Modelling Batch and Fed-batch Mammalian Cell Cultures for Optimizing MAb Productivity

by

Penny Dorka

A thesis
presented to the University of Waterloo
in fulfillment of the
thesis requirement for the degree of

Master of Applied Science
in
Chemical Engineering

Waterloo, Ontario, Canada, 2007

AUTHOR'S DECLARATION

I hereby declare that I am the sole author of this thesis. This is a true copy of the thesis, including any required final revisions, as accepted by my examiners.

I understand that my thesis may be made electronically available to the public.

Penny Dorka

Abstract

The large-scale production of monoclonal antibodies (MAb) by mammalian cells in batch and fed-batch culture systems is limited by the unwanted decline in cell viability and reduced productivity that may result from changes in culture conditions. Therefore, it becomes imperative to gain an in-depth knowledge of the factors affecting cell growth and cell viability that in turn determine the antibody production. An attempt has been made to obtain an overall model that predicts the behaviour of both batch and fed-batch systems as a function of the extra-cellular nutrient/metabolite concentrations. Such model formulation will aid in identifying and eventually controlling the dominant factors in play to optimize monoclonal antibody (MAb) production in the future.

Murine hybridoma 130-8F producing *anti-F-glycoprotein monoclonal antibody* was grown in D-MEM medium (Gibco 12100) with 2% FBS. A systematic approach based on Metabolic Flux Analysis (MFA) was applied for the calculation of intracellular fluxes for metabolites from available extracellular concentration values. Based on the set of identified significant fluxes (from MFA), the original metabolic network was reduced to a set of significant reactions. The reactions in the reduced metabolic network were then combined to yield a set of macro-reactions obeying Monod kinetics. Half saturation constants were fixed empirically to avoid computational difficulties that parameter estimation for an over-parameterized system of equations would cause. Using Quadratic Programming, the proposed Dynamic Model was calibrated and model prediction was carried out individually for batch and fed-batch runs. Flux distribution for batch and fed-batch modes were compared to determine whether the same model structure could be applied to both the feeding profiles. Correlation analysis was performed to formulate a Biomass Model for predicting cell concentration and viability as a function of the extracellular metabolite concentrations in batch and fed-batch experiments. Quadratic Programming was applied once again for estimation of growth and death coefficients in the equations for viable and dead cell predictions. The prediction accuracy of these model equations was tested by using experimental data from additional runs. Further, the

Dynamic Model was integrated with the Biomass Model to get an Integrated Model capable of predicting concentration values for substrates, extracellular metabolites, and viable and dead cell concentration by utilizing only starting concentrations as input.

It was found that even though the set of significant fluxes was the same for batch and fed-batch operations, the order of these fluxes was different between the two systems. There was a gradual metabolic shift in the fed-batch system with time indicating that under conditions of nutrient limitation, the available energy is channeled towards maintenance rather than growth. Also, available literature with regard to cell kinetics during fed-batch operation suggests that under nutrient limited conditions, the cells move from a viable, non-apoptotic state to a viable apoptotic state. This is believed to lead to variations in antibody production rates and might explain inaccurate predictions for MAb obtained from the model proposed in the current work. As a result more detailed analysis of the system and in particular, the switch from non-apoptotic to apoptotic state is required.

As a continuation of efforts to study the system in-depth, fluorescence imaging is currently being applied as a tool to capture the changes in cell morphology along the course of experimental batch and fed-batch runs. These experiments maybe able to elucidate the transition from non-apoptotic to apoptotic cells and this information maybe used in the future to improve the accuracy of the existing mathematical model.

.

Acknowledgements

I would like to thank my supervisor Prof. Hector M. Budman for his constant guidance, unwavering support and an objective criticism of my work that helped in shaping up my subsequent research efforts.

Also, I express my gratitude to Prof. Scharer for offering his extensive knowledge in the field of biotechnology and being a constant source of motivation.

Worth mentioning is the help and advice received from Jana Otruba who shared her knowledge of fermentations with me. Also, I am thankful to Jianying Gao who trained me in basic cell culture techniques and related lab protocols.

My work would never have been successful without the support of my friends- Niju Narayan, Luis Ricardes and Keyvaan Nowruzi, who helped me figure out bottlenecks in my research and M. Kolla for providing the motivation to meet targets. I must also thank Rosendo Diaz and Khurram Aftab for helping me with roadblocks in my work. A special thanks to Suad Al-adwani for her friendship and advice.

I must also thank NSERC for providing financial assistance for this project.

Most importantly, my gratitude goes to my family for teaching me the value of education, hard work and perseverance and instilling in me a ‘Never Say Die’ attitude.

Dedication

This thesis is dedicated to the many people in my life that I appreciate and love more than words can say:

- My parents, who instilled in me the strength to never give up and persevere to overcome obstacles. Mom and Dad, you always believed in me and taught me to stand up for what I believe in. You encouraged me to rise above the ordinary and expect more than average from myself. I love you even for the moments when I felt you pushed me too hard but now I know that you believe I am capable of greater things.
- My Grandmother, for her love and support. May God rest your soul in peace.
- My dearest brother, Gundeep whose constant banter was sometimes quite irritating, yet I love him for teaching me to look at the lighter side of life. Gundeep, on occasions you displayed wisdom beyond your years and I admire you for that. You Rock!

Table of Contents

List of Figures

List of Tables

Chapter 1
Introduction

1.1 Need for Large Scale Production of Monoclonal Antibodies (MAb)

The last decade has seen an unprecedented increase in the demand for biopharmaceuticals produced from animal cell culture processes, primarily due to their application in diagnostics and therapeutic treatments. Mammalian cells are widely used to produce recombinant proteins such as hormones, enzymes, cytokines and antibodies for therapeutic purposes. Despite increasing demand, the manufacturers are faced with the challenge of meeting lower cost expectations of the health system and competition from other manufacturers. All these factors make it crucial that a more efficient production strategies than the ones currently in practice are devised for the large-scale manufacture of these drugs.

1.2 Fermentation Strategies for Large Scale Production

There are three possible fermentation strategies commonly utilized for antibody production on an industrial scale:

- Batch Operation
- Continuous Operation
- Fed-batch Operation

These operations are discussed in more detail below.

1.2.1 Batch Operation

Suspension cultures were initially propagated in batch operated bioreactors in which cells grow in a finite volume of liquid nutrient medium and follow a sigmoid pattern of growth. All cells are harvested at the same time. However, batch processes suffer from problems of nutrient limitation, low cell densities, low productivity and high toxin accumulation that leads to product degradation. Also, the stand-by time between batches is too long.

1.2.2 Continuous Operation

In continuous fermentations fresh nutrient medium is added continuously to the fermentation vessel, accompanied by a corresponding continuous withdrawal of a portion of the medium for recovery of cells or fermentation products. Operating with continuous cultures makes it possible to achieve high cell density and high productivity without any nutrient limitation or growth inhibition due to toxin build-up in the system. But the drawback of continuous culture is that it requires a higher level of technical skill to operate and loss of productivity due to genetic changes may also occur. Additionally, continuous fermentations often waste nutrient substrate.

1.2.3 Fed-batch Operation

Fedbatch operations combine the advantages of batch and continuous modes and minimize the disadvantages that either of the two possesses. Just like batch operations, they are relatively easy to perform and simple to scale-up and unlike continuous culture systems, no additional special pieces of equipment are required to switch from batch to fed-batch operation. At the same time, they ensure prolonged cell growth (high cell densities) and product formation due to extension of working time that is particularly important in the production of growth-associated products.

1.3 Challenges in MAb Production

The large-scale production of MAb by mammalian cells in batch and fed-batch culture systems is limited by the unwanted decline in cell viability and reduced productivity that may result from changes in culture conditions. Therefore, it becomes imperative to gain an in-depth knowledge of the factors affecting cell viability and subsequently antibody production. By understanding these effects it will become possible to impose the necessary conditions during a fed-batch operation to maximize product formation.

1.4 Past Efforts and Scope of the Research

Some limited research work has been conducted on hybridoma cells (Ljunggren and Haggstrom, 1994) that illustrates that a dual substrate (glucose and glutamine) limited feeding profile reduces overflow metabolism of the two major growth inhibitors- lactate and ammonia without a decline in growth rate. Such reports have led to the exploration of fed-batch culture mode in the current work to explore the possibility of developing an optimum feeding profile. In further studies, the kinetics of apoptosis onset and the correlation with exhaustion of nutrients in hybridoma cultures has been revealed (Franek and Dolnikova, 1991; Mercille and Massie, 1994). Since the overall cell population in a bioreactor culture is comprised of individual cells going through the various transitions of the cell cycle, a better understanding of the system response necessitates a better understanding of cells on an individual level. The existing models lack in the level of detail required to explicitly model and predict system properties affecting MAb production and quite often use experimental values along the duration of the run as inputs. Overcoming these shortcomings of existing models may lead to substantial improvements in process efficiency and MAb production. Additional details on relevant research are presented in Chapter 2.

1.5 Identification of Apoptosis and Necrosis

There have been accounts in literature of an increase in the rate of MAb production associated with the onset of cell death in hybridoma cultures (Simpson *et al.*, 1997). It has been documented that cell morphology is a clear indicator of the state of a cell. Each stage of the cell-life cycle exhibits characteristic morphology. Fluorescence imaging provides the means of identifying the different stages of cell growth and death by capturing the changes in cell morphology as the cell progresses through the various stages of its life-cycle (Mercille and Massie, 1994; Renvoize *et al.*, 1997; Ziegler *et al.*, 2004).

1.6 Summary

The focus of the thesis is the identification of an accurate mathematical model that accounts for the heterogeneity in the cell population and predicts the optimum feeding profile for a

fed-batch culture to enhance MAb productivity. A fluorescence imaging protocol/technique has been developed as a tool to capture the changes in cell morphology along the course of experimental batch runs to build on the model proposed in the current work. Identification of an active death process like apoptosis and the factors controlling it (as opposed to a passive one, i.e., necrosis) may lead to new strategies for the minimization of cell death during commercial animal cell culture. Ultimately, this may lead to substantial improvements in process efficiency. A switch from hybridoma to CHO cell cultures has been done as the CHO cell line has been reported to have better specific MAb productivity and it might lead to an appreciation of the differences in the kinetics of the two cell lines, if there are any.

Chapter 2
Literature Review

This chapter provides an overview of past literature with regards to the work presented in later chapters and has been sub-divided into three sections. The three sections discuss-

(i) Biological Background

(ii) Measurement Techniques

(iii) Model Development

The first section of this chapter discusses the common fermentation strategies for large-scale MAb production and the cell growth in a fermentation process. The second section provides an overview of the imaging techniques available for the quantification of cell sub-populations and similar measurements. The third section focuses on the various classical mathematical models utilized for modelling animal cell cultures.

2.1 Biological Background

2.1.1 Common Fermentation Strategies

2.1.1.1 Batch Fermentation

Suspension cultures were initially grown in batch operated bioreactors in which cells grow in a finite volume of liquid nutrient medium and follow a sigmoid pattern of growth. All cells are harvested at the same time. For years, batch fermenters were prepared, inoculated, and run to completion with nothing added except air and some agent to control foaming. According to the reports that address animal cell culture in stirred bioreactors, production in stirred batch bioreactors is easy to perform and simple to scale-up with cell density varying between 10^6 and 10^7 cells/ml (Chisti, 1993; Shuler, 1999; Griffiths, 1988; Glacken *et al.*, 1983). However, batch processes suffer from problems of nutrient limitation, low cell densities, low productivity and potential high toxin accumulation that may lead to product degradation. Also, the down-time between batches may be too long and amounts to a wastage

of operation time. It seems obvious that the batch process changes should affect formation of the product and that these changes can be controlled by nutrient addition or process modification. However, it took a long while for this concept to gain momentum.

2.1.1.2 Continuous Fermentation

On the other hand, in continuous fermentations nutrient medium is added continuously to the fermentation vessel, accompanied by a corresponding continuous withdrawal of a portion of the medium for recovery of cells or fermentation products. Operating with continuous cultures makes it possible to achieve high cell densities and high antibody productivity without any nutrient limitation or growth inhibition due to toxin build-up in the system. But on the other side, it requires a higher level of technical skill to operate a continuous culture. Another drawback is that there may be loss of productivity due to genetic changes in the culture. Product quality control is often a serious problem. Additionally, continuous fermentations often waste nutrient substrate. The fermentation broth as it is continuously withdrawn for product recovery contains a certain amount of residual unused nutrients of the medium as well as a portion of the fresh nutrient constituents being continuously added to the fermentation (http://www.raifoundation.org).

2.1.1.3 Fed-batch Fermentation

Fed-batch operations combine the advantages of batch and continuous modes and minimize the disadvantages that either of the two possesses. In fed-batch culture, nutrients are continuously or semi-continuously added to the bioreactor, while effluent is removed discontinuously.

Just like batch operations, they are relatively easy to perform and simple to scale-up (http://fachschaft.bci.unidortmund.de). Furthermore, unlike continuous culture systems, no additional special piece of equipment is required to convert from batch to fed-batch operation (Longobardi, 1994). At the same time, they ensure prolonged cell growth (high cell densities) and cell maintenance due to extension of working time, which is particularly important in the production of non-growth-associated products such as antibodies (Agrawal *et al*., 1989). It is

possible to exercise control over the production of by-products, or catabolite repression effects, due to limited provision of only those substrates solely required for product formation. In addition, fedbatch operation allows for the replacement of water lost by evaporation (McNiel, and Harvey, 1990). However, in a cyclic fed-batch culture, due care must be taken in the design of the process to ensure that toxic metabolites do not accumulate to inhibitory levels, and that nutrients other than those incorporated into the feed medium do not become limiting. Also, if many cycles are run, the accumulation of nonproducing or low-producing mutants may result.

2.1.2 Phases of Culture Growth during Fermentation

When operating a mammalian cell culture, one encounters various different phases of growth and/or death starting from the point of inoculation of the medium with cell culture right until shut-down. The cell population in a batch culture, that happens to be the simplest mode of operation, typically has the following phases of development: (1)lag phase, (2)logarithmic or exponential growth phase, (3)deceleration phase, (4)stationary phase, (5)death phase (Shuler and Kargi, 1992). Figure 2-1 on the next page describes a batch growth cycle.

2.1.2.1 Lag Phase

Upon inoculation of cells into fresh medium, the cells take some time to acclimatize to the new nutrient/growth environment by means of reorganizing their molecular constituents. Depending on the composition of the new medium, new enzymes are synthesized, the synthesis of some other enzymes is repressed, and the internal machinery of cells is adapted to the new environmental conditions. These changes reflect the intracellular mechanisms for regulation of the metabolic processes. During this phase, the cell mass increases a little while the cell number remains essentially constant. However, at times when the seed density for the culture is too low or the cell viability of the seeding culture is not high enough, there may be encountered a pseudo-lag phase. It must be understood that this phase of arrested growth is not because of adaptation of cells to new culture environment but due to small inoculum size or poor condition of the inoculum (Shuler and Kargi, 1992).

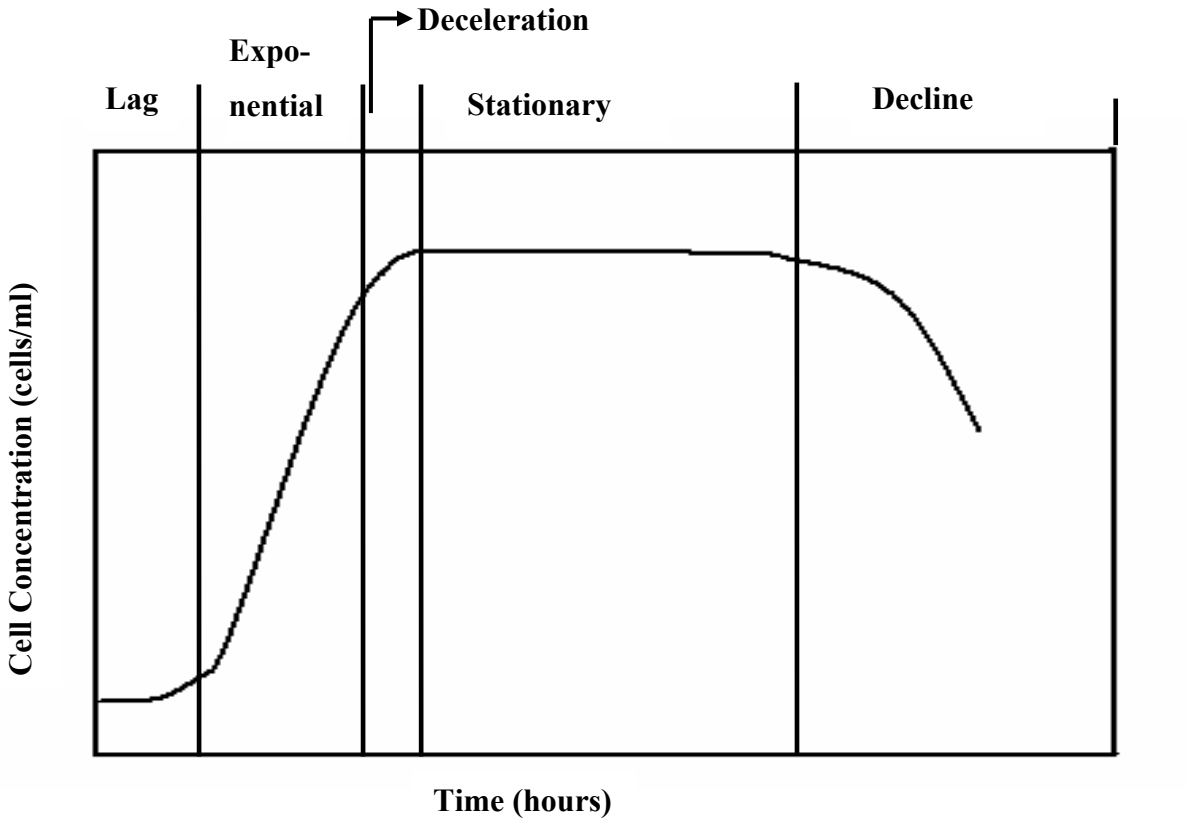

Figure 2-1 Typical Growth Curve for a Mammalian Batch Culture

2.1.2.2 Exponential Growth Phase

The lag phase is followed by the exponential growth phase, also known as the logarithmic growth phase. In this phase, the cells have adjusted to their new environment and are able to multiply rapidly which is indicated by a steady exponential increase in cell number density with time. The exponential phase is often regarded as a period of balanced growth in which all components of a cell grow at the same rate. This means that the average composition of a single cell remains approximately constant during this phase of growth. Thus, during balanced growth, the specific growth rate determined from either cell number or cell mass will be the same. The exponential growth rate follows first order kinetics (Shuler and Kargi, 1992):

$$\frac{dX}{dt} = \mu X, \qquad X=X_0 \text{ at } t=0 \qquad (2.1)$$

where X and X_0 are the instantaneous and initial viable cell concentrations, respectively; t represents the culture time from the instant of inoculation and μ signifies the growth rate constant.

2.1.2.3 Deceleration Phase

Since in a batch process there is no subsequent addition of nutrients to the system during the course of its operation, there is an eventual depletion of one or more essential nutrients. As there is no product recovery during the course of the batch either, there may be a gradual build-up of toxic or inhibitory by-products. The rapidly changing culture environment results in unbalanced growth. This state corresponds to the deceleration phase of growth. While in the exponential growth phase the cellular metabolic control system is directed to achieve maximum rates of reproduction, the deceleration phase witnesses the restructuring of the cell to increase the prospects of cell survival in response to the rapidly changing conditions. This phase is rather short-spanned and is often considered as a continuum between the exponential and stationary phase rather than as a separate phase by itself (Shuler and Kargi, 1992).

2.1.2.4 Stationary Phase

The deceleration phase is succeeded by the stationary phase, when cell division ceases. In other words, the growth rate is equal to the death rate. Even though the net growth rate is zero during the stationary phase, cells are still metabolically active and produce secondary metabolites (non-growth related products). In fact, the production of some metabolites is enhanced during the stationary phase (antibodies, hormones, etc.) due to metabolite deregulation (Suzuki and Ollis, 1990). During the course of the stationary phase, one or more of the following phenomena may take place:

1. Total cell concentration stays constant but the number of viable cells decreases.
2. Cell lysis is observed and there is a decline in viable cell concentration. A second growth phase may occur as cells may grow on products of lysed cells (cryptic growth).
3. Cells do not grow but are metabolically active and produce secondary metabolites as a result of metabolite deregulation.

Reasons attributed to termination of growth may be either exhaustion of an essential nutrient or accumulation of toxic products. If there is production of an inhibitory product during the course of the batch operation, the growth rate will slow down with accumulation of that inhibitory substance and above a certain concentration of this inhibitor the growth will cease completely (Shuler and Kargi, 1992). In some studies, the kinetics of apoptosis onset and the correlation with exhaustion of nutrients in hybridoma cultures has been revealed (Franek and Dolnikova, 1994; Mercille and Massie, 1994). Incidence of cell death in *A. fumigates*, a pathogen has been reported by Mousavi and Geoffrey (2003) during the stationary phase, that appears to share similarities to apoptotic cell death in higher eukaryotes and seems to be dependent on a caspase-like activity. This was proved by the association of the pattern of death observed with markers for apoptotic death. Although, a connection between cell cycle and apoptosis has been suggested in mammalian cells, its nature is not clear yet (Frame and Balmain, 2000; Shapiro, 2001; Sears and Nevins, 2002). It has been hypothesized in the current work that an exit from stationary phase might be a prerequisite for apoptosis.

2.1.2.5 Death Phase

The death phase or decline phase follows the stationary phase. However, there is an overlap between these two stages of growth as some cell death may have already started in the stationary phase. The rate of death follows first order kinetics (Shuler and Kargi, 1992):

$$\frac{dX}{dt} = -k'_d X \qquad (2.2)$$

where X is the instantaneous cell concentration at time t; and k_d' is the death rate constant.

2.1.2.6 Fedbatch culture mode: Extension of Stationary Phase

The fed-batch culture is initiated in the same way as a batch culture starting with inoculation of nutrient volume with seed culture. The Lag and Exponential phase progress in the same way as in batch culture mode. In a batch culture, stationary phase occurs when the cells run out of their carbon and energy source or a particular nutrient. Many products are produced when cell growth slows down; i.e., during the stationary phase of a batch culture. A batch

culture, however, will produce relatively small amounts of these products as without sufficient nutrients, cells will not be able to maintain homeostasis and thus lyse or become biochemically inactive.

However, in a fedbatch culture small nutrient volumes are gradually added to the culture in such a way that the nutrient(s) do not get exhausted and there is little or no toxin build-up over time. This intermittent feeding serves in replenishing the exhausted nutrients and/or dilution of toxified medium which promotes further growth and alleviates the adverse effects of toxin on cell growth. In this way, cells can have sufficient nutrients to either grow slowly or to maintain their internal integrity. Thus, the cells are maintained in an apparent stationary phase mode longer than in batch cultures (i.e., slow or no growth), but at the same time continue to produce products. Thus, a fed-batch reactor is expected to extend the stationary phase in fermentation (http://www.np.edu.sg/home/sitemap.html).

2.1.3 Cell Cycle

Since a cell culture comprises of individual cells, it is not possible to develop an understanding of the overall system without an understanding of the processes taking place within a single cell itself. Typically, the life-cycle of an individual cell progresses through the following 4 stages (http://users.rcn.com/jkimball.ma.ultranet/BiologyPages/C/CellCycle.html):

- G1 - Gap1
- S - Synthesis
- G2 - Gap2
- M - Mitosis

During the initial phase of a fermentation run, a cell feeds on nutrients available in the system, producing RNA and synthesizing protein. This stage is called the G1 phase where the cell grows in size and prepares itself for cell-division. Increase in cell size is followed by DNA replication; this is the S phase. After DNA replication is complete, the cell enters the

G2 phase, where it grows further and produces new proteins. Finally, it enters the mitosis stage where the cell divides into two daughter cells. This process of cell growth can continue indefinitely and has been illustrated in Figure 2-2 (http://www.cellsalive.com).

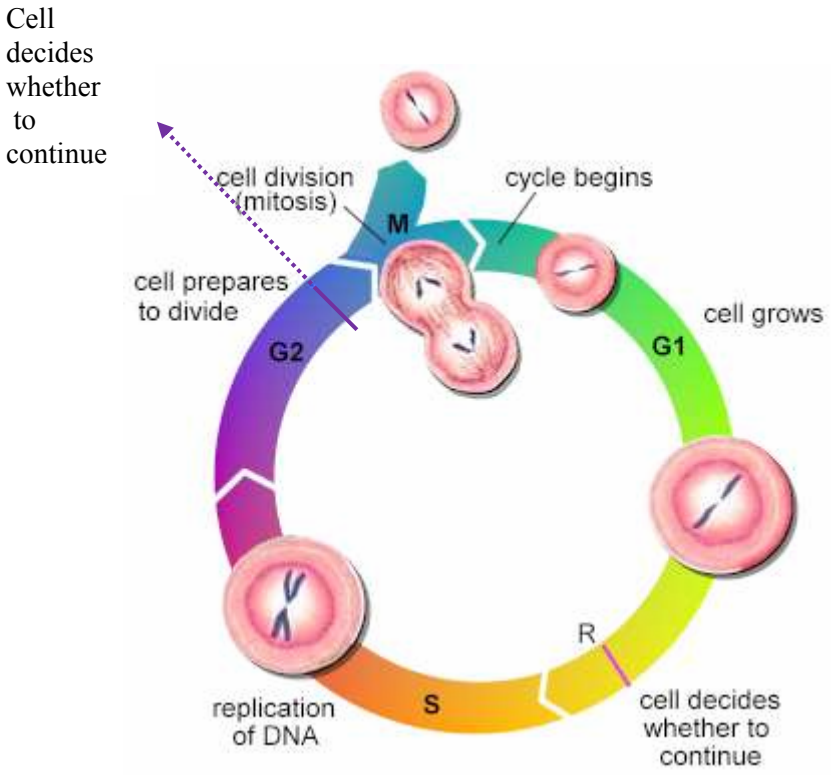

Figure 2-2 Illustration of a Cell-cycle modified from (http://users.rcn.com)

At times there may be errors in functions performed during the cell cycle. To remedy the errors that may be introduced during cell development, there are in-built checkpoints in the cell cycle that interrupt/abort the cell cycle if such an event occurs (http://users.rcn.com/jkimball.ma.ultranet/BiologyPages/C/CellCycle.html).

- G1 checkpoint- Before the cell enters the S-phase, the checkpoint mechanism in place senses DNA damage. Damage to DNA stops the progression of the cell

cycle until the damage can be repaired. If the damage is irreparable, the cell enters the death phase and self-destructs by apoptosis.

- G2 checkpoint: A check is made on the successful replication of DNA that takes place during S phase. If replication stops at any point on the DNA, progress through the cell cycle is halted until the problem can be fixed. If not, cell death by apoptosis is triggered.

(http://users.rcn.com/jkimball.ma.ultranet/BiologyPages/A/Apoptosis.html).

2.1.4 Association of Cell Cycle with the Progress of Culture

In a bioreactor that contains a large cell population, there are cells going through the various developmental stages of the cell-cycle all at the same time. Thus, there exist a number of sub-populations that are in different stages of the cell-cycle and make up an average overall cell population. In other words, the lag phase represents the state of the system where the population/culture is dominated by cells in the G1 stage that are feeding and growing in order to multiply, although there will be cells that are in any of the other three cell-cycle stages. Over time, majority of the cells progress from G1 to the mitosis stage where they divide and it is classified as the exponential stage of culture growth. With the subsequent exhaustion of nutrients, the cell growth slows down which is broadly regarded as the stationary phase. Due to lack of substrate, the cells go into growth arrest as they are unable to clear the checkpoints set in place by the cell machinery
(http://users.rcn.com/jkimball.ma.ultranet/BiologyPages/A/Apoptosis.html).

The progression of cell culture from stationary phase to decline phase marks the onset of death.

2.1.5 Cell Death in Bioreactors- Apoptosis and Necrosis

Cell death can be broadly classified into two categories (Wyllie, 2004; Renvoize et al., 1997):

- Apoptosis

- Necrosis

Apoptosis, also called programmed cell death, is a physiological process that occurs under normal conditions by which unwanted or useless cells are eliminated during development or other biological process. Apoptosis is an energy requiring process.

Necrosis also known as accidental cell death is a passive, catabolic pathological process that occurs when cells are exposed to as serious physical or chemical insult like heat stress or toxic agents.

2.1.5.1 Causes of Apoptosis

There has been evidence in literature (Mercille and Massie, 1994; Singh *et al.*, 1994) supporting the incidence of apoptosis due to the following factors:

- Nutrient limitation (namely, glucose and glutamine)
- Oxygen deprivation
- Cystine deprivation
- Serum limitation
- Hypoxia

2.1.5.2 Causes of Necrosis

- Ammonia accumulation (lowest concentration reported = 2mM)
- Lactate accumulation (lowest concentration reported = 20mM)
- Osmotic pressure
- pH

The lowest concentration of ammonia and lactic acid reported to cause necrosis in culture is 2mM and 20 mM, respectively (Newland *et al.*, 1990). It must be mentioned however, that when both are present in the culture, lactate and ammonia have a negative cumulative effect on cell growth and viability at concentrations lower than what have been reported for each of them individually. (Newland *et al.*, 1990) reported lactate concentrations greater than 12mM

and ammonia in the range (1-4mM) to be growth inhibitory. Osmotic pressure may cause cell death via necrosis by cell implosion from hypertonic solutions, or cell explosion from hypotonic solutions (http://www.extravasation.org.uk). Some substances have been reported to cause tissue damage by having an osmolality greater than that of serum (281-289 mOsmol/L) (Upton *et al.*, 1979).

2.1.5.3 Identification of Apoptosis and Necrosis

It has been documented that cell morphology is a clear indicator of the state of a cell. Each stage of the cell-life cycle exhibits characteristic morphology. Fluorescence imaging provides the means of identifying the different stages of cell growth and death by capturing the changes in cell morphology as the cell progresses through the various stages of its life-cycle (Mercille and Massie, 1994; Renvoize *et al*., 1997; Ziegler *et al.*, 2004).

2.2 Cell Culture Related Measurement Techniques

2.2.1 Estimation of Cell Viability

The most widely practiced method for estimation of cell viability is the Dye Exclusion test which is based on the principle that live cells possess intact cell membranes that exclude certain dyes, such as Trypan Blue, Eosin, or propidium iodide, whereas dead cells do not. In this test, a cell suspension is mixed with a pre-determined volume ration of the dye. The mixture is transferred to a hemacytometer and visually examined under a microscope to determine whether cells take up or exclude dye. A viable cell will have a clear cytoplasm whereas a nonviable cell will have a blue cytoplasm (http://www.invitrogen.com).

2.2.2 Amino-acid Analysis

Amino acid analysis was pioneered by Moore *et al.* (1958). Over time the method was modified for suitability of the reagents being analyzed.

2.2.2.1 HPLC

A pre-column derivatization method for the analysis of primary and secondary amino-acids developed by Bidlingmeyer (1984) based upon the formation of a phenylthiocarbamyl derivative of the amino acids.

2.2.2.2 Ion Chromatography (IC) - An Alternative

Ion Chromatography that uses amperometry as the principle for amino acid detection is an improvement over HPLC as it does not require derivatization and is therefore a much faster method of analysis. This method is designed specifically for analytes that can be oxidized at a selected potential, leaving all the other compounds undetected. The Integrated Pulsed Amperometric Detection (IPAD) as it is formally called is a powerful method that provides a broad linear range of detection with very low detection limits (Hanko *et al.*, 2004).

2.2.3 Assays for Apoptosis Detection

A series of morphological changes distinct to the incidence of death by apoptosis in comparison to necrosis still remain the standard method its identification (Kerr *et al.*, 1972; Renvoize *et al.*, 1997). The different techniques that apply morphology of apoptotic cells for their identification have been mentioned as follows (Renvoize *et al.*, 1997).

2.2.3.1 Electron and Light Microscopy

This method utilizes the detailed structural aspects of apoptosis, such as the loss of microvilli and pseudopodia and dilation of the endoplasmic reticulum. However, centrifugation and spreading of apoptotic cells on a glass slide can be damaging to the cells and lead to biased results.

2.2.3.2 DNA Electrophoresis

Apoptosis identification by means of agarose gel electrophoresis of DNA remains a significant method for identifying the oligonucleosomal digestion of chromatin. However, the application of this technique is limited to a qualitative analysis only.

2.2.3.3 Flow Cytometry

This method of analysis is based on the principle that apoptotic cells, among other typical features, exhibit DNA fragmentation and loss of nuclear DNA content. Use of a fluorochrome, such as propidium iodide, that is capable of binding and labeling DNA which makes it possible to obtain a rapid (within about 2 hours) and precise quantitative evaluation of cellular DNA content by flow cytometric analysis (Riccardi and Nicoletti, 2006). The only drawback of this method is that nuclear fragments of clumps of chromosomes could be counted as apoptotic cells (Darynkiewicz *et al*., 1997).

2.2.3.4 Fluorescence Light Microscopy

This technique utilizes the DNA-binding properties of fluorescent dyes for the purpose of characterization of apoptosis and necrosis. Apoptotic index and membrane integrity can be simultaneously determined and there is no cell-fixation step involved unlike flow cytometry. This protocol has been described in greater detail in Chapter 3 that discusses various experimental methods adopted. Due to the reasons states before, fluorescence light microscopy presents a simplistic way of quantitative determination of the apoptotic index.

2.2.3.5 Caspase Measurement- FRET

Most forms of apoptosis involve activation of caspases (Xiang *et al.*, 1998). FRET is an experimental method that allows the continuous monitoring of caspase activity in individual mammalian cells. Caspases are proteases, which play essential roles in apoptosis and cleave (cut) other proteins. They are called cysteine proteases, because they use a cysteine residue to cleave other substrate proteins at the aspartic acid residue (http://www.wikipedia.org). More than a dozen caspases have been identified in mammalian systems using fluorescence resonance energy transfer (FRET) - a method, based on covalent linkage of a green fluorescent protein (GFP) with a and blue fluorescent protein (BFP) by a short peptide. FRET allows caspase activity in individual cells to be measured over time. Using this method, the kinetic differences in caspase activity between cells in a population can be correlated with whether the cells live or die within a particular time frame. These differences in caspase activity can be detected several hours before death actually occurs (Xiang *et al.*, 1998).

2.3 Mathematical Modelling

The performance of cells, in large, cell cultures can be controlled and enhanced provided that the system properties can be maintained at the required state. Mathematical models are especially useful for simulation, optimization and control purposes. A realistic cell model will not only aid in optimizing productivity but once such a model is formulated, prediction results can be obtained for metabolite concentrations that may otherwise be difficult to measure.

2.3.1 Principles behind Model Formulation

In general, the quantitative description of a bioprocess in terms of a mathematical model involves formulation of three fundamental types of equations (Tziampazis and Sambanis, 1994)

- Mass Balance equations
- Yield equations
- Rate equations

The mass balance equations that are developed based on the reactor configuration and are essentially same for all cell systems if intrinsic kinetics of the culture is not taken into account. The yield and rate equations that describe cellular metabolism are independent of the reactor configuration. The yield equations are based on material and energy balances and relate the amounts/rates of the metabolite consumption and production. Although they may involve several underlying assumptions about metabolism, they have a theoretical basis and hence are reliable. The rate equations describe the kinetics of various processes, generally as functions of intracellular parameters and the composition of the extracellular medium. Being empirical in nature, rate equations are the most unreliable segment constituting a model (Tziampazis and Sambanis, 1994). The process mass balances and the yield equations are not sufficient to fully describe the system. To remove the remaining degrees of freedom, formulation of rate equations or measurements of the rates on-line is required (Andrews, 1993; Hu and Himes, 1986). However, it is not always feasible to make on-line rate

measurements but for a few compounds. Consequently, certain rate equations need to be specified. In the absence of sufficient knowledge, experimental results are utilized to obtain information about cellular processes and hypothesize kinetic expressions (Glacken *et al.*, 1988).

2.3.2 Classical Mathematical Models for Animal Cell Cultures- A Classification

In cell process technology, models for animal cell cultures can be classified into the following categories (Tziampazis and Sambanis, 1994):

- Segregated/ Unsegregated,
- Structured/ Unstructured, and
- Deterministic/ Stochastic.

Figure 2-3 offers a schematic view of the above categorization.

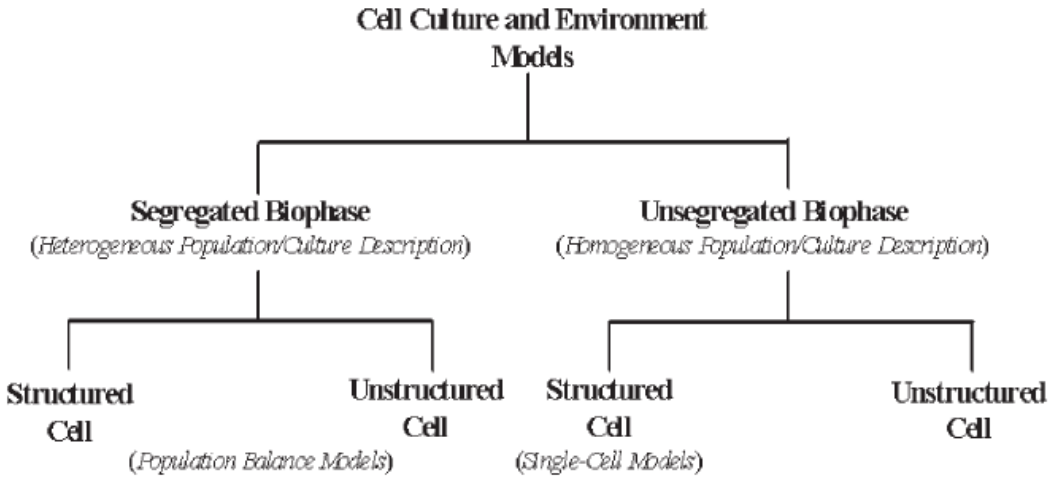

Figure 2-3 Model Classification for Cell Culture Systems adapted from (Sidoli *et al.*, 2004)

Structured models attempt to elucidate intracellular processes in that they possess structure either in the physical sense, namely the organelles, cell shape or size, or in the biochemical sense where biomass is subdivided into its intracellular biochemical components. Structured models can provide a measure of the quality of the cell population and are based on more fundamental processes (Sidoli *et al.,* 2004). On the other hand, unstructured models do not account for the intracellular processes and acknowledge only implicitly the change of cellular physiological state with the environment (Fredrickson, 1976). Such models treat the cell as a single homogeneous unit, hence their biological basis is limited, and the mathematical equations involved are only phenomenological descriptions of the actual system. Unstructured models are of limited applicability in situations where the cellular environment is highly dynamic in nature. Being highly empirical in nature, they are primarily used in cases where only parameter estimation is required for developing the full model in light of lacking physical knowledge of the system. Although their extrapolating ability is limited, these models are relatively easy to build, and are generally suitable for simulating steady-state or slowly-changing systems. Structured models are superior to unstructured models as they attempt to imitate the biological system by separating/lumping the biomaterial into compartments that are chemically and/or physically distinct. The compartments' interactions with each other and with the environment are described by stoichiometric equations that account for various metabolic pathways and/or kinetic rate expressions. The evolution of concentrations with respect to time is mainly based on mass and energy balances and transport and reaction rate terms (Tziampazis and Sambanis, 1994). Structured models have wider applicability and have better extrapolating capability than unstructured models. Unstructured models, on the other hand, can provide a simplistic but quick alternative for the development of process systems applications (Tziampazis and Sambanis, 1994).

Not all cells in a mammalian cell culture are alike; they are heterogeneous in composition. By classifying a model as being segregated or unsegregated, it is possible to account for the heterogeneity of the cell culture with regards to cell age, size, growth rate and metabolic state. Referring to a cell culture as segregated implies that it is composed of cells in different

stages of development and it is therefore heterogeneous. Conversely, an unsegregated model views the population as consisting of identical "average cells" and uses a lumped variable such as total biomass per unit volume, to describe the entire population. Segregated models build on the heterogeneous composition of a culture and offer the advantage of relating cell properties and biochemical activities within distinct parts of the population. Segregated models based on cell cycle relate the kinetics of growth, metabolic processes and product formation to the distribution of the population among the phases. Considering the differences between cells in the population is more representative of the true physical state. However, segregated models are also more computationally difficult to handle (Bailey and Ollis, 1986).

Variability within a cell culture can be accounted for by means of stochastic models that describe random processes. For systems in which the cellular processes are not subject to variability, a deterministic model is applied. Stochastic models use probability distribution functions to describe process dynamics at the cell and population levels. Since they account for randomness in the culture, they are more accurate than deterministic models but that is the case only as long as the systems contains a small numbers of cells (Tziampazis and Sambanis, 1994). A more detailed description of the various categories discussed above follows.

2.3.2.1 Unstructured Non-segregated Models

The simplest way to model cell culture systems will be to consider an unstructured, unsegregated model. As these models do not require system details for their generation, they are essentially based on experimental data to derive information on cellular processes and postulate kinetic expressions. Generally, in the starting phase of model development for animal cell culture systems researchers and bioengineers focused on empirical models.

For such a model, the growth rate expression can be written as (Shuler and Kargi, 1992):

$$r_x = dX/dt = \mu X \qquad (2.3)$$

where, r_x is the rate of cell generation, X is the cell concentration and μ is the specific growth rate.

Many cell culture processes exhibit saturation type kinetics, i.e., the rate of the process μ is limited by a certain factor when its concentration c is low, but the limiting effect disappears and the process rate reaches a maximum value μ_{max}, as the concentration increases. This behavior can be described by a Monod-type equation which is the most commonly used expression that relates the specific growth rate of the cell to the substrate concentration. Monod's equation is given as (Shuler and Kargi, 1992):

$$\mu = \mu_{max} \frac{S}{K_S + S} \qquad (2.4)$$

where, μ = specific growth rate

μ_{max} = maximum specific growth

S = substrate concentration

K_S = saturation constant for substrate

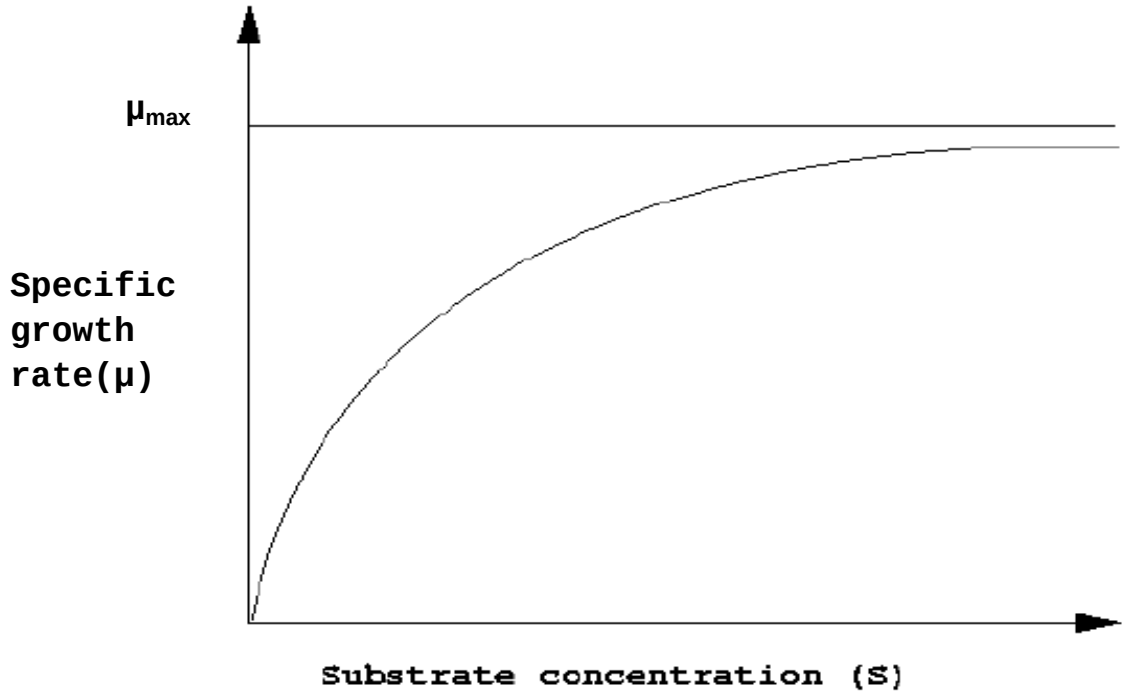

Figure 2-4 Monod's Growth Curve

Figure 2-4 depicts the dependence of μ on S according to Monod's equation. One should note that Monod's equation is empirical and does not have any mechanistic basis. This equation is only valid for an exponentially growing or steady state culture under condition of balanced growth. The equation does not fair well during transient conditions. Despite its simplicity and no fundamental basis, it works surprisingly well in a large number of steady state and dynamic situations. This characteristic has important implications in control of bioreactors.

In contrast to behavior described by Monod kinetics, the effect of an inhibitor on the rate becomes pronounced when its concentration reaches a minimum threshold value; in other words, an inhibitor reduces the rate of a process as its level i increases. Such effects can be modeled by analogy to the various types of inhibition of enzymatic reactions (Bailey and

Ollis, 1986). Of those inhibition models, the simpler and easier to use is that of purely non-competitive inhibition (Tziampazis and Sambanis, 1994):

$$\mu = \frac{\mu_{max}}{1+(i/K_i)} \qquad (2.5)$$

In the above equations, μ and μ_{max} have the same implication as mentioned before. i is the inhibitor concentration while K_i is the inhibition constant.

It is plausible that instead of one metabolite being the controlling factor, there may be a group of metabolites that control the metabolic processes within the culture. In that case, the expressions given above can be modified to incorporate additional terms (thus increasing the number of model parameters). Multiplicative models with concentration terms raised to various powers, introducing dependency of the parameters to other factors through empirical functions have been illustrated (Barford *et al.*, 1992; Glacken *et al.*, 1989). Factorial experiments may be considered to study and model the individual and interactive effect of many variables, individually and interactively, on the process considered (Sidoli *et al.*, 2004). These models are rudimentary but offer insight into which of the variables are important and need to be studied further.

2.3.2.2 Structured Non-segregated Models / Single cell models

Although unstructured models may provide information on how the system properties affect the growth kinetics, they lack the level of detail necessary to understand change in cell kinetics and/or physiology in response to change(s) in culture conditions as such an approach does not consider intracellular processes. On the other hand, structured unsegregated models collectively known as single-cell models (SCMs) offer the advantage of explicitly accounting for intracellular phenomenon such as cell cycle changes, alterations in cell size and shape; this feature is particularly important during transient or unbalanced growth conditions. In addition, cases where the rate of transport between organelles is potentially rate-limiting, SCMs explicitly consider intracellular spatial organization within the cell. Under the SCM approach, a cell is divided into compartments on the basis of difference in

composition/concentration. However, it is assumed that each compartment is a lumped phase i.e., concentrations are constant throughout the compartment (Tziampazis and Sambanis, 1994).

In order to describe these biochemical processes, the same basic engineering formulations are utilized, as discussed previously under unstructured non-segregated models, namely mass balance, yield and rate equations. Cellular metabolism can be incorporated into an SCM model by defining terms like (i) transport, (ii) primary metabolism, (iii) product synthesis, and (iv) cell growth and death with respect to the system (Tziampazis and Sambanis, 1994). Transport processes include transport kinetics of biochemical species across membranes and between the various compartments that the cell has been divided into. In addition to transport, primary metabolism and product synthesis relates conceptually to two or more linked compartments within which either particular metabolic pathways and/or entire metabolic cycles operate. Conservation equations written for each compartment and for each biochemical species, result in a set of ordinary differential equations. Equation (2.6) illustrates the generic form of these conservation equations (Tziampazis and Sambanis, 1994). The accumulation of any given component i depends on its flow into or out of the compartment j as a result of transport across the compartment barrier (first and second terms on the RHS of equation (2.6)), intra-compartmental reactions generating and consuming the component (third and fourth terms on the RHS) and its dilution due to growth of the cell and thus increasing compartment size (last term on the RHS):

$$\underbrace{\frac{dC_{ij}}{dt}}_{\text{Accumulation}} = \underbrace{\left\{ \sum_{l=1}^{N_{gen}} r_{ijl} - \sum_{l=1}^{N_{con}} r_{ijl} \right\}}_{\text{Reaction}} + \underbrace{\left\{ \sum_{k=1}^{N_{in}} R_{ijk} - \sum_{k=1}^{N_{out}} R_{ijk} \right\}}_{\text{Transport}} - \underbrace{\{\mu C_{ij}\}}_{\text{Dilution}} \qquad (2.6)$$

where C_{ij} is the concentration of the ith component in the jth compartment, R_{ijk} represents the transport rate of species i into or out of compartment j from the k^{th} source or sink compartment; N_{in} is number of source compartments; N_{out} is number of sink compartments; r_{ijl} – reaction rate of component i in compartment j in the l^{th} i-generating or i-consuming

reaction; N_{gen} – number of reactions generating component i; N_{con} – number of reactions consuming component i;

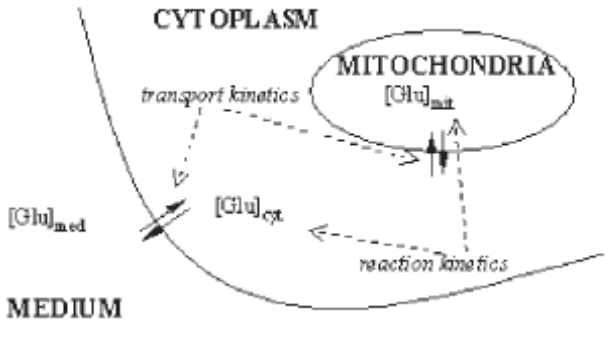

Figure 2-5 Single Cell Compartmentalization
adapted from (Sidoli *et al*., 2004)

Figure 2-5 represents compartmentalization of the cell in the physiological context with cellular structures, such as organelles, pooled biochemical components or the cell environment being treated as compartments. However a problem with multi-compartment models is that the ODEs in equation (2.6) that represent distinct pooled concentrations do not give any idea of spatial distribution of concentration gradients along the surface of the compartment but rather at a single point and do not represent physical dimensions or cell geometry. To overcome this drawback, instead of assuming constant concentration throughout a compartment as per the lumped phase assumption, a concession is made allowing concentration gradients to exist in some compartments. Hence, the resulting conservation equations will then include partial derivatives and additional diffusion equations that are required to compute the diffusive fluxes within the spatial geometry of each compartment. However, the addition of these terms and equations makes the model mathematically and computationally more complex (Tziampazis and Sambanis, 1994). There are two ways in which an SCM can be applied, via a kinetic approach or via a stoichiometric approach.

(i) Kinetic Approach

There are numerous reactions occurring within the cell at any time, and further within the compartments themselves. Kinetic models follow a deterministic approach where one can account for intracellular dynamics by rate and transport mechanisms that give rise to a set of differential algebraic equations (DAEs), which are then integrated over the domain of interest, generally the culture time and results in well-defined time trajectories for all model variables (Gombert and Nielson, 2000). The most commonly used form of expression to describe the reaction rates is the Michaelis–Menten equation. However, one must keep in mind that incorporating a greater level of detail into the system means that the more complex the reaction kinetics will be and the greater the number of parameters required in the SCM. It is important not to over-parameterize the model as this will result in parameter estimation problems due to measurement noise and make the model very time consuming to solve. An additional drawback in incorporating greater detail in terms of complex dynamic expressions is that it normally results in non-linearity in both parameters and variables which makes the models really difficult to solve. In addition, kinetic models are unable to incorporate regulation and control of cellular activity, which requires dynamic simulation (Tziampazis and Sambanis, 1994).

(ii) Stoichiometric Approach

Stoichiometric modelling represents an alternative to the kinetic approach. Such a model yields a static instance of metabolic activity and is represented by a system of flux balance equations based on reaction stoichiometry of a metabolic network with accompanying constraints on flux values. The resulting equations are solved as a constrained optimization problem using some assumed objective; there exists a mathematical and therefore physiological feasible region in which a range of possible mathematical solutions or phenotypes are acceptable though not optimal (Gombert and Nielson, 2000).

The key advantage of stoichiometric models is that they can account for competing reactions, which enables us to study the relative activity of certain pathways under various culture

conditions. For example, the existence of more than one physiological steady state, known as steady-state multiplicity, has been observed by a number of investigators using stoichiometric models and metabolic flux analysis (Follstad *et al.*, 1999; Europa *et al.*, 2000; Cruz *et al.*, 1999; Zhou *et al*., 1997; Linz *et al.*, 1997; Paredes *et al*., 1999).

Generally, most existing SCMs are only partially mechanistic and contain empirical mathematical functions that best seem to describe the observed phenomenon. This is due to the fact that many cellular processes that these models seek to describe have not yet been accurately described. The development of SCMs requires the incorporation and integration of either parts or the entirety of other smaller models each of which describe specific sub-processes. Utilizing the most accurate sub-models that correspond to the components of cellular metabolism is, therefore, of key importance to the construction of a good SCM. On the whole, the SCM approach is a very effective tool to relate hypotheses about molecular level mechanisms to the whole cell and population response to changes in the local environment (Tziampazis and Sambanis, 1994).

2.3.2.3 Segregated Models- Population Balance Models

All segregated (or corpuscular) models can be collectively grouped under the category of population balance models (PBMs). PBMs have been available since the 1960s and are the most mathematically concise way of elucidating the property variation of cells within a population and recognize the individuality of cells within a population.

PBMs are further classified into (Mantzaris *et al.*, 2001):

(i) Single- or Multi-variable,

(ii) Single- or Multi-staged, and

(iii) Mass or Age-structured

A single-variable model differentiates on the basis of one cell property which is generally cell mass. Whereas a multi-variable model uses more than one cellular characteristic to distinguish between cells and can be used to account for any number of biochemical constituents within the cell. Using a multi-stage model, it is possible to describe multiple

developmental phases in the population with each stage of growth added representing each additional phase considered.

Finally, if population differentiation is done on the basis of mass conservation laws, then the model is mass structured, whereas if cell age/maturity is used, the model is said to be age structured (Tziampazis and Sambanis, 1994).

Three parameters are required in a generalized PBM, each having physiological significance. They are: (i) the single cell growth rates, (ii) the transition rates between each of the cell cycle phases, and (iii) the partition function. Together, these three process parameters define the collective state of the cell population (Sidoli *et al.*, 2004; Tziampazis and Sambanis, 1994).

In essence, PBMs are a number balance on a cell population. Unfortunately, they are also particularly difficult to solve, being partial-integro-differential equations and the accurate determination of model parameters imposes a more limiting restriction. Hence, in general, numerical methods must be used for their solution (Villadsen, 1999).

(i) A Single-stage Single-variable PBM

Single stage PBMs consider cell growth as a single stage in that there is no subdivision of the cell cycle. The cell mass (m) is used to distinguish the physiological states of cells- parent or daughter cells. The key variable of interest is the total number of cells or cell number distribution, N(m,t) which is treated as a function of time (t) and cell-mass (Sidoli *et al.*, 2004).

$$\underbrace{\left\{\frac{\partial N(m,t)}{\partial t}\right\}}_{\text{Accumulation}} + \underbrace{\left\{\frac{\partial [r(m,S)N(m,t)}{\partial t}\right\}}_{\text{SingleCellGrowth}} = \underbrace{-\{\Gamma(m,S)N(m,t)\}}_{\text{Division}} + \underbrace{\left\{2\int_{\Gamma}^{\infty}\Gamma(m',S)p(m,m',S)N(m',t)dm'\right\}}_{\text{Birth}} \tag{2.7}$$

In equation (2.7) above, LHS of the equation changes as a result of specific cell lifecycle events represented by RHS of the equation. The first derivative term on the LHS accounts for accumulation of cells over time while the second term on the LHS accounts for loss of cells of a given mass due to their transition into larger cells – single cell growth. The RHS of the equation represents the two fundamental life-cycle processes, namely cell division, which results in the loss of dividing cells of mass m with a division rate $\Gamma(m, S)$ and cell birth, which gives rise to two daughter cells from the division of a single parent cell of mass m'. Thus, the product ΓN represents the total number of parent cells in the culture at any time t. The partition function, $p(m, m', S)$ expresses the probability of a parent cell of mass m' giving birth to a daughter cell of mass m so that $2p\Gamma N$ quantifies the number of newborn cells originating from parent cells of a single mass. As parent cells take on a range of masses m_0 along the mass continuum, to include all parent cell divisions, integration is required for calculating all possible parent cell masses ranging from the minimum, τ, to the theoretical maximum, i.e., infinity. To completely define the model, the physiological functions r, Γ and p expressed in equation (2.7) and the substrate variation S must be specified along with initial and boundary conditions (Sidoli *et al.*, 2004).

Initial Condition:

At the start of the culture process (t =0), the number distribution of cells (N_0) is known and can be expressed as:

$$N(m,0)=N_0(m) \qquad (2.8)$$

Boundary Conditions:

The boundary condition is derived from knowledge of the fact that cells can't have zero mass.

$$N(0,t)=0 \qquad (2.9)$$

The most widely used representation for substrate, S is by relating it to biomass production rate via a yield coefficient, Y (Mantzaris *et al.*, 1999).

For a well-mixed system,

$$\frac{dS}{dt} = \frac{1}{Y}\int_0^{\infty} r(m,S)N(m,t)dm \qquad (2.10)$$

where, the initial substrate concentration (at t=0) S_0 is known.

The partition function, p, which is mathematically a distribution function and specifies distribution of cellular material of a parent cell amongst its two daughter cells, is expressed as a unimodal symmetric beta distribution B(q, q) (implying the shape parameters are equal):

$$p(m,m') = \frac{1}{B(q,q)}\frac{1}{m'}\left(\frac{m}{m'}\right)^{q-1}\left(1-\frac{m}{m'}\right)^{q-1} \qquad (2.11)$$

Other distributions of cell partition function that have been used in previous studies are a Gaussian-type distribution implemented by Eakman *et al.* (1966) where the underlying assumption made is that the partition function variance is very small which translates to equal partitioning always occurring.

The division rate, Γ is proportionally related to growth r by the expression as most commonly reported in literature, for example, Mantzaris *et al.* (1999):

$$\Gamma(m,S) = \frac{f(m)}{1-\int_0^m f(m')dm'} r(m,S) \qquad (2.12)$$

where, f(m) is the division probability density function assumed to be a LHS truncated normal distribution with a mean of μ_f and standard deviation σ_f.

The normal distribution is truncated to exclude cells of mass less than zero. The denominator of the density function represents the proportion of all cells that have reached a mass m and remain undivided. It is used to re-normalize f (m) in order to yield the fraction of cells of mass m that will divide, given that no division of cells with mass less than m has yet taken place. For detailed derivation the reader is referred to Eakman *et al*. (1966).

Various forms have been used to describe the growth rate, including constant, linear and quadratic growth forms.

(ii) Single-stage Multi-variable PBM.

It is possible to distinguish cells on the basis of more than one physiological state. Mathematically, this translates to the use of a 'physiological state' vector (x) in place of the cell-mass (m) only as done in the previous section. Otherwise, the form of this PBM is analogous to the single-variable form:

$$\frac{\partial \mathbf{N}(\mathbf{x},t)}{\partial t} + \nabla_x[\mathbf{r}(\mathbf{x},\mathbf{s})\mathbf{N}(\mathbf{x},t)] = -\Gamma(\mathbf{x},\mathbf{s})\mathbf{N}(\mathbf{x},t) - \mathbf{D}\mathbf{N}(\mathbf{x},t) + 2\int_{x}^{xmax} \mathbf{\Gamma}(\mathbf{x}',\mathbf{s})\mathbf{p}(\mathbf{x},\mathbf{x}',\mathbf{s})\mathbf{N}(\mathbf{x}',t)d\mathbf{x}' \quad (2.13)$$

Here, the variables used have the same meaning as mentioned before. D is the dilution rate and r(x,s) is the single cell growth rate.

Once again, the corresponding initial and boundary conditions may be specified as follows (Sidoli *et al*., 2004).

Initial Condition:

$$\mathbf{N}(\mathbf{x},0)=\mathbf{N_0}(\mathbf{x}) \quad (2.14)$$

Boundary Conditions:

$$\mathbf{r}(\mathbf{x},\mathbf{S})\mathbf{N}(\mathbf{x},t)=0 \qquad \forall \mathbf{x} \in \mathbf{B} \quad (2.15)$$

where, B represents the physiological state space boundary and at least one element of x is at its maximum or minimum value. The cell environment is considered as multi-component represented by a vector form s. The physiological state vector x has maximum (xmax) and minimum (xmin) states of daughter cells, and parent cells cannot divide unless in a minimum physiological state (xmin).

The equation for the substrate utilization- equation (2.16) has been taken from Liou and Fredrickson (1997) that applies PBMs to a CSTR setup. An extra term has been included to account for the effect of continuously fed and removed substrate in (2.16).

$$\frac{\partial \mathbf{N_1}(\mathbf{x},t)}{\partial t} = D(\mathbf{S_f} - \mathbf{S}) - \int_{xmin}^{xmax} \mathbf{q}(\mathbf{x},\mathbf{S})\mathbf{N}(\mathbf{x},t)dx \qquad (2.16)$$

where, q is a nutrient consumption vector.

The equation (2.16) is subject to the following initial conditions:

$$\mathbf{S}(0)=\mathbf{S}_0 \qquad (2.17)$$

(iii) A Multi-stage Multi-variable PBM

Unlike single stage PBMs that are based on the premise that cell life cycle is represented by one stage from birth to death, multistage PBMs divide the overall culture population into subpopulations based on a distinct classification of cell cycle phases. Thus each subpopulation is treated to be in a distinct phase of growth. Hatzis *et al.* (1995) illustrated the general structure and framework of a multivariable multi-staged PBM as follows.

$$\underset{\text{Accumulation1}}{\frac{\partial N_1(\mathbf{x},t)}{\partial t}} + \underset{\text{SingleCellGrowth1}}{\nabla_x[\mathbf{r_1}(\mathbf{x})N_1(\mathbf{x},t)]} = \underset{\text{Transition1}\to 2}{-\Gamma_1(\mathbf{x},t)N_1(\mathbf{x},t)} + \underset{\text{Birth}}{2\int \Gamma_3(\mathbf{x}')p(\mathbf{x}',t)N_3(\mathbf{x}',t)d\mathbf{x}'} \qquad (2.18)$$

$$\underset{\text{Accumulation2}}{\frac{\partial N_2(\mathbf{x},t)}{\partial t}} + \underset{\text{SingleCellGrowth2}}{\nabla_x[\mathbf{r}_2(\mathbf{x})N_2(\mathbf{x},t)]} = \underset{\text{Transition2}\to 3}{-\Gamma_2(\mathbf{x},t)N_2(\mathbf{x},t)} + \underset{\text{Transition1}\to 2}{\Gamma_1(\mathbf{x},t)N_1(\mathbf{x},t)} \qquad (2.19)$$

$$\underset{\text{Accumulation3}}{\frac{\partial N_3(\mathbf{x},t)}{\partial t}} + \underset{\text{SingleCellGrowth3}}{\nabla_x[\mathbf{r}_3(\mathbf{x})N_3(\mathbf{x},t)]} = \underset{\text{Division}}{-\Gamma_3(\mathbf{x},t)N_3(\mathbf{x},t)} + \underset{\text{Transition2}\to 3}{\Gamma_2(\mathbf{x},t)N_2(\mathbf{x},t)} \qquad (2.20)$$

Each equation in (2.18)-(2.20) provides a population balance for each cycle phase population N_i for 3 phase cycle, i.e., i=1…3. Since a 'constant environment' has been assumed, substrate concentration s does not feature in the model equations. Consequently, an equation for expressing the substrate utilization is not required in this case. The distribution of the cellular

properties at the phase transitions can either be measured directly and used to generate a histogram that can be used directly to describe the transition rate, or be approximated by a parametric distribution.

Irrespective of which approach is used the shape of the distribution will determine the transition rate. Also, the physiological functions r, Γ, and p are related to experimentally obtainable cell properties and can thus be determined from known experimental population data. This eliminates the need for simulating the behavior of a population based on assumed functions for single cell parameters (Tziampazis and Sambanis, 1994).

2.3.2.4 Combined Single Cell and Population Balance Models

Single cell models describe detailed intracellular structure but introduce no population heterogeneity. On the other hand, population Balance models emphasize characterization of overall cell population into subpopulations based on differences in growth phases of the cell cycle but fail to take into account intracellular detail. Thus combining the two models may help to address inaccuracies associated with either of the two approaches.

The single cell-population balance model developed by Sidoli *et al.* (2006) uses SCMs to describe growth and death mechanisms that appear as part of the bigger PBM.

2.3.3 Common Models Proposed for Antibody Production

Ultimately, the key motivation to improve cell culture Modelling is the need to optimize the system for achieving increased productivity. Since protein production is the ultimate goal of many cell culture operations, accurate quantitative descriptions of this process are important for simulation and optimization of product formation. For this, it is necessary to have predictive models relating the growth and death rates, and the specific rates of substrate consumption and product formation to the environmental state of the culture (Seamans and Hu, 1990).

Cell growth and death depend on the chemical composition of the medium and the age of the culture. As is evident from the vast amount of literature available, a lot of work has been done in this respect till date. This section focuses on the gradual development and improvement of models in cell process technology over the years.

An unsegregated, unstructured model for explaining growth and antibody production in hybridoma cultures was developed by Barford *et al*. (1992). Their work laid the foundation for more detailed and extensive models capturing cellular kinetics to a greater detail than had been done previously.

The model was unique in the sense that

(i) A detailed stoichiometry (for catabolic, anabolic reactions and their interactive effects) was included and was capable of explaining both continuous and fedbatch behavior.

(ii) A large number of nutrients were simulated through the model. The nutrients were clubbed into 6 groups that were then solved for. The reader is referred to Barford *et al.* (1992) for details.

(iii) The model was more extensive than previous models as it could simulate both fedbatch and continuous behavior.

Nutrient consumption rates were explained by Monod expressions and simple linear kinetics was used for internal metabolism.

A number of unstructured models for cell-specific antibody production have been compared by Portner and Schafer (1996) for hybridomas in chemostat cultures. Specific growth rate, substrate concentration, serum and death rate have all been proposed as being the variables on which productivity depends, although which of these should be used and to what extent productivity is sensitive to them is very much cell line dependent.

Table 2-1 that follows illustrates the common factors considered to model animal cell cultures. Most of the correlations for the specific growth rate are Monod type but differ in their choice of glucose or glutamine as the growth limiting substrate. Some models consider both of them as growth limiting species. Some models include additional terms to account for growth inhibition. Metabolites such as lactate and ammonia were found to be inhibitory or toxic for the system. Some models allow for the absence of cell growth at non-zero substrate concentrations by incorporating a 'threshold term'. In one particular case, serum has been included as a variable affecting specific growth rate. However, serum is subject to batch to batch variability and some of the components in serum cannot be accounted for. Consequently, there is a general tendency to work with serum-free media, which may eliminate the need to consider serum effects in any future models. Antibody production seems to follow non-growth associated kinetics, negatively growth-associated kinetics increased specific productivity (at reduced growth rates) or a combination of the two. Exceptions, however, exist.

Table 2-1: Correlations for the Specific Growth Rate and the Specific Death Rate adapted from (Portner and Schafer, 1996)

Serial No.	Specific Growth Rate	Specific Death Rate
1	$\mu_{max}\frac{Glc}{Glc+K_{Glc}}\frac{Gln}{Gln+K_{Gln}}$	$\frac{K_{d,max}}{(\mu_{max}-K_{d,Lac}Lac)(\mu_{max}-K_{d,Amm}Amm)}$
2	$\mu_{max}\frac{(\mu_{max}-\mu_{min})(Glc-Glc_{th})}{K_{Glc}+(Glc-Glc_{th})}\frac{Gln}{Gln+K_{Gln}}$	$(\mu_{min}-D_{min})-\frac{K_{d,max}(Glc-Glc_{th})}{K_d+(Glc-Glc_{th})}$
3	$\mu_{max}\frac{Gln}{Gln+K_{Gln}}\frac{K_{Amm}}{Amm+K_{Amm}}\frac{K_{Lac}}{Lac+K_{Lac}}$	$K_d\frac{K_{d,Gln}}{Gln+K_{d,Gln}}\frac{Amm}{Amm+K_{d,Amm}}\frac{Lac}{Lac+K_{d,Lac}}$
4	$\mu_{max}(Ser)\frac{Gln}{Gln+K_{Gln}}$	$K_{d,min}+(K_{d,max}-K_{d,min})\frac{K_d}{Gln+K_d}$

5	As a function of intracellular constituent pools	$K_d \frac{Amm}{Amm+K_{d,Amm}} \frac{Lac}{Lac+K_{d,Lac}}$
6	$D + d_0 e^{\frac{d1}{\mu}}$	$d_0 e^{\frac{d1}{\mu}}$

Non-segregated structured models have also been developed to describe product formation. Compartmental models describe the system as a set of distinct pools which may be defined either by location or by kinetic behavior. Interactions between compartments occur via unidirectional substance transfer, usually following first order kinetics with or without time delays (Noe and Delenick, 1989). Other types of kinetic equations, such as Michaelis-Menten, can be incorporated, notwithstanding increasing mathematical complexity. (Sambanis *et al.*, 1991) developed a model incorporating chemical and physical structure to describe intracellular protein trafficking and secretion in a pituitary cell line. Sanderson (1997) has been reported to have developed a structured, unsegregated, deterministic SCM for mammalian cells that may be applicable to any type of suspension culture. The model incorporates glycolysis, glutaminolysis, the TCA cycle, the pentose-phosphate pathway, and fatty and amino acid metabolism in addition to cell growth and death and antibody production into a compartmental form. There are three cell-related compartments: the medium, cytoplasm and mitochondria. The concentrations of some 49 biochemical components are modeled using Monod-type kinetics. The model accounts for the effects of feedback inhibition in certain reactions and competitive reactions by modifying the Michaelis–Menten expression. Transport equations account for membrane transport and link the various intracellular and extracellular concentrations. A simplified concentration driving force has been used to quantify flux. The model's practical accuracy is accessed by using certain experimental data set for model calibration and then performing a second experiment under different conditions and comparing the data with the model's simulation. The ratio of the difference (error) between measured and predicted concentration values of the reaction species provides an indication of the model's accuracy. The error lies in the range of 10% to

15%. Simulations for glutamine and antibody concentration, however, are significantly inaccurate.

Segregated models for mammalian cell cycle have been developed with population characterization based on differences in cellular activities, morphology, and even mechanical properties (Mitchison, 1971; Needham *et al.*, 1990; Ramirez and Mutharasan, 1990; Henderson *et al.*, 1992).

Segregated models can be enhanced by incorporating additional biological information to create models of higher structure. For example, the cell cycle theory can be combined with intracellular processes like the translation of messenger RNA (mRNA) to protein product (Suzuki and Ollis, 1990). There also exist cell cycle models that take into account the reportedly different antibody synthesis rates in each of the cell cycle phases (Garatun *et al.*, 1976; Liberti and Baglioni, 1973; Mitchison, 1971; Abraham *et al.*, 1976; Ramirez and Mutharasan, 1990). The advantage offered by these models is that no particular productivity function is needed. Instead, the productivity is described as a function of the population fractions in each cycle phase that are in turn dependent on the growth rate and can be described either with the aid of deterministic (Suzuki and Ollis, 1990) or stochastic models (Linardos *et al.*, 1992; Cazzador and Mariani, 1993). An underlying assumption made here is that the synthesis rate is constant in each cycle phase; the culture conditions affect only the viable cell number and the distribution of cells among the phases. The validity of this assumption probably depends on the particular system under consideration and the range of conditions employed.

2.4 Summary

From the above description it is evident that a structured, segregated, stochastic model is the ideal form of cell model. A major challenge presented by these models, however, is that they easily get so intensive computationally with increasing detail in the model that they cannot be easily handled by computers. Parameter and process lumping and timescale separation methods can be used as tool for providing the necessary simplifications. In the future, such

models could be further improved by incorporating new biological knowledge, which rapidly accumulates with the advent of new techniques, and by simplifying the final expressions so that the resulting descriptions remain computationally manageable.

Since currently available experimental data is limited, a compromise needs to be made on the level of detail incorporated into the proposed model to avoid over-parameterization and non-linearity in the model. Hence, an unstructured, segregated, deterministic model has been proposed. A systematic approach has been adopted for model development based on Metabolic Flux Analysis (MFA) proposed by Provost and Bastin (2004) that has been applied by Gao *et al*. (2006) with some modifications for batch production of MAb. However, in the mentioned works, in the development of the MFA and the resulting dynamic model of metabolites, the viable and dead cell concentrations and their corresponding rates of change have not been explicitly modeled. Instead, their experimental values have been used as an input for the metabolites model.

The current work addresses these issues as follows:

1. MFA is applied to a fed batch situation in order to obtain a dynamic model for this mode of operation. In this context, this study compares the flux values obtained in batch and fed batch operations and investigates whether the same structure of the dynamic model is applicable to both.
2. The viable and dead cell concentrations are explicitly modeled. Correlation analysis is used to investigate the dependencies of growth and death rates on nutrient and product concentrations. Then, the cell concentrations model is coupled to the metabolites dynamic model that utilizes experimental starting values to come up with an integrated model that predicts for all significant system variables, including viable and dead cell concentrations, independent of subsequent experimental values.

The dynamic metabolic model proposed is based on a combination of stoichiometric and dynamic mass balances and has been explained in detail in further sections. First,

stoichiometric flux balances based on a comprehensive metabolic network were constructed. Second, the metabolic network was simplified by systematic elimination of fluxes that were deemed insignificant.

The objective of the experimental and modelling efforts presented in the thesis is the identification of an accurate mathematical model that accounts for the heterogeneity in the cell population and predicts the optimum feeding profile for a fed-batch mode culture to enhance MAb productivity. Fluorescence imaging has been applied as a tool to capture the changes in cell morphology along the course of experimental batch runs to build on the model proposed in the current work. Identification of an active death process like apoptosis and the factors controlling it (as opposed to a passive one, i.e., necrosis) may lead to new strategies for the minimization of cell death during commercial animal cell culture. Ultimately, this may lead to substantial improvements in process efficiency. A switch from hybridoma to CHO cell cultures might lead to an appreciation of the differences in kinetics of the two cell lines, if there are any.

Chapter 3
Materials & Methods

A set of batch and fed-batch experiments were conducted using a hybridoma 130-8F cell line and a Chinese Hamster Ovary IgG1-9B8 cell line. The details of the experimental infrastructure and the experimental settings have been summarized in this chapter. The experimental techniques applied for analysis of the experimental samples have been covered as well.

3.1 Sources of Materials

Bellco, N.J., U.S.A.: 250 mL Bellco Spinners; 1000 mL Bellco Spinners

Corning *(from various locations)*: 75 cm^2 T-Flask

Invitrogen Canada Inc., Burlington, Ontario: Gibco D-MEM containing glutamine and glucose (12100), Gibco D-MEM w/o glutamine and glucose (23800), DMSO (Gibco 11101-011), D-MEM high Glucose (10566), Ham's F-12 Nutrient Mix (11765), L-Glutamine (25030), D-Glucose (15023)

JRH Biosciences - *A Division of* **Sigma-Aldrich Corp.** *(from various locations)*: Fetal Bovine Serum (FBS, JRH 12107-78P)

Nalgene *(from various locations)*: 1.8 ml cryovials

Sigma, Burlington or Oakville, ON: sodium hydrogen carbonate (S-5761), pluronic F68 (P-1300), insulin (I-6634), transferrin (T-1283), $FeSO_4$* (F-8633), $ZnSO_4$* (Z-0251), sodium pyruvate (P-5280), lipoic acid* (T-1395), biotin* (B-4639), putrescine* (P-5780), $CuS0_4$* (C-8027), cholesterol (C-8503), linoleic acid (L-1012), β-cyclodextrin (C-4805), proline (Sigma P-8449), 66 mg/L l-asparagine (Sigma A-4159), and 33.5 mg/L l-aspartic acid (Sigma A-4534), glutamine (Sigma G-8540) and glucose (Sigma G-6152), histidine (Sigma H-5659), threonine (Sigma T-8625), arginine (Sigma A-3784), tyrosine (Sigma T-3754), valine (Sigma V-0500), methionine (Sigma M-2893), tryptophan (Sigma T-0271), phenalanine (Aldrich 16,261-2), isoleucine (Sigma I-2952), leucine (Sigma L-1512), and

lysine (Sigma L-5626); Sigma Ammonia Kit (Sigma 171-B), Acridine Orange (Aldrich A6014), Ethidium Bromide (Aldrich E8751), Amino Acid Standard (AA-S-18)

VWR *(from various locations)* **-** SFX-CHO-GLN-GHT (CA16777) , Glass Slides and cover-slips: 3in.x1in.; 1mm thickness glass-slides and 25mm^2 cover-slips.

Caution: Acridine Orange and Ethidium Bromide have been found by the Ames test to be highly mutagenic and must be handled carefully.

3.2 Cell Line

The cell line, hybridoma 130-8F, used in this study was obtained from Sanofi Pasteur Ltd. Toronto, Ontario. The cell strain was produced by the fusion of Sp 2/0 myeloma cells with spleen cells from 12 to 20 week old immunized BALB/c mice (De Alwis Seneviratne, 2004).

The CHO cell line, IgG1-9B8, used for the second set of experiments involving fluorescence imaging was obtained from Cangene Corporation, Mississauga, Ontario. The cell line was produced as a result of modifications performed on another CHO cell line originally produced by ATCC.

In addition, seed-bank for two other cell lines was created. The first cell line was a hybridoma CRL-10463 obtained from ATCC. The other cell line was a CHO CRL-9606 also obtained from ATCC. CRL-9606 is a producer of human tissue plasminogen activator (t-pA). However, they were not utilized for experimental work because the focus was attached to the first two cell lines mentioned.

3.3 Media Formulation

3.3.1 Hybridoma 130-8F

The hybridoma cells were cultured in basal medium consisting of D-MEM containing 25 mmol/L glucose and 4 mmol/L L-glutamine. The medium was further supplemented with additional reagents that have been specified in Table 3-1 along with their final concentration in the medium (De Alwis Seneviratne, 2004).

Table 3-1: Supplements added to Basal Medium

Component	Concentration
Sodium hydrogen carbonate, $NaHCO_3$	2.2 g/L
PluronicF68	0.7 g/L
Insulin	9mg/L
Transferrin	5 mg/L
Zinc Sulphate, $ZnSO_4$*	0.86 mg/L
Sodium pyruvate	0.11 mg/L
Lipoic acid*	0.1 mg/L
Biotin*	0.1 mg/L
Putrescine*	0.161 mg/L
Copper Sulphate anhydrous, $CuS0_4$*	0.0025 mg/L
Cholesterol	0.5 mg/L
Linoleic acid	0.08 mg/L
ß-cyclodextrin	0.1 g/L
Proline	29 mg/L
L-asparagine	66 mg/L
L-aspartic acid	33.5 mg/L

Solutions marked with an asterix (*) were added from pre-made concentrate solutions.

It must be noted that amino acids originally present in the medium were taken into consideration when creating supplemented medium based feed solutions for fed-batch runs. For feed solutions, glutamine and glucose were added to "glutamine and glucose free basal

media" as required. Additional amino acids added to fed-batch feed medium have been specified in Table 3-2 that follows.

Table 3-2: Additional Amino-acids added to Feed Medium

Histidine	Tryptophan
Threonine	Phenalanine
Arginine	Isoleucine
Tyrosine	Leucine
Valine	Lysine
Methionine	

Basal medium from powdered DMEM was prepared by dissolving it in 18.0 mOhm-cm Milli-Q water. The resulting concentrate was diluted to the desired volume, pH equilibrated to 7.2 and, filtered through a 0.2 μm filter. Basal medium was stored at 4°C for a maximum of 3 weeks prior to use. Insulin was dissolved in 10 mL of Milli-Q water with the aid of a few drops of 2.0M HCl. Fetal Bovine Serum (FBS, JRH 12107-78P) was added prior to use on a per liter basis.

3.3.2 CHO IgG1-9B8

For CHO cells grown in serum free conditions, the basal medium used was HyQ-SFX CHO containing 17.5 mmol/L glucose but no glutamine; it was supplemented with glutamine upon use to be brought to a final concentration of 3 mmol/L glutamine. For CHO cells grown in serum supplemented conditions, the basal medium used was D-MEM containing 4mmol/L glutamine, 4500mg/L glucose, 1mmol/L sodium pyruvate and 1500 mg/L sodium bicarbonate. For both serum-supplemented and serum-free cultures, no amino-acid supplementation was done.

3.3.3 Hybridoma CRL-10463

The basal medium was D-MEM containing 4mmol/L glutamine, 4500mg/L glucose, 1mmol/L sodium pyruvate and 1500 mg/L sodium bicarbonate. For passaging cells, the basal medium was supplemented 10% v/v fetal bovine serum (FBS) but no amino-acid supplementation was done.

3.3.4 CHO CRL-9606

Ham's F-12 Nutrient Mix was utilized as the basal medium. It contained 4mmol/L glutamine, 4.5 g/L glucose. The culture medium contained 90% v/v basal media and 10% v/v fetal bovine serum (FBS). No amino-acid supplementation was done.

3.4 Pre-Experiment Protocols

All cultures were grown in a CO_2 incubator (Sanyo IR Sensor, 37 °C) at 8.0% CO_2 for hybridoma 130-8F and 5.0 % CO_2 for the other cell lines mentioned in section 3.3. In case of the hybridoma 130-8F, the culture pH was maintained in the range 7.1-7.4 by adding a solution of 7.5% $NaHSO_4$ as per requirements (De Alwis Seneviratne, 2004).

3.4.1 Developing a Cell Bank

3.4.1.1 Cell Bank for 130-8F

Cells for 130-8F were adapted to growth in 2% serum conditions over a period of two months prior to performing the actual experiments. It was observed that the reduction in serum did not result in a reduction of overall productivity or robustness of the cell-line. The cell bank was established using these adapted cells.

Cells in the late exponential growth phase (>90% viability) were centrifuged, re-suspended at a concentration of 30 x 10^6 cells/mL, and aliquoted into 100x1-1.8 mL cryovials. The vials were initially frozen at -80°C and half of the cell bank was transferred to liquid nitrogen storage. The cells used in subsequent experiments were obtained from the vials stored at -80°C (De Alwis Seneviratne, 2004).

3.4.1.2 Cell Bank for IgG1-9B8

One of the frozen vials received from Cangene was thawed upon arrival and transferred to a T-flask. The cells were passaged a number of times to ensure that they had adapted to the new culture environment. Cells in late exponential growth phase (>90% viability) were centrifuged, re-suspended at a concentration of 1.0 x 10^6 cells/mL, and aliquoted into 40x1-1.8 mL cryovials. The vials were initially frozen at -80°C for 24 hours and then transferred to liquid nitrogen storage. Two vials from the freeze-down were stored in the -80°C freezer as backup.

A supplementary cell bank of serum adapted cells for this cell line was also created. Cells in late exponential growth phase (>90% viability) were centrifuged, re-suspended at a concentration of 0.5 x 10^6 cells/mL, and aliquoted into 40x1-1.8 mL cryovials. The vials were initially frozen at -80°C for 24 hours and then transferred to liquid nitrogen storage.

3.4.1.3 Cell Bank for CRL-10463 and CRL-9606

For hybridoma CRL-10463, the frozen vial was thawed and the contents of the vial were transferred to a T-flask. The vial for CHO CRL-9606 cell was received from ATCC and was thawed upon arrival and its contents transferred to a flask.

Thereafter, the procedure for the two cell lines was the same. The cells were passaged a number of times to ensure that they had adapted to the culture environment. Cells in late exponential growth phase (>90% viability) were centrifuged, re-suspended at a concentration of 10^7cells/mL for CRL-10463 and 4x10^6 cells/ml for CRL-9606, and aliquoted into 40x1-1.2 mL cryovials. The vials were initially frozen at -80°C for 24 hours and then transferred to liquid nitrogen storage. Two vials from the freeze-down for each of the cell lines were stored in the -80°C freezer as backup but were lost due to a freezer malfunction.

For freezing down a cell bank, the composition of the freezing medium is as described in Table 3-3.

Table 3-3: Freezing Medium

Component	% Concentration for 130-8F	% Concentration for IgG1-9B8	% Concentration for CRL-10463	% Concentration for CRL-9606
Fresh culture medium, i.e., the basal medium	80	45	80	80
Spent cell culture medium	0	45	0	0
DMSO	10	10	10	10
Serum	10	0	10	10

3.4.2 Initiation of Cell Culture from Thawed Vials

Cell culture was initiated by thawing a cryovial in a 37°C water bath for under 2 minutes.

3.4.2.1 Hybridoma 130-8F

The contents of the thawed vial were suspended in 10mL of fresh media, centrifuged for 4 minutes at 1000 rpm. The supernatant was removed in order to eliminate DMSO that may inhibit cell growth to some extent. The cell pellet was resuspended in a 75 cm^2 T-Flask containing 21mL fresh media with 15% (or 10%) serum. The T-flasks were incubated for two to three days (depending on the rate of cell growth) before passaging (De Alwis Seneviratne, 2004).

3.4.2.1.1 Serum Reduction

The hybridoma cells were grown in serum containing medium. Cells were passaged every two days during the week and every three days if it was a weekend, i.e., a Monday, Wednesday, and Friday. At high serum concentrations some cell attachment was observed on the bottom of the flask. Cells were detached by sharp tapping. The T-flasks were repeatedly

monitored under a microscope to ensure that almost all the cells had detached from the surface of the flask. If the attachment of cells to the surface still persisted, the flask was tapped a few more times. Cell concentration and viability were determined and cells were further passaged using an inoculation density of 0.1 x 10^6 cells/ml. The serum concentration was gradually decreased as outlined in Table 3-4. Once the cells reached 2% serum conditions, it was observed that cell attachment was considerably less. At least two weeks were required from initial thaw to the commencement of experiments the details of which have been covered in later sections. The cells were grown in suspension using spinners for two or three consecutive passages prior to the start of the batch and fed-batch experiments.

Table 3-4: Procedure for Serum Reduction

(De Alwis Seneviratne, 2004)

Passage	Percentage Serum
1	15 (10)
2	10 (7.5)
3	7.5 (5)
4	5 (3.5)
5	3.5 (2)
6	2 (2)
7	2 (2)

3.4.2.2 CHO IgG1-9B8

The contents of the thawed vial were suspended in 5 ml fresh medium containing 3mmol/L glutamine and 17.5 mmol/L glucose. The T-Flask was incubated for a day (depending on the rate of cell growth) before passaging. After the cell density was appreciably high, the cells were passaged to a higher volume of 20 ml. This diluted the DMSO present to an insignificant concentration. Thereafter, the T-flasks were incubated for two to three days

(depending on the rate of cell growth) before passaging. The glutamine concentration was gradually reduced to 2 mmol/L for performing spinner experiments.

3.5 Experiments

The first set of experiments that was utilized for model development was performed at the Sanofi Pasteur facilities at Sunnybrook Health Sciences Centre with a hybridoma cell line. Two different modes of reactor operation were adopted: batch culture (3 to 9 days) and fed batch culture (>7 days duration) and were carried out in 250 mL and 1000 mL spinners.
The second set of batch experiments was performed at the University of Waterloo as part of efforts to generate fluorescence images along the course of the run to gain an understanding of the incidence of apoptosis. The cell line utilized was a CHO cell line (De Alwis Seneviratne, 2004).

3.5.1 Batch Experiments- Set 1

Batch experiments (se Set 1, Batch Experiment in Appendix A) were performed in 250 mL and 1 L spinners inoculated with 0.1 x 10^6 cells/mL to start with. The same spinners were re-inoculated by replacing spent media with fresh media again every 3 days, two times in a row before the start of the experiment (i.e., 2 passages prior to start of experiment). Spinners were stored at random positions in two incubators at 37.0 ºC and 8.0 % CO_2. The starting basal medium waș MDMEM with 4mmol/L Glutamine, 25 mmol/L Glucose, 2% FBS.

Samples of 1-3 mL volume were taken daily and analyzed for viable cell concentration, percent viability, and pH. Thereafter, samples were sent for analysis for total mouse IgG assay by ELISA and amino acid analysis by HPLC. Cell concentration and viability were determined using a haemocytometer and 0.5% trypan blue in PBS diluted to a ratio of 1:1.

3.5.2 Fed-batch Experiments- Set 1

Fed-batch experiments (see Set 1, Fed-batch Experiment in Appendix A) were performed in 500 mL spinners inoculated with 0.1 x 106 cells/mL in 300 mL medium to start with. The experiment duration was 8 days. Initial volume of the culture was 300 mL with 4 mmol/L

glutamine and 25 mmol/L glucose. The starting basal medium taken was MDMEM containing 2% FBS without glutamine and glucose.

For the fed-batch experiment, the ratio of glutamine to glucose in the feed was kept at 0.32 while the glutamine concentration was 4mM in one spinner and 2mM in the other. After initial sampling, the spinners were left in the incubator undisturbed for about 20 hours. Thereafter, samples were taken regularly for analysis of viable cell concentration, percent viability, pH, total antibody titre, and amino acid composition. Samples were taken every 3 hours during the day and every 12 hours overnight. Sample volume of 0.5 mL was taken for glucose and glutamine concentration analysis and cell viability analysis; 1.5 mL for pH analysis. Sample volumes were replaced with fresh medium containing 4 mmol/L glutamine, 25 mmol/L glucose, and 2% serum. The feeding schedule was adjusted over the course of the study from 4-hour to 6-hour schedules. Since fed batch experiments ran the duration of at least seven days, 8 to 12-hour periods of 'night-time non-feeding' occurred. When possible, these periods were minimized.

Also, aliquots of a 1 mL sample were taken for cell count and in/out lab sample retention. Cell concentration and viability were determined by Trypan Blue dye exclusion test using a hemacytometer. Aliquots were frozen at -80°C to be sent out of the lab for total mouse IgG assay by ELISA and amino acid analysis by HPLC.

Once fed batch feeding commenced after 60 hours, sample volumes removed from fed batch spinners were not replaced. 7.5 % $NaHCO_3$ was added for any necessary pH adjustments during the experiment (pH was maintained between 7.1-7.3). The experiment was terminated after 194 hrs.

3.5.3 Batch Experiments- Set 2

Batch experiments (see Set 2, Batch Experiment in Appendix A) were performed in spinners: 2x1-100 and 2x1-250 mL spinners inoculated with 0.3 x 10^6 cells/mL inoculum. Spinners were stored at random positions in two incubators at 37.0 °C and 5.0 % CO_2.

The starting basal medium was HyQ SFX-CHO with 17.5 mmol/L glucose in all spinners while the glutamine concentration was 4 mmol/L for 1x100 ml spinner and 3 mmol/L glutamine in the rest of the spinners. The cultures were grown in serum free conditions.

Samples of 1 mL and 0.6 ml volume were taken daily and analyzed immediately for viable cell concentration, percent viability, glucose and fluorescence imaging. Thereafter, eppendorfs were centrifuged at 1000rpm for 5 minutes and the culture supernatant was removed and transferred to new eppendorfs and frozen at -30˚C. The samples were kept in a frozen state for further analysis- ammonia analysis using an ammonia meter, total mouse IgG assay by ELISA, amino acid analysis by HPLC. Cell concentration and viability were determined using a haemocytometer and 0.5% trypan blue in PBS diluted to a ratio of 1:1. Fluorescence images were generated by adding 10 µL of a fluorescent dye-mix (Acridine Orange and Ethidium Bromide, mixed together to a final concentration of 50 µg/ml) and added to 250 µL of cell suspension in an eppendorf. The sample was allowed to stand for 1 minute after which a glass slide was stained with 10 µL of the fluorescent sample and images were generated with the use of the imaging software- Image-J.

3.6 Analytical Methods

3.6.1 Viable Cell Concentration

Total cell concentration and viability were determined via the Trypan Blue Exclusion Test using a hemacytometer and a 1:1 dilution with 0.5% trypan blue in PBS. Cell count was made within one minute of dye addition, and within 30 minutes of sampling. The percent viability was determined as a ratio of the number of non-stained i.e., viable cells counted to the total number of cells counted i.e., stained+non-stained.

3.6.2 Substrate Concentration(s)

3.6.2.1 Hybridoma 130-8F

Samples were centrifuged for 4 minutes at 1000 rpm to remove cells. Measurements for substrate concentrations were recorded and the sample was further aliquoted and stored at -80°C for out of lab analysis. The maximum storage time was approximated 1 month.

Glucose, lactate, glutamine, and glutamate concentration was quantified using two YSI Biochemistry Analysers. The detection ranges for each respective substance is summarized in Table 3-5. A fresh 5 mmol/L calibration standard for glutamine was prepared daily. Samples outside this range were diluted with sterile Milli-Q water.

Table 3-5: Detection Range for YSI Bioanalyser

(De Alwis Seneviratne, 2004)

Chemical	Detection Range
D-Glucose	0-25 g/L
L-Lactate	0-2.67 g/L
L-Glutamine	0-8 mmol/L
L-Glutamate	0-10 mmol/L

3.6.2.2 CHO IgG1-9B8

Measurements for glucose concentration were recorded using an Ascensia Contour glucose meter and the samples were centrifuged for 5 minutes at 1000 rpm to remove cells. The sample was further aliquoted and stored at -30°C for further analysis.

3.6.3 Ammonia Assay

For set-1 of experiments, diluted samples (1:10 with Milli-Q water) were stored either at -80ºC or 4ºC (< 1 week) and tested for ammonia content using a Sigma Ammonia Kit (Sigma 171-B).

For set-2 of experiments, acidified samples (with phosphoric acid) were stored at -30ºC and tested for levels of ammonia using an Orion ammonia meter. Fresh standards for calibration of ammonia meter were prepared daily.

3.6.4 Out-of-lab Analysis for Samples from Set-1 Experiments

Samples of volume between 0.2-1.0 mL of supernatant were aliquoted and stored at -80ºC prior to being sent for analysis for monoclonal antibodies and amino acid assay (De Alwis Seneviratne, 2004).

3.6.4.1 Monoclonal Antibody Assay

Total IgG titre or monoclonal antibody concentration was determined using the competitive Enzyme Linked ImmunoSorbent Assay (ELISA). The assay was carried out by the Research Microbiology Group at Aventis Pasteur Ltd. The assay involves standard ELISA techniques.

3.6.4.2 Amino Acid Assay

Amino Acids were assayed using High Performance Liquid Chromatography (HPLC, Agilent 1100 Series, Hypersil AA-ODS column). Analysis was carried out by the Process Development Formulations & Stability Platform of Aventis Pasteur Ltd. Samples were run in groups according to each cell culture growth run. The samples were filter centrifuged in Millipore Microcon YM-10 and microcentrifuged for 15 minutes at 8000 rpm to deproteinize the cell culture media. The filtrate was further diluted as required. Twenty amino acids, listed in Table 3-6, in deproteinized cell culture media were quantified using an automated a two step precolumn derivatization method for reverse phase HPLC analysis with fluorescence detection. The two step pre-column derivatization reaction occured first with OPA (o-phthaldehyde and 3-mercaptopropionic acid in borate buffer, Agilent 5061-3335), which

reacts with primary amino acids; and then with FMOC (9- fluorenylmethylchloroformate in acetonitrile, Agilent 5061-3337), which reacts with secondary amino acids. The OPA derivatives elute chromatographically before the FMOC derivatives.

Table 3-6: Amino Acids Quantified in Assay

ASP	Aspartic Acid	**TYR**	Tyrosine
GLU	Glutamic Acid	**CYS**	Cystine
ASN	Asparagine	**VAL**	Valine
SER	Serine	**MET**	Methionine
GLN	Glutamine	**TRP**	Tryptophan
HIS	Histidine	**PHE**	Phenylalanine
GLY	Glycine	**ILE**	Isoleucine
THR	Threonine	**LEU**	Leucine
ALA	Alanine	**LYS**	Lysine
ARG	Arginine	**PRO**	Proline

3.6.5 Fluorescence Imaging

3.6.5.1 Protocol

Basic Protocol has been adapted from Coligan (1994) and the work of Mercille and Massie (1994). According to this assay, a cell suspension is mixed with fluorescent DNA-binding dyes and the sample is then observed under a fluorescence microscope to examine chromatin organization. 100µg/ml Acridine Orange (AO) and 100 µg/ml Ethidium Bromide (EB) are mixed in a ratio of 1:1. 10 µl of this dye mixture is added to 250 µl of cell suspension having cell concentration in the range $5x10^5$ to $6x10^6$ cells/ml in an eppendorf that is then allowed to stand for a minute. 10 µl of the sample is then placed on a glass slide and covered with a

cover-slip. The specimen is examined under a fluorescence microscope (Coligan, 1994; Mercille and Massie, 1994; Wyllie, 2004).

3.6.5.2 Instrument Settings

Microscope used: Zeiss Axiovert 200 with eppiilumination.

Objective lens: Nikon 40X Plan Neofluar with numerical aperture 0.75.

Digital Camera: Sony, Model No.XCD-X700; DC8-30V

Filter settings: as specified in Table 3-7 below.

Table 3-7: Filter Specification for Fluorescence Imaging

Filter set	Fluorochrome	Excitation	Beam Splitter	Emission
Blue Filter	Acridine Orange (both DNA and RNA)	475-495 nm	510 nm	515-565 nm
Red Filter	Ethidium Bromide	515-560 nm	565 nm	580-630 nm

3.6.5.3 Image Processing

The images captured by the available set-up were gray-scale images and needed to be processed to colored images by a software called Image-J. Image-J is a public domain, Java-based image processing program that can open and save all supported data types as TIFF (uncompressed) or as raw data. It is capable of opening and saving GIF, JPEG, BMP, PNG, PGM, FITS and ASCII, DICOM, TIFFs, GIFs, JPEGs, DICOMs and raw data using a URL and many other formats using plugins (http://rsb.info.nih.gov/ij/features.html).

3.6.5.4 Assays for Identification of Apoptosis and Necrosis

Before progressing to the classification of cells in regular cell culture, it is imperative to be able to independently identify apoptosis and necrosis. In order to do so, assays for apoptosis and necrosis were performed whereby apoptosis and necrosis was induced in a cell culture in the exponential phase of growth.

(i) Induction of Apoptosis

For the induction of apoptosis, the protein synthesis inhibitor cycloheximide was added. Cycloheximide was added at a final concentration of 25 μg/ml to a T-75 flask containing over $1x10^6$ cells/ml. The flask was then incubated in a CO_2 incubator at 37 ˚C. Images were taken after addition of the mentioned reagents and incubation overnight.

(ii) Induction of Necrosis

Although several different methods have been suggested for the induction of necrosis by artificial means in a cell culture (Mercille and Massie, 1994), the easiest method was considered for application. For induction of necrosis, 25 % v/v HPLC grade ethanol was added to a T-75 culture flask with cells at a concentration of over $0.6x10^6$ cells/ml and viability equal to 98%. The flask was then incubated in a CO_2 incubator at 37 ˚C. After overnight incubation, the flask was tested for necrotic morphology every few hours for the next day since it was not known for certain what the time span for induction of necrosis was using this approach. 24 hours after incubation, all cells were necrotic; the Trypan Blue exclusion test confirmed this.

Chapter 4
Model Development

The importance of model development has been highlighted in the literature review section. In this section, the exercise of model development and the mathematical concept behind it have been explained.

The large-scale production of MAb by mammalian cells in batch and fed-batch culture systems is limited by the unwanted decline in cell viability and reduced productivity that may result from changes in culture conditions. Therefore, it becomes imperative to gain an in-depth knowledge of the factors affecting cell viability and subsequently antibody production. Although considerable effort has been made to understand the kinetics of hybridoma growth and metabolism, it has become evident that a model structure is not a priori obvious. A common limitation of the currently available models is that they focus on individual characterization of selected aspects of the overall cell metabolism (exponential or post-exponential).

The aim of the present work is to obtain an overall dynamic model that predicts the behaviour of both batch and fed-batch systems as a function of the extra-cellular nutrient/metabolite concentration at any time and utilize this model for optimization of MAb production in the future. A systematic approach has been adopted for model development based on Metabolic Flux Analysis (MFA) for animal cell culture proposed by Provost and Bastin (2004) that has been applied by Gao *et al.* (2006) with some modifications for batch production of MAb. However, in the development of the MFA and the resulting dynamic model of metabolites, the viable and dead cell concentrations and their corresponding rates of change have not been explicitly modeled. Instead, their experimental values have been used as an input for the metabolites model.

The current work addresses these issues as follows:

1. MFA has been applied to a fed batch situation in order to obtain a dynamic model for this mode of operation. In this context, this study compares the flux values obtained in batch and fed batch operations and investigates whether the same structure of the dynamic model is applicable to both.
2. The viable and dead cell concentrations are explicitly modeled. Correlation analysis is used to investigate the dependencies of growth and death rates on nutrient and product concentrations. Then, the cell concentration model is coupled to the dynamic model for metabolites that utilizes experimental starting values to come up with an integrated model that predicts for all significant system variables, including viable and dead cell concentrations, independent of subsequent experimental values.

The dynamic metabolic model proposed here is based on a combination of stoichiometric and dynamic mass balances as is explained in detail in further sections. First, stoichiometric flux balances based on a comprehensive metabolic network are constructed. Second, the metabolic network is simplified by systematic elimination of fluxes that are deemed insignificant.

4.1 Metabolic Flux Analysis (MFA):

4.1.1 Theory

A powerful methodology for the determination of significant metabolic pathways is MFA, whereby intracellular fluxes are calculated by utilizing a stoichiometric model for the major intracellular reactions and applying mass balances around intracellular metabolites (Papoutsakis and Lee, 1999). The final outcome of flux calculation is a metabolic flux network representing the biochemical reactions included in the calculation along with an estimate of the steady state rates, referred to as the fluxes, at which the reactions occur. Thus, MFA permits to calculate values of intracellular fluxes from available extracellular fluxes, some of which are significant and some are negligible. Based on the set of the most significant fluxes, the original metabolic network can be reduced to contain only the reactions corresponding to significant fluxes. The reactions in the reduced network are further used to formulate a set of elementary macro- reactions linking the substrates to the products, thus eliminating involvement of intracellular metabolite concentrations in the mathematical model. A set of dynamic mass balances is then devised that involves rate expressions for the consumption/ production of substrates/ metabolites.

Furthermore, MFA provides additional information on the following aspects (Papoutsakis and Lee, 1999):

(i) Identification of Alternative Pathways:

Often the actual biochemical route by which a substrate is converted into products is not evident as there are many alternate pathways available for the conversion to take place. MFA is important in identifying pathways that can reproduce the macroscopic flux measurements of extracellular metabolites equally well and eliminate alternate pathways that are not possible because of their inability to satisfy material balances.

(ii) Calculation of Non-measured Extracellular Fluxes:

In case of under-determined systems, where the number of extracellular measurements available is less than what is required to calculate intracellular fluxes, we can still compute their values by applying the stoichiometric model proposed under MFA approach.

(iii) Calculation of Maximum Theoretical Yields:

Although a*d hoc* theoretical yield determination is possible and is often performed; however, in complex metabolite networks MFA provides a more formalized approach.

4.1.2 Metabolic Network for Hybridoma Cells

The starting point of MFA is obtaining the reaction network stoichiometries describing the conversion of substrates into metabolic products and biomass constituents (or macromolecular pools). The overall metabolic network for hybridoma has been taken from (Gao *et al.*, 2006) and is shown in Figure 4-1. This figure represents the system under study and accounts for all the major energy producing pathways in hybridoma, namely the TCA cycle, Embden-Meyerhoff Fermentative pathway, Glutaminolysis and Respiration that produce both energy and precursors for biosynthesis (Barford *et al.*, 1992). A key component of the metabolic network is the TCA cycle or Citric Acid cycle that is involved in the catabolism of all three major food groups: carbohydrates, lipids and proteins. As Figure 4-1 illustrates, the complete reaction network involves m(=30) metabolites and n(=32) fluxes corresponding to 32 reactions.

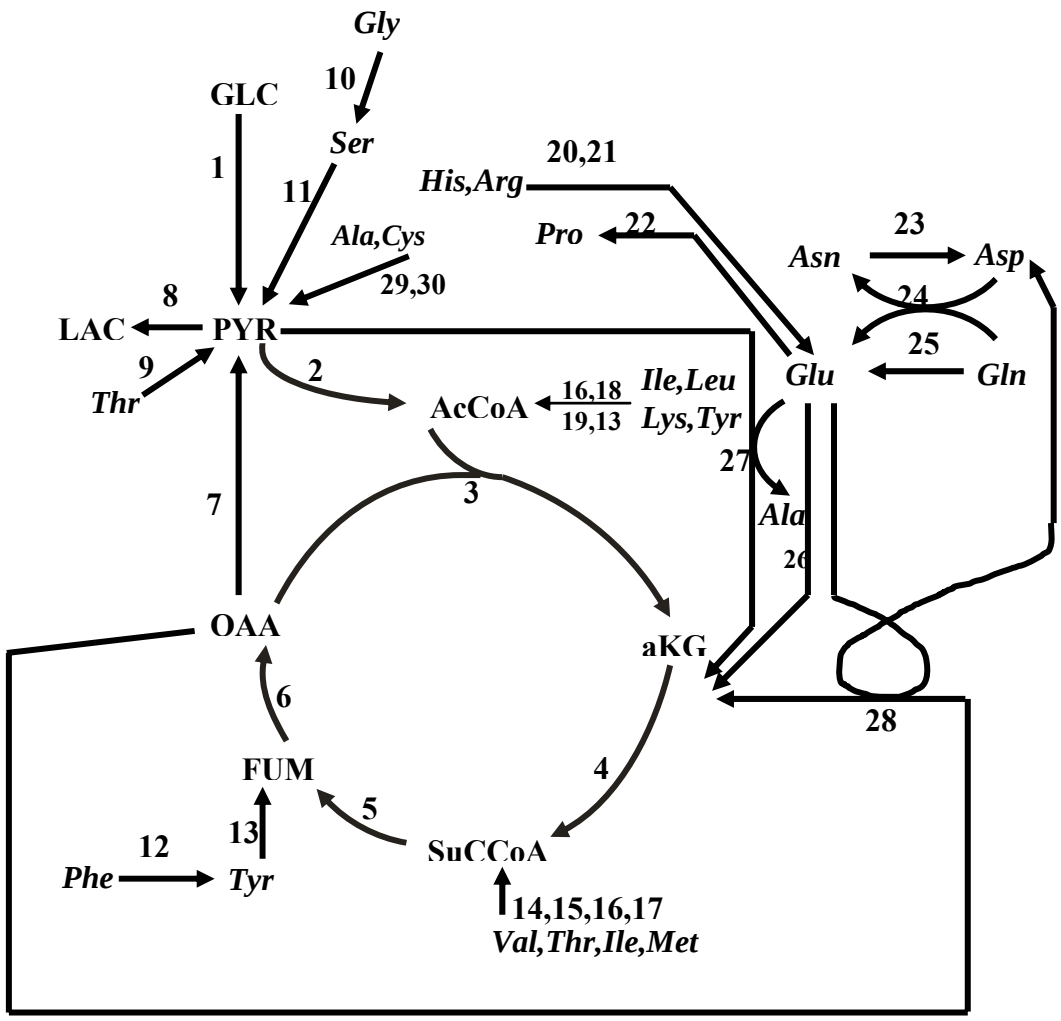

Figure 4-1 Simplified Metabolic Network of Hybridoma Cells adapted from (Gao *et al.* 2006)

The reactions corresponding to the metabolic flux network are given in Table 4-1.

Table 4-1: List of Stoichiometric Equations

ji. (i=1,2,…,32)	**Reaction**
j1.	GLC→ 2PYR + 2NADH + 2ATP

j2. PYR→ AcCoA + CO2+NADH

j3. AcCoA + OAA→ aKG + NADH + CO2

j4. aKG→ SuCCoA+ NADH + CO2

j5. SuCCoA→ FUM + NADH

j6. FUM→ OAA + NADH

j7. OAA→ PYR + NADPH + CO2

j8. PYR + NADH→ LAC

j9. THR→ PYR + CO_2 + NH_3 + 2NADH

j10. 2GLY→ SER+CO_2+NH_3 + NADH

j11. SER→ PYR+NH_3

j12. PHE→ TYR + NADH

j13. TYR→ FUM + 2AcCoA + NH_3 + CO_2 + NADPH

j14. VAL→ SuCCoA + CO_2 + NH_3 + NADPH

j15. THR→ SuCCoA + NH_3

j16. ILE→ SuCCoA + AcCoA + NADPH + NH_3

j17. MET + O2→ SuCCoA + SO2 + NADPH + NH_3

j18. LEU→ NH3 + 3AcCoA + NADPH

j19. LYS→ 2 AcCoA + 2CO_2 + 2NADPH + 2NH_3

j20. HIS→ GLU+2NH3+CO_2

j21. ARG→ aKG + 2NH_3 + UREA + 3 NADH

j22. GLU + ATP + 2 NADPH→ PRO

j23. ASN→ ASP + ATP + NH_3

j24. GLN + ASP + 2 ATP→ ASN + GLU

j25. $GLN \rightarrow GLU + ATP + NH_3$

j26. $GLU \rightarrow AKG + NADPH + NH_3$

j27. $PYR + GLU \rightarrow ALA + AKG$

j28. $GLU + OAA \rightarrow ASP + AKG$

j29. $CYS + O_2 \rightarrow PYR + SO_2 + NADH + NH_3$

j30. $ALA \rightarrow PYR + NADH + NH_3$

j31. 0.0508GLC +0.0577GLN +0.0133ALA +0.007ARG +0.006ASN
+0.020lASP +0.0004CYS +0.0016GLU +0.0165GLY +0.0033HIS
+0.0084ILE +0.0133LEU +0.0101LYS +0.0033MET +0.0055PHE
+0.0081PRO +0.0099SER+0.008THR+0.004TYR+0.0096VAL→BIOMASS

j32. 0.0104GLN +0.011ALA +0.005ARG +0.0072ASN +0.0082ASP
+0.005CYS +0.0107GLU +0.0145GLY +0.0035HIS +0.005ILE
+0.0142LEU +0.0145LYS +0.0028MET +0.0072PHE +0.0148PRO
+0.0267SER +0.0160THR +0.0085TYR +0.0189VAL→ MAb

4.1.3 Calculation of Conversion Rates and Fluxes

Mass balances for the intracellular and extracellular metabolites involved in the system can be represented as follows:

$$\frac{d\boldsymbol{\psi}(t)}{dt} = \mathbf{R}X_V(t) \qquad (4.1)$$

where $\boldsymbol{\psi}$ is the vector of intracellular and extracellular metabolite concentrations and t is the culture time. **R** is the vector of specific uptake/production rate of substrates/metabolites. $X_v(t)$ is the viable cell concentration and is a function of culture time, t. Here, an assumption of balanced growth condition has been made. This implies that the system is at a quasi-steady state and consequently the net conversion rate of all intracellular metabolites is equal to zero.

This is a common assumption made in the literature for this type of flux analysis (Provost and Bastin, 2004).

Upon integration of equation (4.1) and assuming an average value of R over the integration interval:

$$\int_0^t d\psi(t) = \int_0^t \mathbf{R} dX_v(t) \qquad (4.2)$$

$$\Rightarrow \quad \psi_t - \psi_0 = \mathbf{R}(CH_t - CH_0) \qquad (4.3)$$

CH is referred to as the cumulative volumetric cell hours (Dutton *et al.*, 1998) and can be mathematically expressed as:

$$CH = \int_0^t X_v(t)dt \qquad (4.4)$$

The integral expression in equation 4.4 can be approximated by an algebraic expression as shown by Dutton *et al.* (1998):

$$CH = \sum_0^t \frac{\left(X_{v_{t+\Delta t}} - X_{v_t}\right)}{\ln\left(\frac{X_{v_{t+\Delta t}}}{X_{v_t}}\right)} \times \left(t_{t+\Delta t} - t_t\right) \qquad (4.5)$$

where X_v is the viable cell concentration and t is the culture time.

The use of the cumulative volumetric cell hours allows for an assessment of productivity and biological capacity for production on the same cumulative basis (Dutton *et al.*, 1998).

R is calculated from linear regression between measured concentrations of metabolites and volumetric cell hours (CH) based on equation (4.3). The need for concentration measurements for intracellular metabolites is eliminated by assuming that the system operates under balanced growth conditions and consequently, the reaction rates corresponding to intracellular

metabolites(1 to 6 according to the numerical designation given in Figure 4-1) are assumed to be equal to zero (Provost and Bastin, 2004; Gambhir *et al.*, 2003).

The growth curve for batch or fed-batch run has been broadly divided into two phases: exponential and post-exponential. Essentially, all data points corresponding to the peak viable cell density and before are part of the exponential phase. Conversely, the data points from the peak viable cell density and beyond constitute the post-exponential phase. This is schematically shown in Figure 4-2(a).

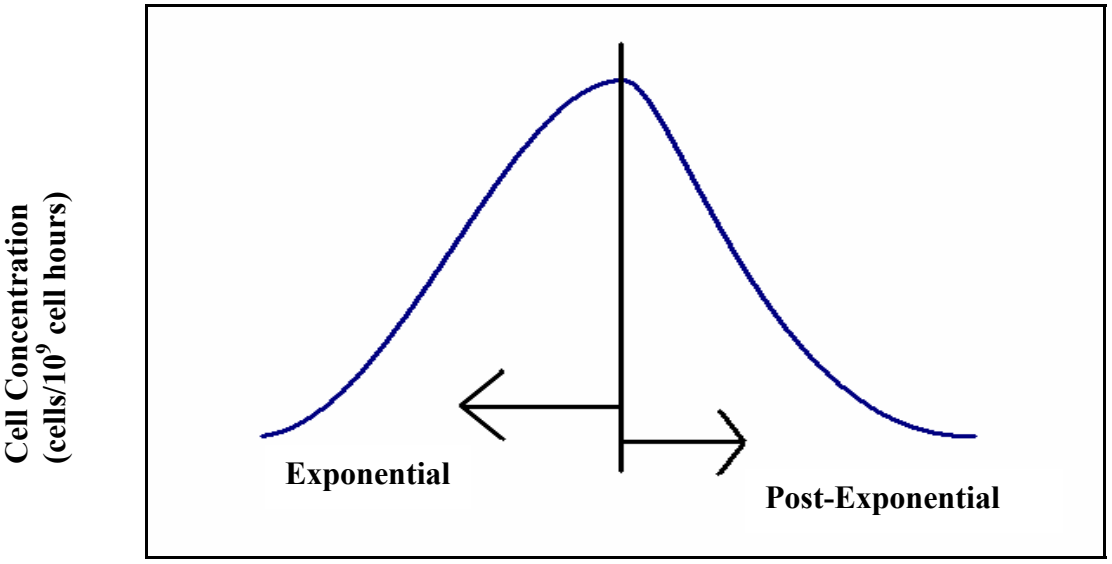

(a)

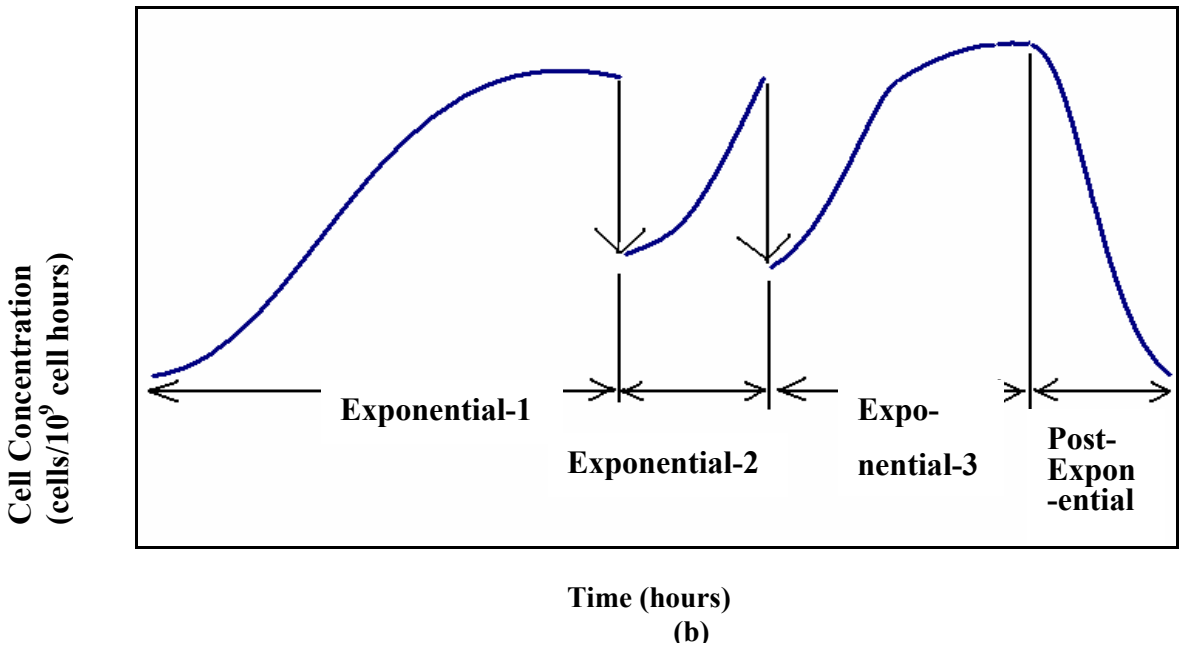

Figure 4-2 Division into Phases for Calculation of R for (a) Batch Run and (b) Fed-batch Run, respectively

The division into various growth phases requires special attention for fed-batch culture as addition of feed at several instances during the run caused abrupt drop in biomass concentration. The separation of data into intervals was done as shown in Figure 4-2(b) by classifying all time intervals immediately after a feed addition as exponential and the point in time where the viable cell concentration started to fall was considered as the beginning of the post-exponential phase. In the experiments under study, there were 10 successive exponential phases followed by a post-exponential phase. Thus, an average R value was calculated for the exponential phase, one for the post-exponential phase and another for the overall experiment.

Under the assumption of quasi-steady state, the conversion or production rate, R(m) of a nutrient or metabolite in a biological system can be expressed as (Bonarius *et al*., 1996):

$$\mathbf{R}(m) = \sum_i \alpha_{i,m} j_i \qquad (4.6)$$

where **R** is the uptake or production rate of metabolite m (=1,2,…M) in reaction i (=1,2,…N). $\alpha_{i,m}$ is the stoichiometric coefficient for metabolite m in reaction i. $\alpha_{i,m}$ has a negative value for substrates that get consumed and is positive for metabolites that are produced. j_i is the intracellular flux for reaction i. In matrix notation, equation (4.6) may be written as:

$$\mathbf{R}=\mathbf{Aj} \qquad (4.7)$$

where **R** is the vector of average uptake or production rates, **j** is the vector of all intracellular and extracellular species fluxes and **A** is the matrix of stoichiometric coefficients of the corresponding reaction species involved in the system metabolic network as shown in Figure 4-1.

$$\mathbf{A}=\{\alpha_{i,m}\}_{i=1,2,\ldots N;\ m=1,2,\ldots M} \qquad (4.8)$$

In the case under study, N=32 and M=28.

Referring back to system of equations in (4.7), experimental data was available to determine values of the vector **R** while the expression for the stoichiometric matrix **A** was be extracted from the reaction scheme in Figure 4-1. Thus, values for the flux vector **j** were easily determined using regression under the Quadratic Programming approach.

$$\text{Min}\left(\mathbf{R}-\mathbf{Aj}\right)^{\mathrm{T}}\left(\mathbf{R}-\mathbf{Aj}\right) \qquad (4.9)$$

Now, it must be remembered that only 28 extracellular and intracellular measurements were known using which 32 flux values needed to be determined. Henceforth, the system of equations was underdetermined i.e., less equations than unknowns. Among the unknown quantities were concentrations for cystine and ammonia. Fortunately, a unique solution for the system was possible by imposing additional constraints on the system. These additional constraints were based on the assumption that all reactions should proceed in the direction

indicated in the metabolic flux network shown in Figure 4-1. This implies that all fluxes will have values at least greater than or equal to zero. Since there were 32 unknowns with 28 equations, a unique solution is assured as long as the number of active constraints in the solution of the QP is greater than or equal to four. All the solutions found in the current work satisfied this criterion. Also, since cystine measurements were not available, its consumption rate was taken to be equal to zero as opposed to being excluded, because otherwise, a physically unrealistic flux distribution was obtained as solution, i.e. the flux corresponding to cystine consumption was unusually high.

The metabolic flux analysis presented above is strongly based on averaged measured consumption and production rates of extracellular metabolites. Consequently, it is expected that the measurement experimental noise will surely affect the calculated flux distribution. In order to reduce sensitivity to noise, experimental values of **R** for a number of batches or for measured values of **R** at different times during the run in case of a fed-batch experiment were considered together to conduct the QP regression proposed above. For example, if s sets of experimental batches are considered, the augmented system of equations may be expressed as follows.

$$\begin{bmatrix} \mathbf{R_{set1}} \\ \vdots \\ \mathbf{R_{sets}} \end{bmatrix}_{sMx1} = \begin{bmatrix} \mathbf{A} \\ \vdots \\ \mathbf{A} \end{bmatrix}_{sMxN} \qquad (4.10)$$

$$\Rightarrow \mathbf{R_{mod}} = \mathbf{A_{mod}}\mathbf{j}$$

s: is the number of batches/sections considered in a fedbatch experiment.

Then, a solution for the resulting over-determined system of equations given by (8) can be obtained from the following minimization problem:

$$\text{Min}(\mathbf{R_{mod}} - \mathbf{A_{mod}}\mathbf{j})^T(\mathbf{R_{mod}} - \mathbf{A_{mod}}\mathbf{j})$$
$$\text{s.t. } \mathbf{j} \geq 0 \qquad (4.11)$$

The problem in (4.11) can be solved by a Quadratic Programming (QP) algorithm (Gao *et al.*, 2006). The result of flux calculation is a metabolic flux network outlining the various biochemical reactions included in the calculations along with an estimate of the steady state rate (i.e., the flux) at which each reaction in the diagram occurs. Depending on the contribution of each reaction in the network, the smaller flux values that are a negligible portion of the net flux through the system can be eliminated to obtain a reduced metabolic network. The results of this reduction process are given in Chapter 5.

4.2 Reaction Kinetics and Development of the Dynamic Model

A dynamic model was developed for predicting metabolite concentrations over the duration of the culture and is specifically referred to as 'Dynamic Model' elsewhere in the text to differentiate it from other dynamic models developed in this work.

The dynamics involved in a stirred spinner is given by the following macroscopic material balance model:

$$\frac{d\boldsymbol{\xi}(t)}{dt} = \mathbf{K}\mathbf{r}(t) + \mathbf{u}(t) \qquad (4.12)$$

In the equation above, the symbol $\boldsymbol{\xi} = (\xi_1, \xi_2 \ldots \xi_i)^T$ is the vector of concentrations of extracellular species and is a subset of the vector $\boldsymbol{\psi}$ given by equation (4.1). $\mathbf{r} = (r_1, r_2 \ldots r_i)^T$ is the macro-reaction rate vector. **K** is the matrix containing stoichiometric coefficients of the reaction species involved in the elementary macro reactions. The second term on the right hand side of the equation $\mathbf{u}(t)$ represents the vector of net exchange rate of species with the surroundings. The term is zero for all species except for CO_2 which is a gas. However, measurements corresponding to CO_2 were not available and such measurements are difficult to make. As a result, the term $\mathbf{u}(t)$ has been effectively dropped from equation 4.12 and it can in turn be written in the matrix form as follows:

$$\frac{d\boldsymbol{\xi}(t)}{dt} = \mathbf{K}\mathbf{r}(t) \qquad (4.13)$$

Monod kinetics has been assumed for all the reactions according to the general expression:

$$r_i(t) = a_i\left[\prod \frac{\text{Nutrient}_i}{\text{Nutrient}_i + k_i}\right]X_{v,e} \qquad (4.14)$$

where $r_i(t)$ is the reaction rate for i^{th} reaction; Nutrient_i and k_i are the corresponding substrate concentration and half-saturation constant, respectively. a_i is the maximum rate at which the reaction can proceed, while $X_{v,e}$ is the experimental viable cell concentration.

There are two methods for estimation of the specific growth rate, a_i and the associated Monod constant, k_i in equations elucidating behavior of growing cultures. One is the steady state measurement of growth and the limiting substrate concentration in continuous culture at different dilution rates. An alternative method is the measurement of the growth rate at different substrate concentrations in batch culture (Banerjee, 1993).

The assumption of balanced growth made previously implies that the reactions taking place in the system operate at a constant maximum rate during the exponential phase. In the absence of experimental data for estimation of a_i and k_i, the maximal rates, a_i's can be obtained by choosing the half saturation constants k_i's in equation (4.14) to be significantly smaller in comparison to substrate concentration for major part of the experimental run, i.e. $\mathbf{r}(t) \approx \mathbf{a}X_{v,e}(t)$. However, attention was paid that the values were not too small to avoid any numerical stiffness problems (Gao *et al.*, 2006). The dynamic model expressed in (4.13) can thus be stated as:

$$\frac{d\xi(t)}{dt} = \mathbf{K}\mathbf{a}X_{v,e}(t) \qquad (4.15)$$

Additionally, following equation (4.1) the mass balances for the extracellular metabolites specified by the vector ξ can be expressed as:

$$\frac{d\xi(t)}{dt} = \mathbf{R}_\xi X_{v,e}(t) \qquad (4.16)$$

where $\mathbf{R}_\xi$ is the conversion rate vector and is a subset of vector **R**.

Next, utilizing equations (4.13) and (4.14), a system of algebraic equations can be derived as follows.

$$\mathbf{Ka}=\mathbf{R}_\xi \qquad (4.17)$$

As explained before, experimental data is used to compute the values for **R** and the reduced reaction scheme for determining expression for **K**. Again, the system in (4.17) is generally over-determined and correspondingly the **a**-values can be estimated by applying QP to solve the following constrained minimization:

$$\begin{aligned} &\text{Min } (\mathbf{R}_\xi-\mathbf{Ka})^T(\mathbf{R}_\xi-\mathbf{Ka}) \\ &\text{s.t. } \mathbf{a}\geq\mathbf{0} \end{aligned} \qquad (4.18)$$

4.3 Development of the Biomass Model

The second objective of the study was to model the growth and death of the cells. The underlying motive was to develop a general model to balance the viable and dead cell concentrations as a function of system properties at that instant in time. Thus, the fundamental model structure was expected to be of the general form expressed in equation 4.19.

$$\begin{aligned} \frac{1}{X_v}\left(\frac{dX_v}{dt}\right) &= k_g f(\xi) - k_d g(\xi) \\ \frac{1}{X_v}\left(\frac{dX_d}{dt}\right) &= k_d g(\xi) \end{aligned} \qquad (4.19)$$

where X_v and X_d are the viable and dead cell concentration, respectively and k_g and k_d are the parameters of the system.

Here, Biomass Model refers to the dynamic model that predicts the viable and dead cell concentration over the duration of the culture and the metabolite concentrations over time act as inputs to the model. The phrase ‘Biomass Model’ has the same implication as mentioned here elsewhere in the text.

The key challenge in this model was to find from experimental data the explicit dependence of the growth and death rates with respect to the extracellular metabolites. Although no starting assumptions were made as to whether the model would be multiplicative or not, it was expected that the X_v and X_d will show dependence on more than one variable/metabolite. To find these dependencies, it was decided to use correlation analysis between the experimentally measured terms in the left hand side of equation (4.19) and different functional forms of nutrient and product concentrations. Since there was no prior information to indicate the nature of mathematical functions that would account for behavior of $f(\xi)$ and $g(\xi)$, Monod functions for metabolite concentration were initially used for testing correlation. The software- STATISTICA was used to find these explicit functional forms. Results of the correlation analysis for the system under study are presented in Chapter 5. Finally, after these functions were found, the growth and death rate coefficients, k_g and k_d given in (4.19) were found from the following minimization problem.

$$\text{Min [Sum of squares]} = \sum (X_{v,e} - X_{v,p})^2 + \sum (X_{d,e} - X_{d,p})^2 \qquad (4.20)$$

Where $X_{v,e}$, $X_{v,p}$, $X_{d,e}$, $X_{d,p}$ are the experimental and predicted values of the viable and dead cell concentrations, respectively.

4.4 Integration of the Dynamic Model and Biomass Model

Once separate models for predicting metabolite concentrations and biomass concentration over time were developed, an integration of these two models is required to come up with an overall generalized model. Integration of the two models into one overall model is schematically described in Figure 4-3. The advantage of the overall model over the individual sub-models is its ability to predict both metabolite and biomass concentration solely on the basis of starting concentrations of the metabolite/concentration variables involved in the model. The estimated parameters for the two separate models needed to be adjusted in order to fine-tune the predictions as combining the two models led to introduction of greater noise in the overall data-set. The obtained integrated model is presented in greater detail in Chapter 5.

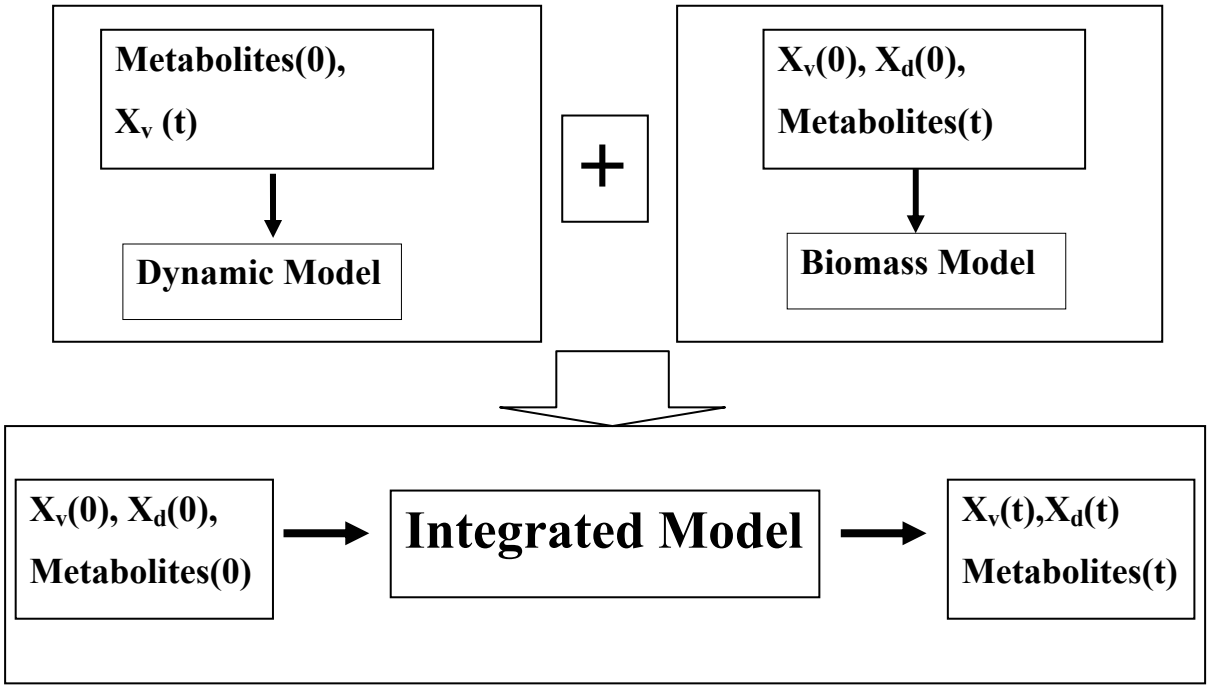

Figure 4-3 Integration of Dynamic and Biomass Model

Chapter 5
Results

As part of the modelling procedure, firstly MFA was applied to a general reaction network for hybridoma cells developed on the basis of published information. A reduced metabolic network was obtained as a result. The reactions in the reduced network were further utilized to develop rate expressions for consumption/ production rates of substrates/products. A dynamic model was then constructed that predicted metabolite concentrations over time. Next, correlation analysis was applied to obtain the dependence of specific growth and specific death rates on metabolite concentration(s). Thus, a multiplicative model was developed for biomass prediction. And finally, individual models were integrated to give an overall model that utilizes starting values for metabolite concentrations and predicts their subsequent concentration values in time.

Two sets each of batch and fed-batch data were available. MFA was applied based on the available data sets. One batch and one fed-batch data set were utilized towards model calibration and the other set of batch/fed batch data was used for model prediction. This enabled us to test the validity of the model(s).

Based on the results obtained from the simulations, hypotheses about the cell metabolism and kinetics of the system have been made in Chapter 7. Additionally, the drawbacks of the study have been highlighted and improvements have been suggested that will be a part of future work.

5.1 Obtainment of the Reduced Metabolic Network

The first step in the process of model development is the MFA. Initially experimental batch data for two separate runs was considered. The complete run was divided into exponential and post-exponential phases as described in the previous chapter. The data included concentration measurements (mmol/L) for 22 extracellular metabolites that were further converted to mmol/(10^9cell-hours). The formula(s) for such a conversion have been given in the previous chapter. Corresponding specific uptake/production rates for these metabolites were calculated for the exponential, the post-exponential and the complete run; and have been denoted by $\mathbf{R}_{\mathbf{exp}}$, $\mathbf{R}_{\mathbf{post\text{-}exp}}$ and $\mathbf{R}_{\mathbf{full}}$ respectively. The uptake/production rate for intracellular metabolites was taken equal to zero under the assumption of balanced growth conditions. Equation (4.3) was used to compute these three **R**-vectors. The calculated values have been expressed in Appendix-B. **R**-values for the intracellular metabolites in the reaction scheme were taken to be equal to zero on the basis of the balanced-growth assumption made earlier.

Now, it must be mentioned that only 28 measurements- extracellular and intracellular were known using which 32 flux values needed to be determined. Henceforth, the system of equations was underdetermined i.e., less equations than unknowns. Among the unknown quantities were concentrations for cystine and ammonia. However, the system can be made over-determined by applying additional constraints to the system; it was stated the solution should be such that all flux values are at least greater than or equal to zero. Furthermore, an assumption was made to the system; the consumption rate of cystine (missing measurement) was taken to be equal to zero rather than being just left out. This is because otherwise a physically unrealistic flux distribution was obtained as solution, i.e., flux corresponding to cystine consumption had an unusually high value. It was found that any time, more than three constraints were satisfied; thus the solution was unique. In order to reduce the sensitivity to noise, experimental values of **R** for a number of batches were considered.

By substituting values of the calculated uptake/production rate vector $\mathbf{R_{mod}}$ into equation (4.10) where the expression for the stoichiometric matrix $\mathbf{A_{mod}}$ is obtained by inspection from Figure 4-1, the flux vector **j** was obtained by applying a Quadratic Programming routine as in equation (4.11). As explained above, three values for vector **R** corresponding to the exponential, post-exponential and overall average phase were obtained. The corresponding values for the flux vector have been denoted by $\mathbf{j_{exp}}$, $\mathbf{j_{postexp}}$, $\mathbf{j_{full}}$.

On observation of the overall flux distribution ($\mathbf{j_{full}}$) in Figure 5-1(a), it is evident that the flux values from j9-j22; and then j26, j29 and j30 have values very close to zero. This implies that the reactions these fluxes represent do not proceed appreciably and hence do not contribute to the overall cellular metabolism. Consequently, they were ignored and henceforth the original reaction network was reduced to Figure 5-2.

To obtain the reduced metabolic network for the fed-batch case, the growth phase of each of the two fed-batch experimental runs was subdivided into 10 time intervals that has been described in detail in Chapter 4. The post-exponential phase of fed-batch experiments has been defined as decline phase when feeding was stopped and there was an irreversible drop in viable cell concentration. Subsequently, average reaction rate values, as per equation (4.3), were calculated for each one of these 10 time intervals ($\mathbf{R_1}$,…,$\mathbf{R_{10}}$). Then, the data corresponding to the 10 intervals was simultaneously used to define the over-determined system of equations given by equation (4.10) and the corresponding fluxes were obtained from the QP solution based on (4.11). And finally, an overall average value of **R** denoted by $\mathbf{R_{full}}$ was computed based on equation (4.3). Again, the calculated values for **R** have been given in Appendix-B while the graphical representation for the average fed-batch flux values follows in Figure 5-1(b).

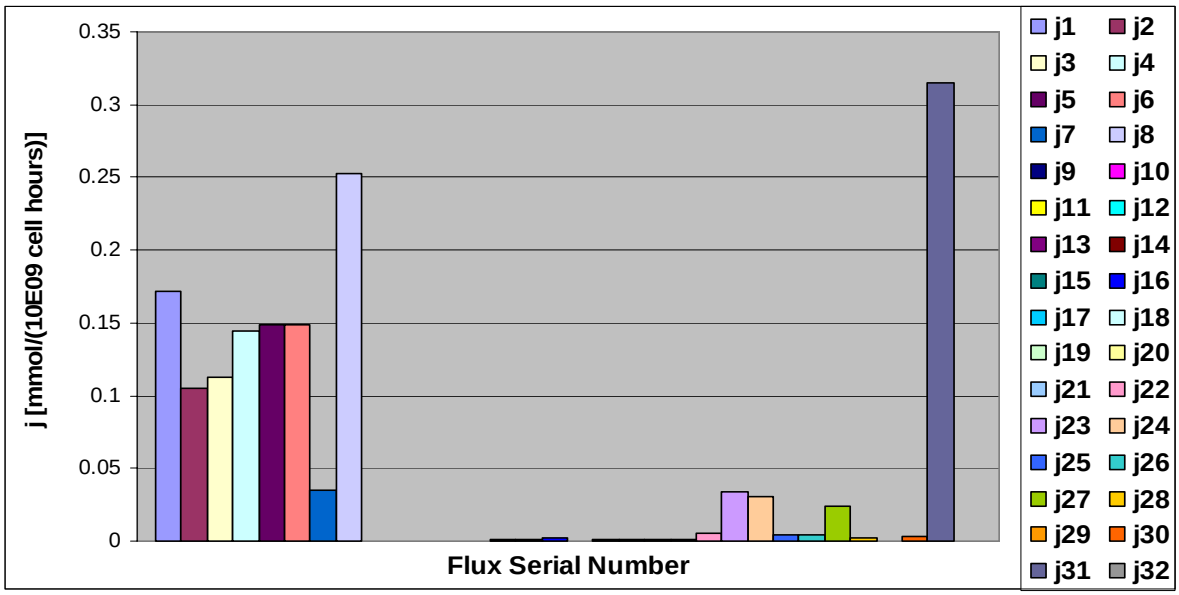

(a)

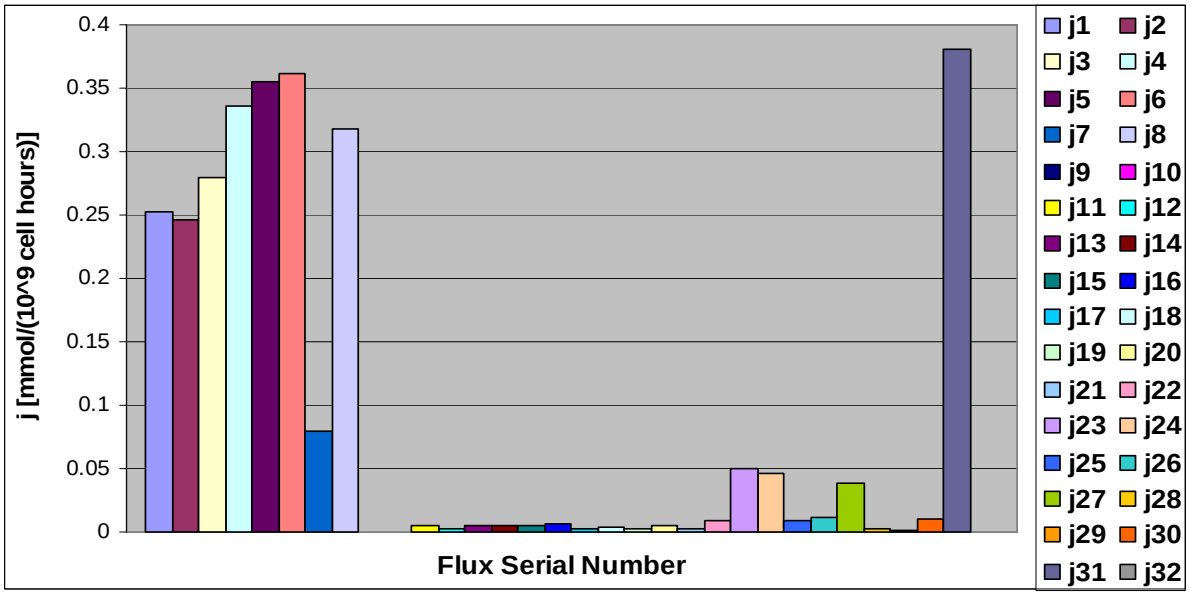

(b)

Figure 5-1 Distribution of Average Fluxes for (a) Batch Run and (b) Fed-batch Run

It is clear from Figures 5-1(a) and 5-1(b) that the distribution trend of fluxes in batch and fed-batch cultures is strikingly similar. Based, on the flux distribution, the same exercise of

eliminating insignificant fluxes from the complete metabolic network was undertaken for the fed-batch case. Since the same fluxes were found to be insignificant in both culture modes, a common reduced metabolic network was obtained and has been shown in Figure 5-2.

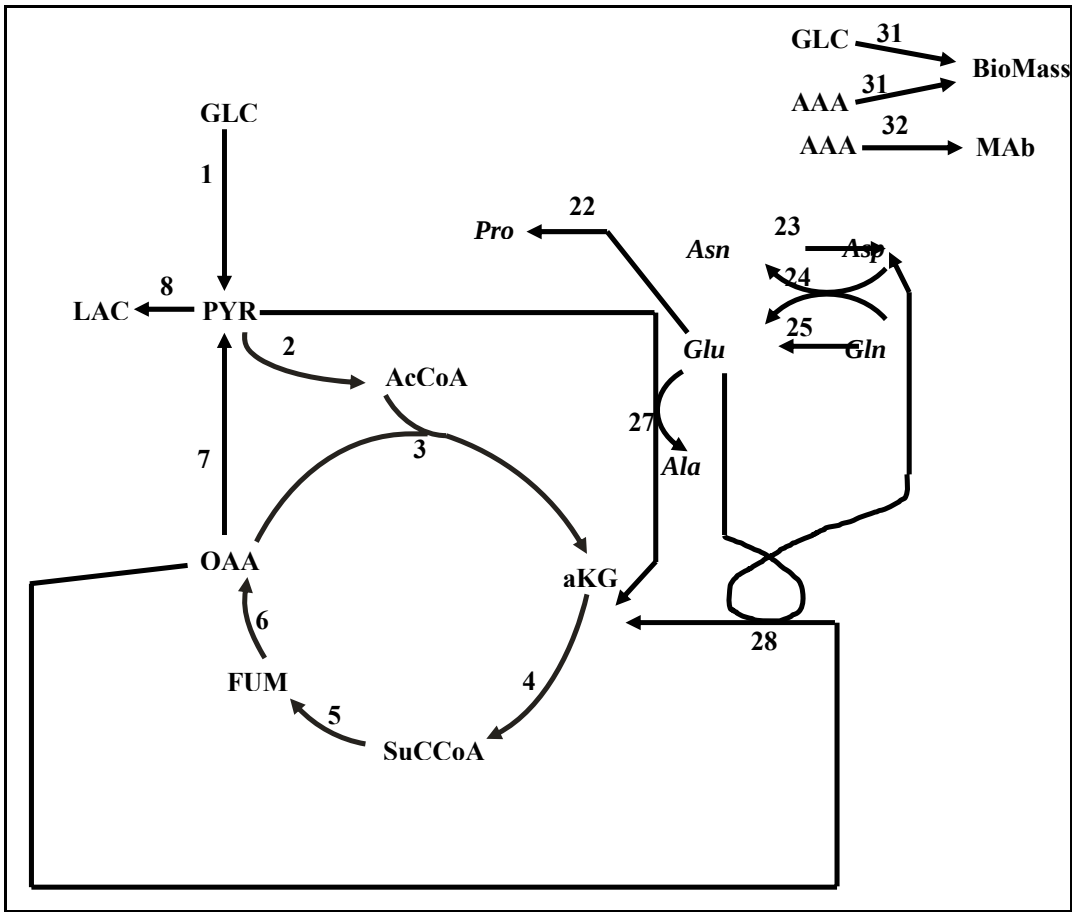

Figure 5-2 Reduced Metabolic Network

The reduced network obtained in the current work is very similar to the one obtained by Gao *et al*. (2006) for hybridoma in batch culture with the only difference being that flux j28 instead of j26 is eliminated, otherwise the reduced metabolic network is identical.

5.2 Obtainment of the Dynamic Model

5.2.1 Developing Fundamental Macro-Reactions

Each reaction species in Figure 5-2 represents a 'flux mode'. Based on the reduced reaction network, the elementary flux modes were computed and in turn, translated into a set of macro-reactions linking/establishing relationships between the various extracellular substrates and products (Provost and Bastin, 2004).

The intracellular metabolites were eliminated by simple algebraic manipulation in light of missing measurements for the same. The intracellular fluxes could not be measured in this work and therefore even if they could be calculated, their values could not be verified due to a lack of experimental data for the same. The process of elimination of the intracellular fluxes can be illustrated by the following example:

J1 Glc→2Pyr …***x***1 *Multiplying equation J1 by 1 and*,

J2 Pyr→Lac …***x***2 *Multiplying equation J2 by 2*

----------*Adding up J1 and J2 so as to eliminate Pyr*

E1: Glc→2Lac

After the elimination of intracellular fluxes from the reduced reaction network, 9 elementary macro-reactions were derived and have been summarized in Table 5-1.

Table 5-1: Elementary Macro Reactions

Ei (i=1,2…9)	**Reaction**
E1	Glc(G) →2Lac

E2 $Glc+2Glu(U) \rightarrow 2Ala+2CO_2+2Lac$

E3 $Glc+2Glu \rightarrow 2Lac+2NH_3+8CO2$

E4 $Glu \rightarrow Pro$

E5 $Asn(S) \rightarrow Asp+NH_3$

E6 $Gln(Q)+Asp \rightarrow Asn+Glu$

E7 $0.0508Glc + 0.0577Gln + 0.0133Ala + 0.007Arg + 0.006Asn + 0.0201Asp + 0.004Cys + 0.0016Glu + 0.0165Gly + 0.0033His + 0.00084Ile + 0.0133His + 0.0084Ile + 0.0133Leu + 0.0101Lys + 0.0033Met + 0.0055Phe + 0.0081Pro + 0.0099Ser + 0.008Thr + 0.004Tyr + 0.0096Val \rightarrow Biomass$

E8 $0.0104Gln + 0.011Ala + 0.005Arg + 0.0072Asn + 0.0082Asp + 0.0005Cys + 0.0107Glu + 0.0145Gly + 0.0035His + 0.0054Ile + 0.0142Leu + 0.0145Lys + 0.0028Met + 0.0072Phe + 0.0148Pro + 0.0267Ser + 0.0160Thr + 0.0085Tyr + 0.0189Val \rightarrow MAb$

E9 $Gln \rightarrow Glu+NH_3$

Based on the above results for the reduced reaction network, the reduced stoichiometric coefficient matrix, K can be written as:

$$\mathbf{K}=\begin{bmatrix} & r1 & r2 & r3 & r4 & r5 & r6 & r7 & r8 & r9 \\ \text{Glc} & -1 & -1 & -1 & 0 & 0 & 0 & -0.0508 & 0 & 0 \\ \text{Gln} & 0 & 0 & 0 & 0 & 0 & -1 & -0.0577 & -0.0104 & -1 \\ \text{Lac} & 2 & 2 & 2 & 0 & 0 & 0 & 0 & 0 & 0 \\ \text{Glu} & 0 & -2 & -2 & -1 & 0 & 1 & -0.0016 & -0.0107 & 1 \\ \text{Asn} & 0 & 0 & 0 & 0 & -1 & 1 & -0.006 & -0.0072 & 0 \\ \text{Asp} & 0 & 0 & 0 & 0 & 1 & -1 & -0.0201 & -0.0082 & 0 \\ \text{Ala} & 0 & 2 & 0 & 0 & 0 & 0 & -0.0133 & -0.011 & 0 \\ \text{Pro} & 0 & 0 & 0 & 1 & 0 & 0 & -0.0081 & -0.0148 & 0 \\ \text{Biomass} & 0 & 0 & 0 & 0 & 0 & 0 & 1 & 0 & 0 \\ \text{MAb} & 0 & 0 & 0 & 0 & 0 & 0 & 0 & 1 & 0 \end{bmatrix} \tag{5.1}$$

The rows in **K** represent the various extracellular metabolites being considered in the model, and the columns represent the number of macro-reactions obtained as a result of the elimination of intracellular measurements that are represented in Table 5-1. It should be noted that unmeasured components such as CO_2 and NH_3 were eliminated in the equations.

5.2.2 Development of Rate Expressions

Since it was assumed that the reactions shown in Table 5-1 proceed by Monod kinetics, the reaction rates could be expressed as Monod functions of the nutrient concentrations involved in the reaction under consideration. For example, the reaction rate for the elementary reaction

E2: $\text{Glc}+2\text{Glu}\rightarrow 2\text{Ala}+2\text{CO}_2+2\text{Lac}$

can be expressed as:

$$r_2 = a_2 \frac{\text{Glc}}{\text{Glc}+k_G} \frac{\text{Glu}}{\text{Glu}+k_u} X_V \tag{5.2}$$

The fundamental macro reactions and their rate expressions are stated in Table 5-2.

Table 5-2: Macro Reactions and Accompanying Reaction Rates

Reaction	Rate Expression	Parameters
E1	$r_1 = a_1 \frac{G}{G+k_G} X_{v,e}$	a_1, k_G
E2	$r_2 = a_2 \frac{G}{G+k_G} \frac{U}{U+k_U} X_{v,e}$	a_2, k_G, k_U
E3	$r_3 = a_3 \frac{G}{G+k_G} \frac{U}{U+k_U} X_{v,e}$	a_3, k_G, k_U
E4	$r_4 = a_4 \frac{U}{U+k_U} X_{v,e}$	a_4, k_U
E5	$r_5 = a_5 \frac{S}{S+k_S} X_{v,e}$	a_5, k_S
E6	$r_6 = a_6 \frac{Q}{Q+k_Q} \frac{F}{F+k_F} X_{v,e}$	a_6, k_Q, k_F
E7	$r_7 = a_7 \frac{G}{G+k_G} X_{v,e}$	a_7, k_G
E8	$r_8 = a_8 \frac{Q}{Q+k_Q} X_{v,e}$	a_8, k_Q
E9	$r_9 = a_9 \frac{Q}{Q+k_Q} X_{v,e}$	a_9, k_Q

5.2.3 Model Calibration and Testing

The half saturation constants, k_{ij} (i= a certain metabolite and j= number of the elementary reaction) in Table 5-2 were chosen by inspection such that they were small enough to be negligible when the nutrient concentration was reasonably high but would be large enough to avoid any stiffness problems (Gao *et al.*, 2006).Their exact values have been given in Table 5-3.

Table 5-3: Values for the Half-saturation Constants

Constant	Batch Mode (in mmol/L)	Fed-batch Mode (in mmol/L)
k_G	4	0.5
k_Q	0.05	0.5
k_U	0.01	0.01
k_S	0.02	0.12
k_F	0.05	0.05

Putting all rate expressions in the matrix form, and utilizing equalities specified in Chapter 4, we get:

$$\frac{d\boldsymbol{\xi}(t)}{dt} = \mathbf{Kr}(t) = \mathbf{Ka}X_{v,e} \qquad \Rightarrow \frac{d\boldsymbol{\xi}(t)}{dt} = \mathbf{Ka}X_{v,e} \tag{5.3}$$

The **a**-coefficients in the reaction rate expressions in (5.3) were calculated by Christian Fischer, a summer co-op student separately for the exponential and post exponential phases of batch and then fed-batch operation. It was seen that the **a**-coefficients determined for batch operation differed from similar estimation for fed-batch operation; and even within one batch, the values of **a**-coefficients for exponential phase of growth were different from the post-exponential phase because of differences in kinetics. The values for the a-coefficients have been given in Appendix-B.

Based on the set of equations derived in (5.3), the model calibration was performed on the basis of one batch and one fed-batch experiment, and the estimated **a**-values were in turn tested for accuracy on an additional batch and fed-batch experiment.

Calibrated batch and fed-batch data sets are given in Figure 5-3 (a) and (b). The model has been tested by a comparison between experimental data and model predictions given in Figure 5-3 (c) and (d). In these figures, experimental cell concentration, also included, was used as input to the dynamic model of metabolites. Viable cell concentration acts as input as model equations for predicting viable cell concentration had not been developed at this stage. Figures are shown on the following page. Figures 5-3(a, b) are the model calibrations and Figures 5-3(c, d) are the corresponding model predictions.

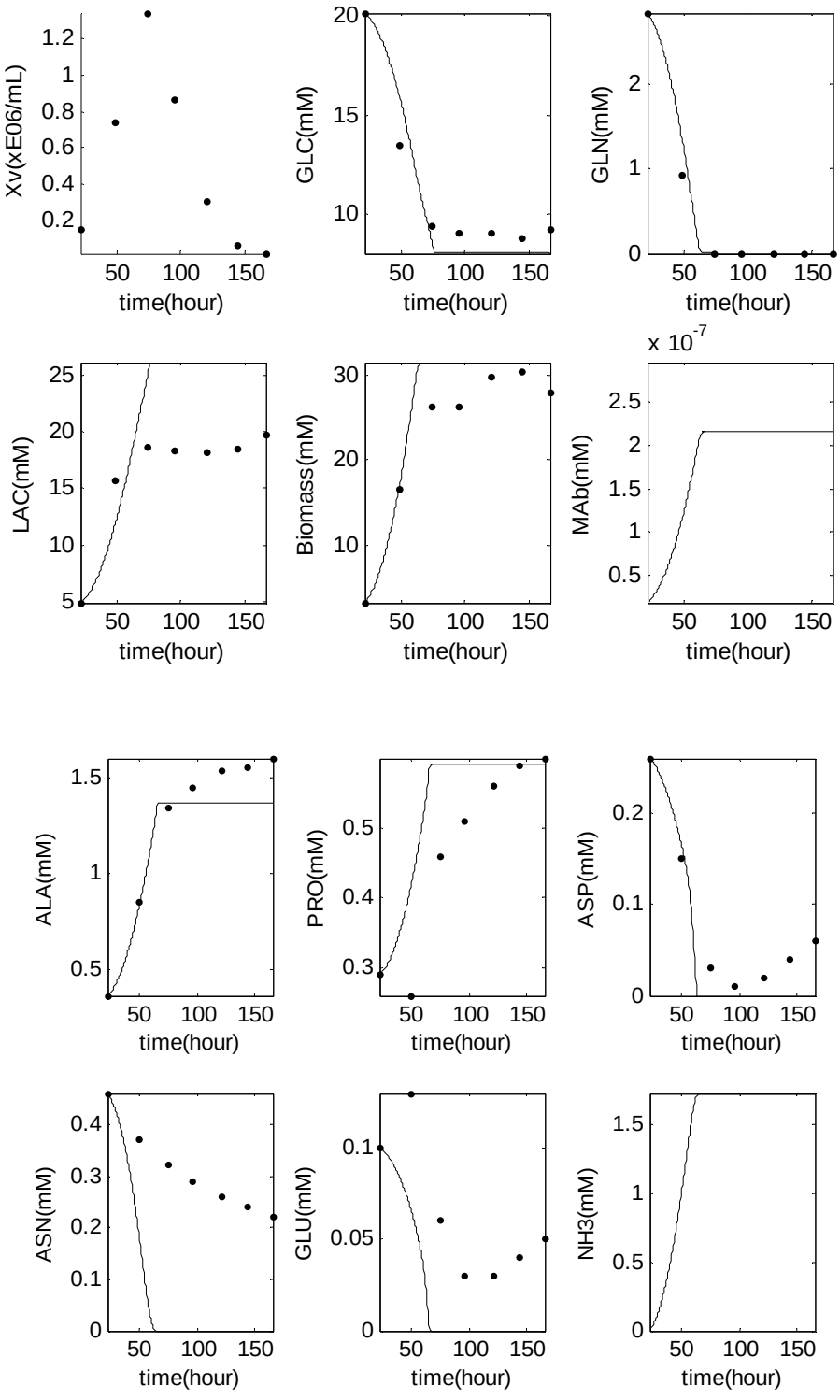
Xv(xE06/mL)
GLC(mM)
GLN(mM)
LAC(mM)
Biomass(mM)
x 10^-7
MAb(mM)
ALA(mM)
PRO(mM)
ASP(mM)
ASN(mM)
GLU(mM)
NH3(mM)
time(hour)

(a)

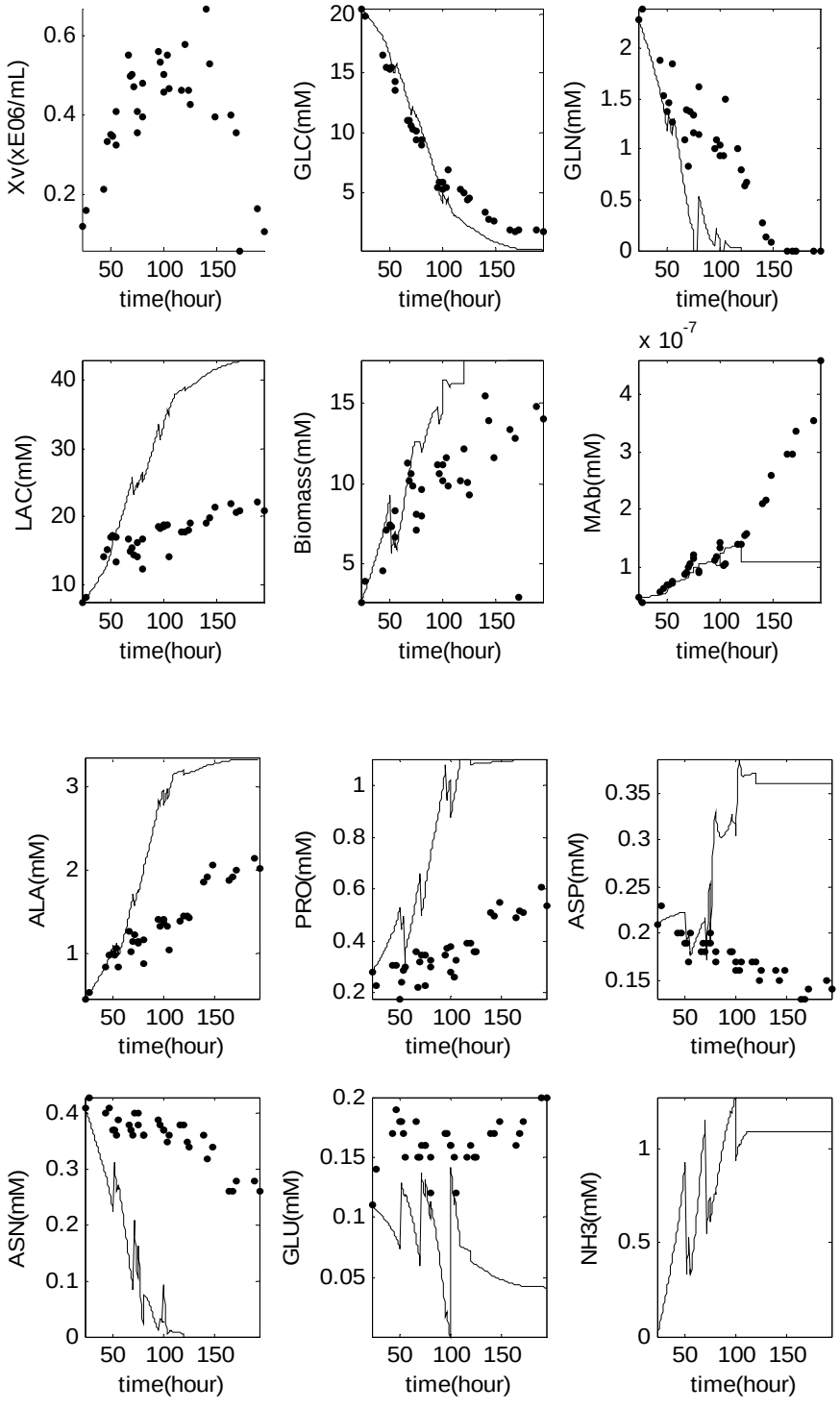
Xv(xE06/mL)
GLC(mM)
GLN(mM)
LAC(mM)
Biomass(mM)
x 10^-7
MAb(mM)
ALA(mM)
PRO(mM)
ASP(mM)
ASN(mM)
GLU(mM)
NH3(mM)
time(hour)

(b)

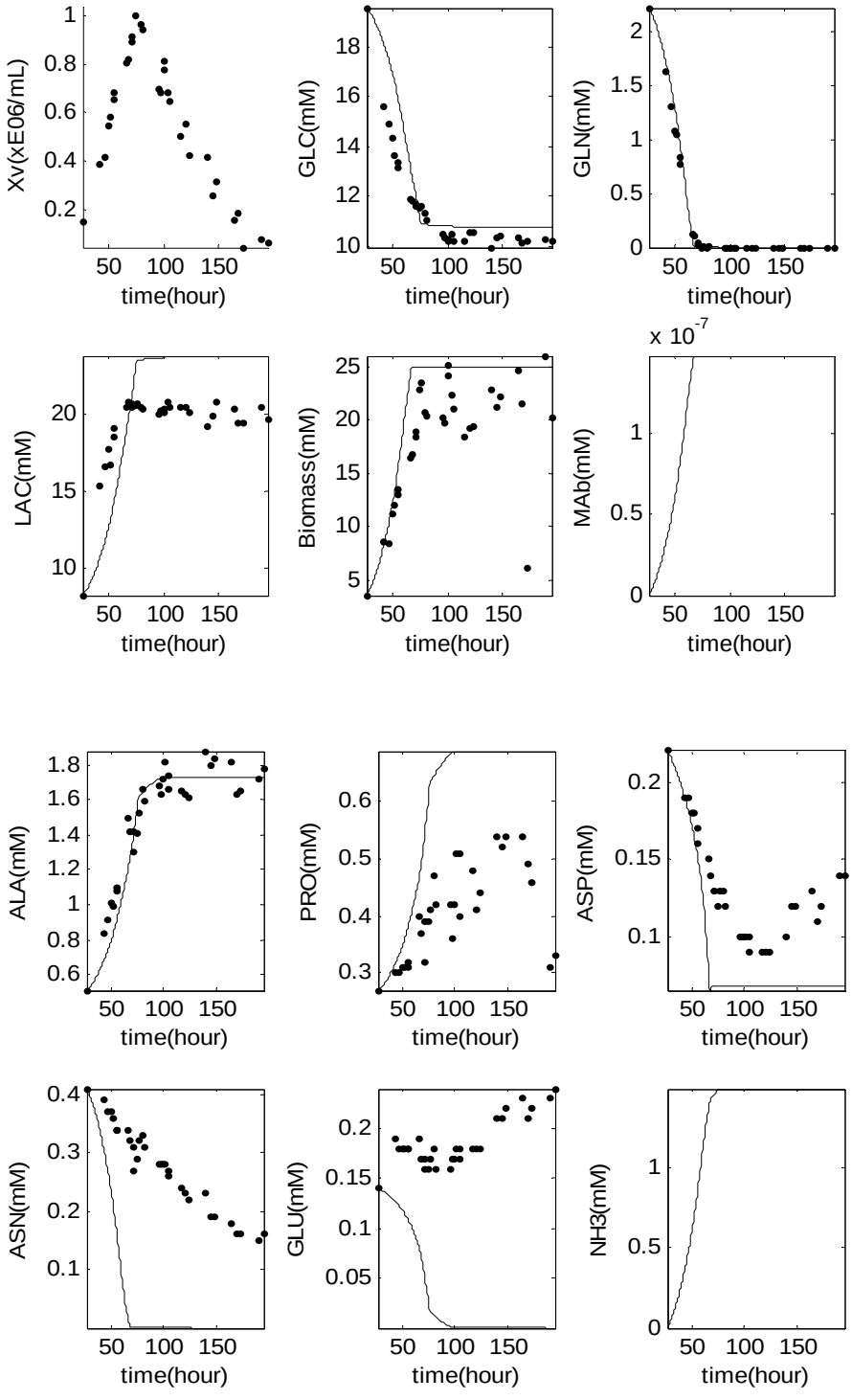
Xv(xE06/mL)
GLC(mM)
GLN(mM)
LAC(mM)
Biomass(mM)
x 10^-7
MAb(mM)
ALA(mM)
PRO(mM)
ASP(mM)
ASN(mM)
GLU(mM)
NH3(mM)
time(hour)

(c)

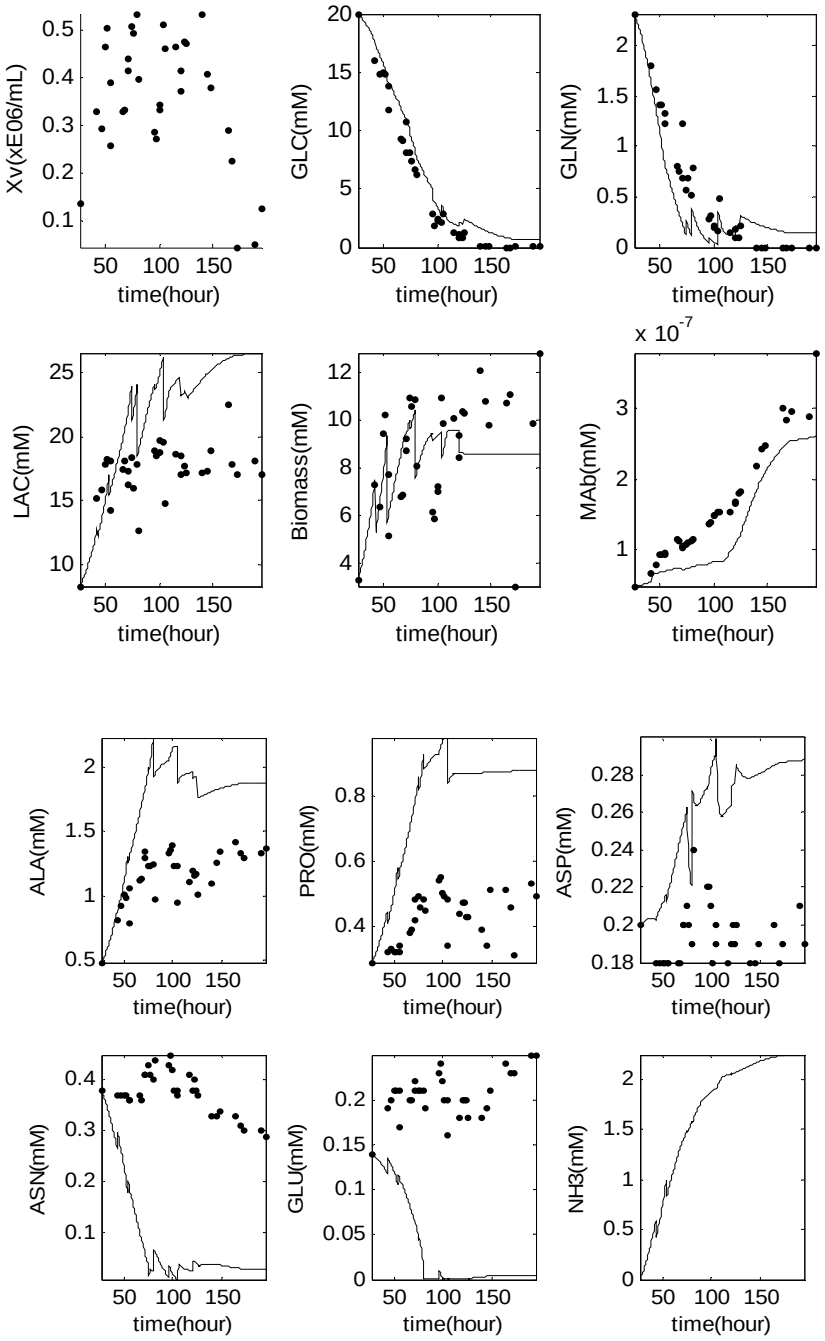

(d)

Figure 5-3 Dynamic Model Simulations (-) vs Experimental (●) Metabolite Concentrations in Batch Run (a,c) and Fed-batch Run (b,d)

5.3 Obtainment of the Biomass Model

5.3.1 Correlation Analysis

To obtain a mathematical model that does not require the experimental data for cell concentration, it was necessary to predict the trends for growth and death of the cells with respect to influencing factors that affect cell growth and viability. To find the exact dependence relationship, the software STATISTICA was used to run the correlation analysis with respect to the various metabolite measurements available including nutrients, amino acids and by-products.

Since Monod expressions are the most common types of mathematical functions used for explaining cellular behavior in systems biology, the first few attempts focused on finding similar functional dependence (Monod) in the system under study. The functions with which the growth and death terms showed correlation were referred to as influencing factors. The terms that did not improve correlation were left out from the overall expression for influencing factors. The results summarized in Table 5-4 show that the influencing factor is a function of glutamine and lactate.

Table 5-4: Results of Correlation Analysis

Expression	Influencing factor	Correlation coefficient highest-value (average-value)
Growth: $\frac{1}{X_v}\frac{dX_v}{dt}$	$\frac{Q}{Q+k_{gQ}}$	0.93 (0.84)
Growth: $\frac{1}{X_v}\frac{dX_v}{dt}$	$\frac{Lac}{Lac+k_{dQ}}$	-0.90 (0.81)
Death: $\frac{1}{X_v}\frac{dX_d}{dt}$	$\frac{Lac}{Lac+k_{dQ}}$	0.92 (0.83)

Thus Biomass Model can be concisely expressed as follows in equation 5.4.

$$\frac{dX_v}{dt} = k_g\left(\frac{Q}{Q+k_{gQ}}\right) - k_d\left(\frac{Lac}{Lac+k_{dQ}}\right)$$
$$\frac{dX_d}{dt} = k_d\left(\frac{Lac}{Lac+k_{dQ}}\right) \quad (5.4)$$

5.3.2 Model Calibration and Testing

The parameters k_{gQ} and k_{dQ} were determined by simply choosing values that gave the best possible fit of the simulations to experimental data. The growth and death coefficients k_g and k_d were estimated by applying a least squares minimization routine in MATLAB using **fmincon** function. The optimized objective function was as follows:

$$\text{Min [Sum of squares]} = \sum(X_{v,e} - X_{v,p})^2 + \sum(X_{d,e} - X_{d,p})^2 \quad (5.5)$$

Where $X_{v,e}$, $X_{v,p}$, $X_{d,e}$, $X_{d,p}$ are the experimental and predicted values of the viable and dead cell concentrations, respectively. Values for the estimated coefficients are furnished in Table 5-5.

Table 5-5: Values for Parameters in Biomass Model

Parameter	Value for Batch Mode	Value for Fed-batch Mode
k_g	0.05	0.05
k_d	0.0004	0.0004
k_{gQ}	0.05	0.05
k_{dQ}	0.43	0.43

It is worth commenting that the parameter values in Table 5-5 for batch and fed-batch mode are the same and the model built on these values is able to capture the process behaviour. To test validity of the model, a separate data set was used for calibration and prediction of the

Biomass model for the batch as well as the fed-batch case. Figure 5-4 shows the calibrations and predictions based on the calibrations.

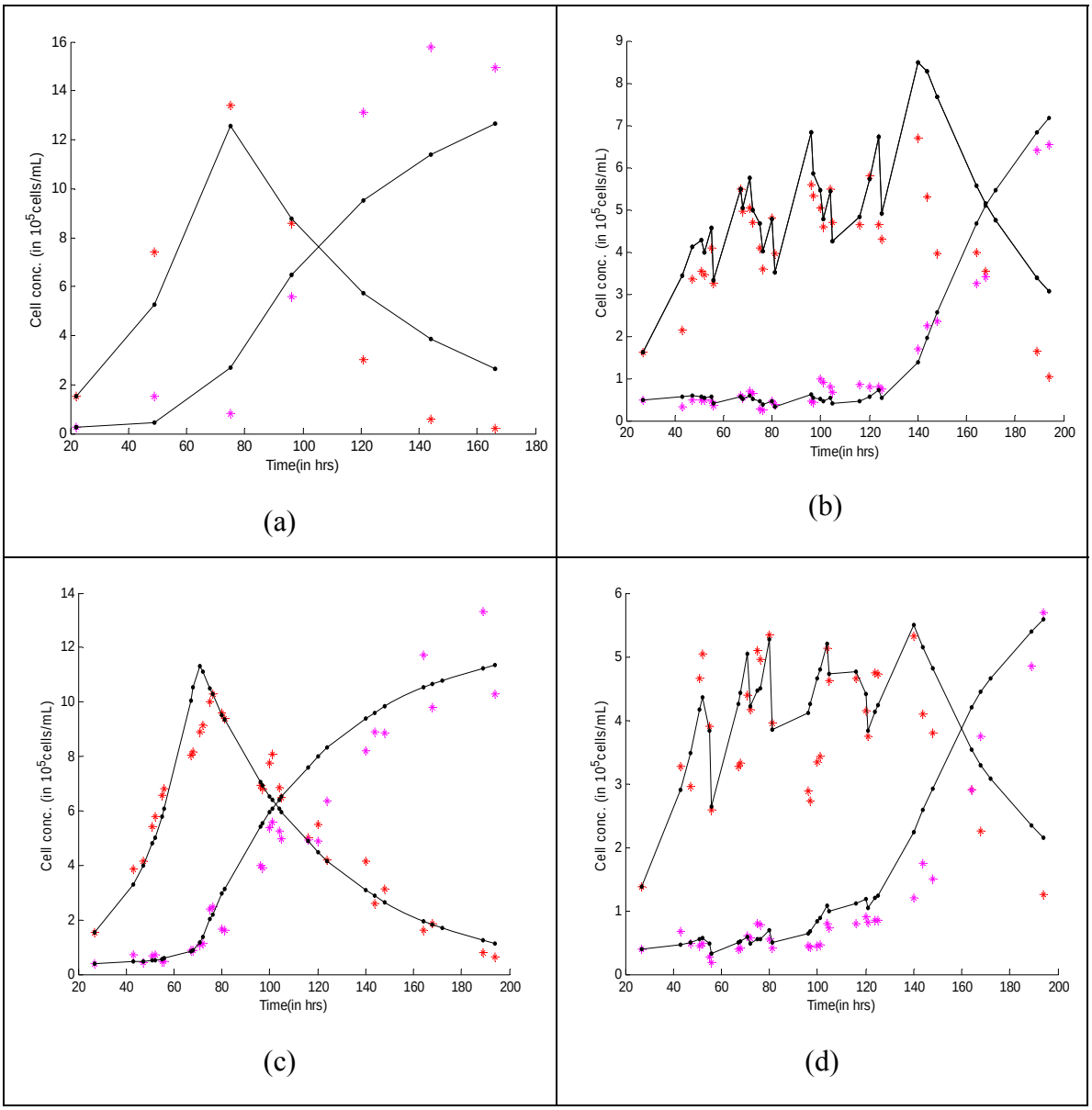

Figure 5-4 Experimental Data for Viable and Dead Cell Concentrations (*) vs Simulated Data (-) for Biomass Model for Batch Mode (a,c) and Fed-batch Mode (b,d)

Note: For fed-batch, the various maxima in the graph for X_v correspond to addition of feed to culture.

Graphs in Figure 5-4(a) are calibration results for batch mode and graphs in Figure 5-4(b) are calibration results for fed-batch mode. The graphs in Figure 5-4(c) are prediction results for batch mode and graphs in Figure 5-4(d) are prediction results for fed-batch mode.

5.4 The Integrated Model

The final step in the formulation of a general model for MAb production was the integration of the dynamic model for extracellular species and the cell concentration model as per the schematic diagram in Figure 4-3. By combining the two sets of equations (5.3 and 5.4) meant that instead of using experimental values (as inputs) for model prediction, only starting values would be used for successively predicting metabolite concentrations and cell concentrations over time. In short, the system of equations for the cell culture system under analysis can be finally stated as in equation (5.6).

$$\begin{aligned} \frac{d\xi(t)}{dt} &= \mathbf{K}\mathbf{r}(t) \\ \frac{dX_v}{dt} &= k_g\left(\frac{Q}{Q+k_{gQ}}\right) - k_d\left(\frac{Lac}{Lac+k_{dQ}}\right) \\ \frac{dX_d}{dt} &= k_d\left(\frac{Lac}{Lac+k_{dQ}}\right) \end{aligned} \qquad (5.6)$$

5.4.1 Model Calibration and Testing

A re-adjustment of growth and death coefficients (k_g and k_d) was required because upon integration of the individual models into one, the predictions were slightly inaccurate. Some of the half saturation constants for fed-batch data required adjustment as well. The coefficients k_g and k_d for batch mode were 0.04 ($x10^6$ cells/ml-hr) and 0.001 ($x10^6$ cells/ml-hr) respectively while for fed-batch these values were 0.04 ($x10^6$ cells/ml-hr) and 0.0001 ($x10^6$ cells/ml-hr) respectively. The values for the half-saturation constants for the integrated model have been summarized in Table 5-6.

Table 5-6: Values for the Half-saturation Constants

Constant	Batch Mode (in mmol/L)	Fed-batch Mode (in mmol/L)
k_G	4	4
k_Q	0.03	0.05
k_U	0.01	0.01
k_S	0.02	0.12
k_F	0.05	0.05

Based on results obtained from equations in (5.6), a separate set of batch and fed-batch experimental runs was taken to test accuracy of estimated parameters in predicting for future runs. The results are shown in Figure 5-5.

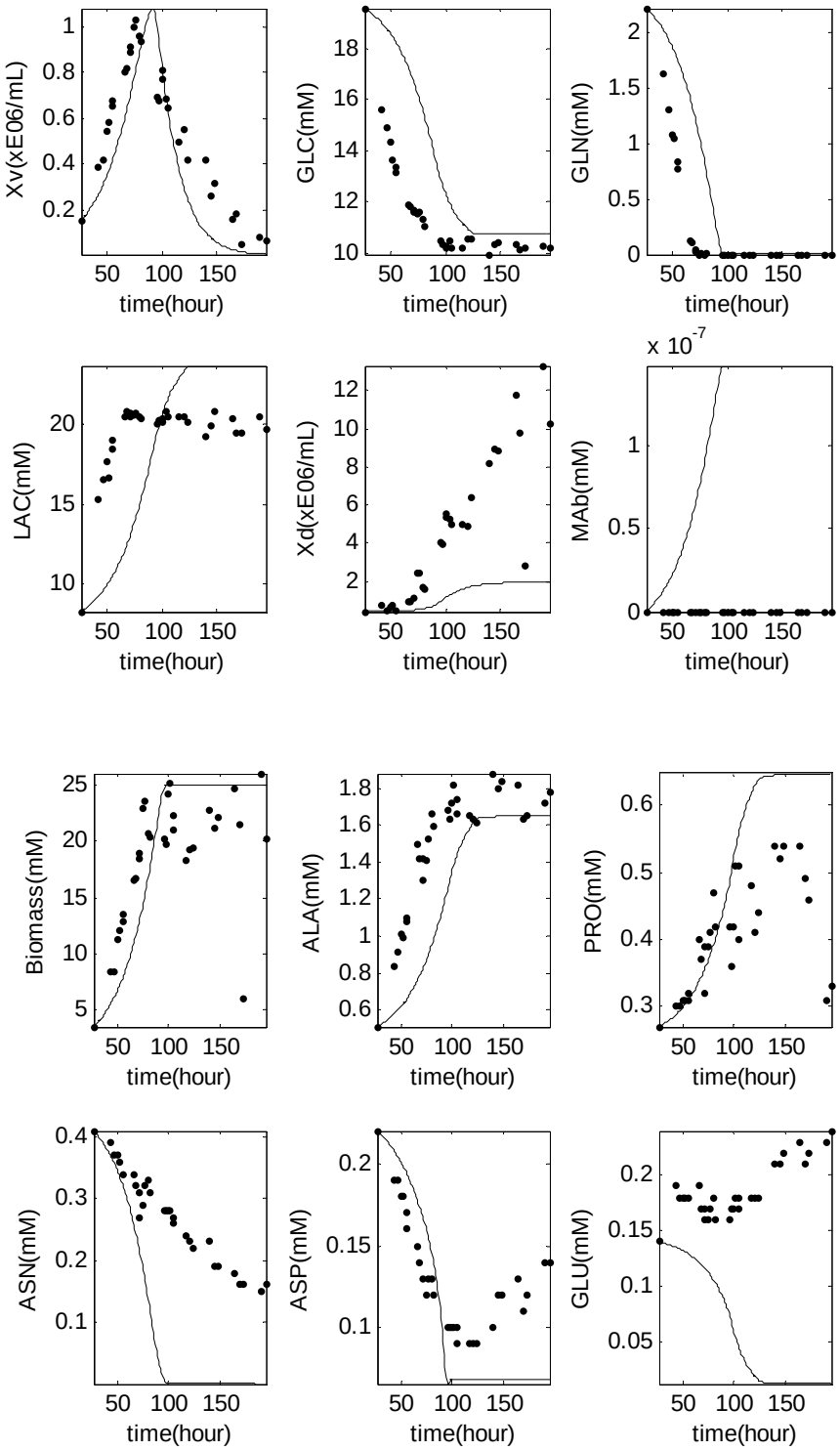
Xv(xE06/mL)
GLC(mM)
GLN(mM)
LAC(mM)
Xd(xE06/mL)
x 10^-7
MAb(mM)
Biomass(mM)
ALA(mM)
PRO(mM)
ASN(mM)
ASP(mM)
GLU(mM)
time(hour)

(a)

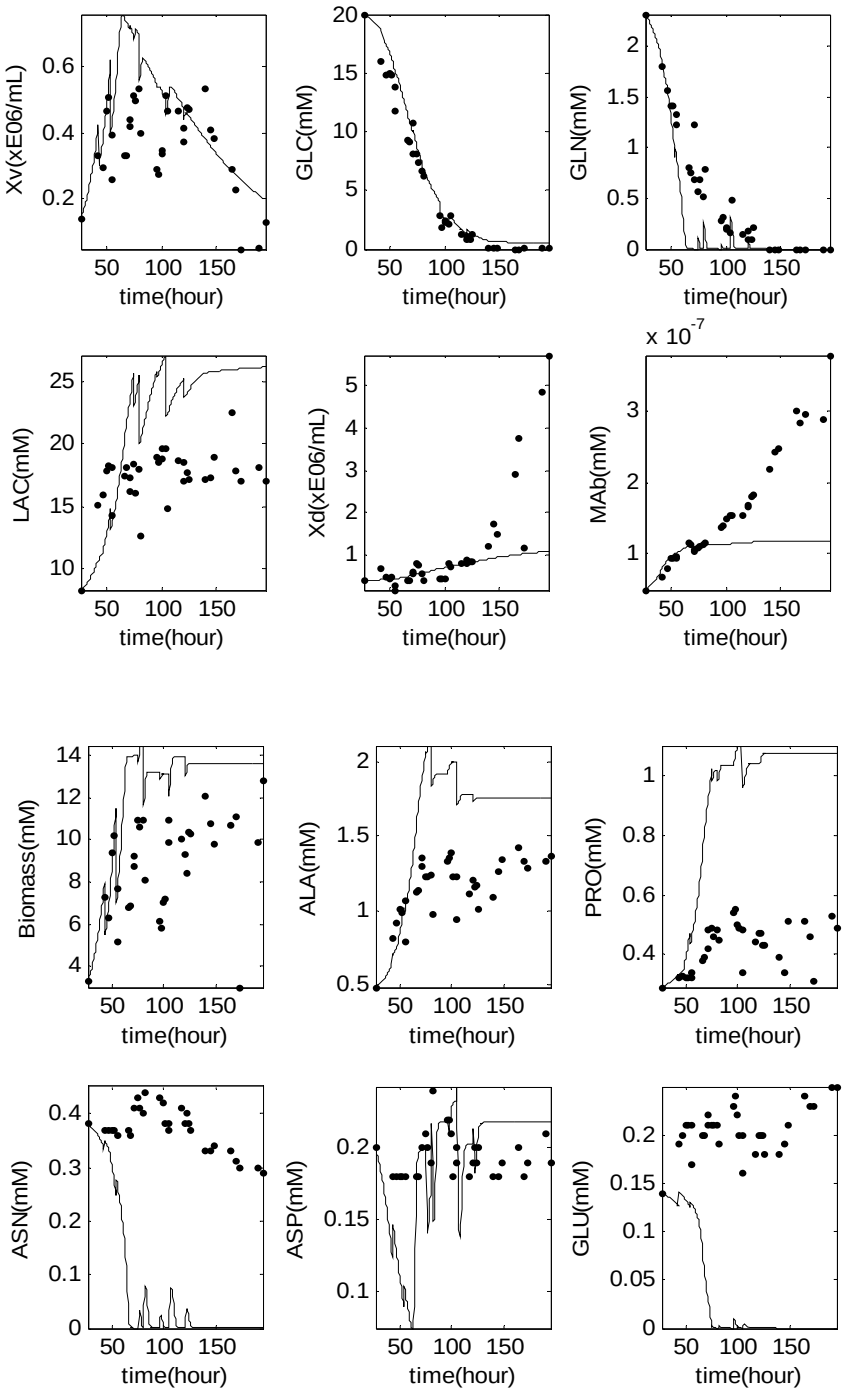

(b)

Figure 5-5 Comparison of Predicted Data (-) with Experimental Data (●) for (a) Batch Culture and (b) Fed-batch Culture.

Note: Experimental MAb data is unavailable for batch experiment

In addition to predicting experimentally measured metabolite concentrations, the model also predicts for ammonia that was not measured during the course of the experiment. The simulated results for ammonia have been given in Figure 5-6.

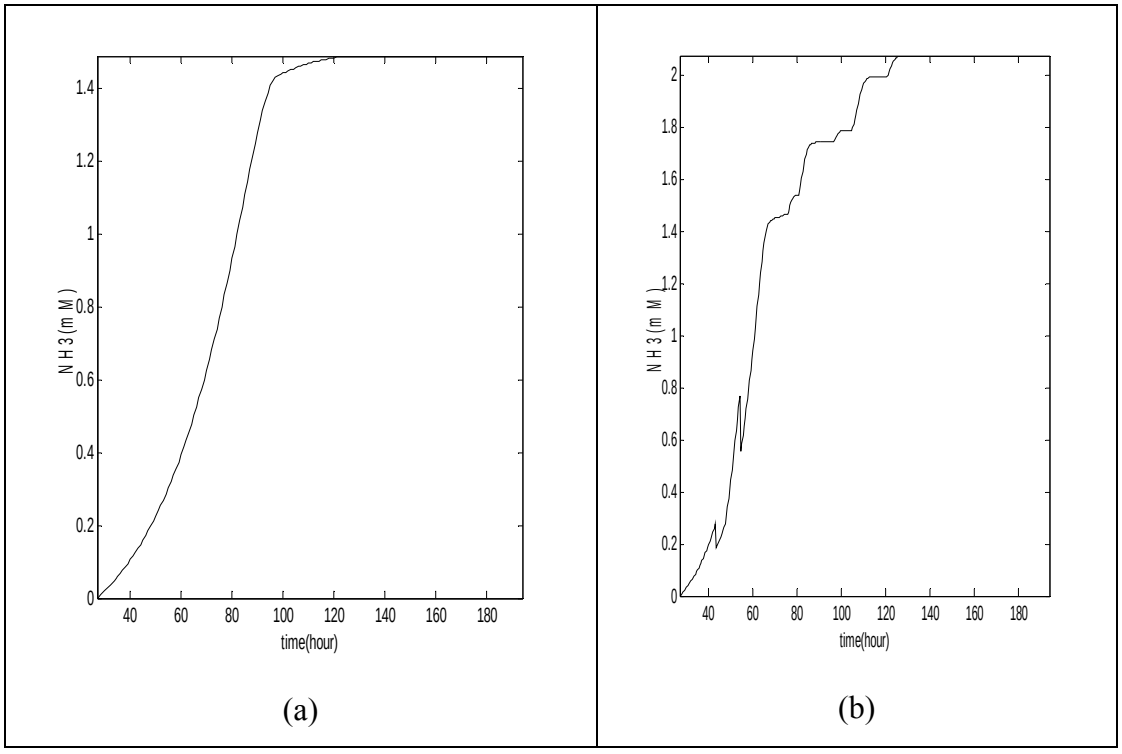

Figure 5-6 Simulations for Ammonia Concentration in (a) Batch and (b) Fed-batch Systems

At this point, the simulation results for ammonia could not be verified experimentally because ammonia measurements were unavailable for the current experiments.

Chapter 6
Fluorescence Imaging

6.1 Overview

Analysis of the modelling results presented in Chapter 5 suggests that a more detailed characterization of the cell population is required. Until now, Trypan blue dye exclusion test was used to characterize the overall population of cells as either viable or dead. However, this staining technique cannot provide any further details about the state of the cell population and hence it is not possible to derive a more detailed characterization of cells based on this technique alone. Compared with the usual Trypan blue dye exclusion method of establishing culture viability, dual staining demonstrated that under stressful conditions a significant proportion of cells that excluded Trypan blue were also moribund through apoptosis, i.e. programmed cell death. This chapter presents preliminary results on the application of fluorescence imaging for a more detailed classification of cells by identifying apoptotic and necrotic cells in-situ.

6.2 Identification of Apoptosis and Necrosis- Why is it Crucial?

Even though cell cultures are sometimes treated as a homogeneous mixture of identical cells, the fact is that individual cells exhibit heterogeneity as a result of small differences in their cellular metabolism and cell-cycle dynamics. Repeated progression through the cell cycle yields a heterogeneous population in which individual cells differ according to their size and intracellular state (Henson, 2003).

There have been accounts in literature of an increase in the rate of MAb production associated with the onset of cell death (Simpson *et al.*, 1997). This negative association between productivity and cell growth has been attributed duly in part to the passive release of MAb stored in cytoplasmic vesicles (Al-Rubeai *et al.*, 1992). As cells die and membrane integrity deteriorates, the cytoplasmic content of the cell is released. Experiments have been

conducted with hybridoma cultures where cell growth was slowed by either a DNA synthesis inhibitor (thymidine or hydroxyurea) or by a selective inhibitor of initiation of nonantibody protein (potassium acetate) and exhibited 50-130 % MAb production rate enhancement for growth slowed up to 50 % (Suzuki and Ollis, 1990).

It has been hypothesized in the current research that cells at different stages of the cell cycle may exhibit different product formation rates and different death rates in the absence of nutrients. Therefore, identifying different patterns of cell death such as apoptosis or necrosis may be essential for obtaining an accurate model of the operation.

6.3 Differentiation between Apoptosis and Necrosis

As apoptosis marks the onset of cell death, it is important to accurately distinguish between the apoptotic and necrotic states from the stand-point of the current work. Table 6-1 and Figure 6-1 enlist the differences between the two modes of cell death based on morphology.

Table 6-1: Differential Features and Significance of Necrosis and Apoptosis

adapted from (Wyllie, 2004)

Apoptosis	**Necrosis**
Morphological Features	
• Protrusions on the cell membrane, but no loss of membrane integrity • Aggregation of chromatin in the nuclear membrane • Begins with shrinking of cytoplasm and condensation of nucleus • Ends with fragmentation of cell into smaller bodies • Formation of membrane bound vesicles	• Loss of membrane integrity • Begins with swelling of cytoplasm and mitochondria • Ends with total cell lysis

(apoptotic bodies) • Mitochondria become leaky due to pore formation involving proteins of the bcl-2 family	• No vesicle formation, complete lysis • Disintegration (swelling) of organelles
Biochemical features	
• Tightly regulated process involving activation and enzymatic steps • Energy(ATP)-dependent process (active process, does not occur at 4˚C)	• Loss of regulation of ion homeostasis • No energy requirements (passive process, can occur even at 4˚C)
Physiological significance	
• Affects individual cells • Induces physiological stimuli (lack of growth factors, changes in hormonal environment) • No inflammatory response	• Affects groups of contiguous cells • Evoked by non-physiological disturbances (complement attack, lytic viruses, hypothermia, hypoxia, hyperoxia, ischemica, metabolic toxins) • Significant inflammatory response

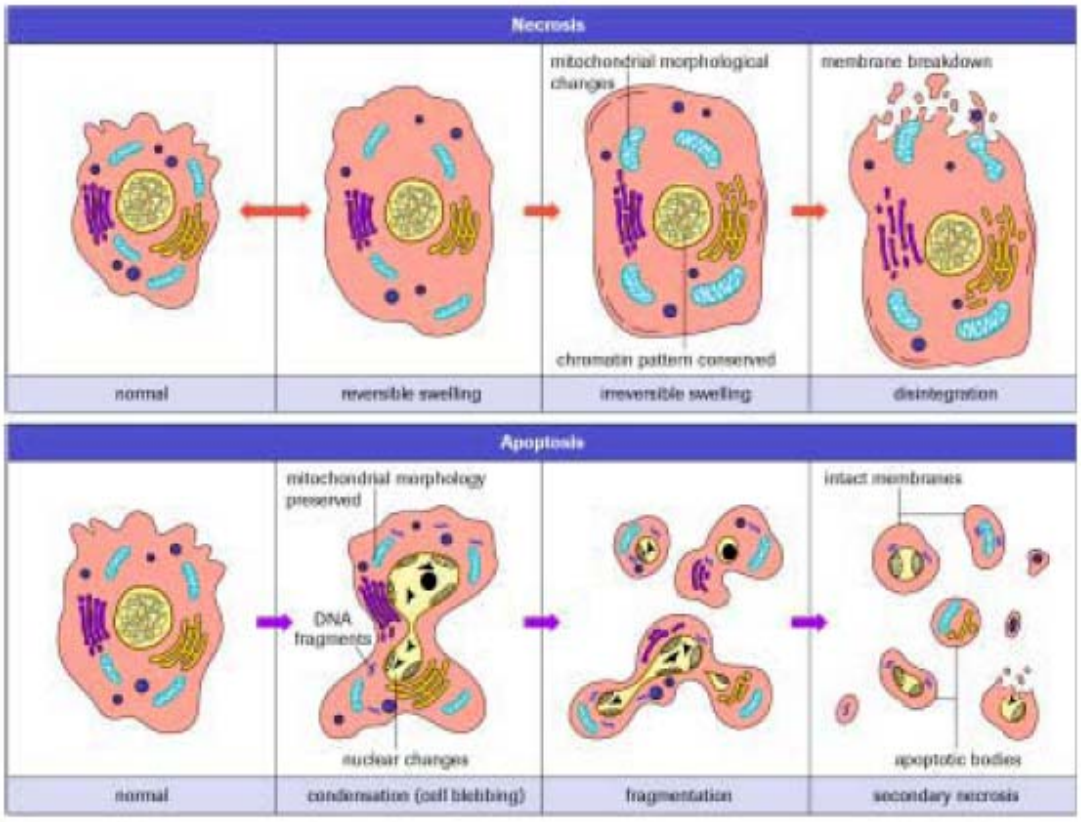

Figure 6-1 Illustration of the Morphological Features of Necrosis and Apoptosis borrowed from (Wyllie, 2004)

6.3.1 Morphology in Apoptosis and Necrosis

It has been documented that cell morphology may be used to infer the state of a cell. Each stage of the cell-life cycle exhibits characteristic morphology. Fluorescence imaging provides the means of identifying the different stages of cell growth and death by capturing the changes in cell morphology as the cell progresses through the various stages of its life-cycle (Mercille and Massie, 1994; Renvoize *et al.*, 1997; Ziegler *et al.*, 2004).

Sources from available literature (Mercille and Massie, 1994: Renvoize *et al.*, 1997; Wyllie, 2004) have classified the various stages of growth and death morphologically as in Table 6-2.

Table 6-2: Morphological Characteristics of Various Stages of Cell Growth and Death

Cell Morphology	Identifying Characteristics
Viable Non-apoptotic (VNA)	Cytoplasm intact, nucleus intact
Viable Apoptotic (VA)	Cell-shrinkage, rounding-up, loss of contact with adjacent cells
Non-viable Apoptotic (NVA)- Early	Highly condensed chromatin in the shape of crescents around the periphery of the nucleus or present as groups of spherical beads/ Surface protrusions
Non-viable Apoptotic (NVA)- Late	Cell fragmentation into apoptotic bodies
Non-viable Necrotic (NEC)	Swelling of entire cell, ruptured plasma membrane, release of intracellular constituents and slow dissolution of the nucleus

6.3.2 Dual Channel Fluorescence Staining for Apoptosis and Necrosis

Before proceeding towards the classification of cells in batch and fed-batch cultures, it is imperative to be able to independently identify apoptosis and necrosis. In order to do so, assays for apoptosis and necrosis were performed whereby cell death was induced in a cell culture in the exponential phase of growth.

The determination of cell death by apoptosis is made primarily on the basis of distinct structural changes in the cell's chromatin that occur prior to the lysis of the membrane. These changes include the aggregation of chromatin in the nuclear membrane and may be accompanied by the appearance of protrusions on the cell membrane, but without any loss of membrane integrity.

Typically, apoptosis begins with the shrinkage of the cytoplasm and condensation of nucleus. Fragmentation of cell into smaller membrane bound vesicles (apoptotic bodies) marks the end of apoptosis (Coligan, 1994; Wyllie, 2004).

Basic protocol adopted for the purpose of characterization of apoptosis/necrosis utilizes the DNA-binding properties of fluorescent dyes- AO and EB. This protocol has been described in greater detail in Chapter 3 that discusses the various experimental methods adopted.

AO and EB are both intercalating fluorochromes that bind to the DNA to emit green and orange fluorescence respectively. AO can penetrate the plasma membrane and is thus taken up by both live and dead cells. It binds to the DNA staining it green and binds to the RNA making it fluoresce as red. On the other hand, EB cannot penetrate the cytoplasm and is therefore only taken up by non-viable cells that have suffered membrane disintegration. EB binds to the DNA making it appear orange and binds somewhat weakly to the RNA present that may give weak red fluorescence. Thus, viewed under a fluorescence microscope, a viable non-apoptotic cells cell stained with both AO and EB will have bright green nucleus with intact structure while early apoptotic cells will display bright green chromatin condensed in the form of crescents in the nucleus. As EB dominates AO fluorescence, a non-viable apoptotic cell will exhibit bright orange nucleus with widespread chromatin condensation and the non-viable necrotic cells will appear to be larger than the average cell in size and will exhibit an orange nucleus with cytoplasm intact and emitting orange-red to bright red fluorescence (Coligan, 1994; Mercille and Massie, 1994).

6.3.2.1 Induction of Apoptosis

Method for induction of apoptosis has been discussed in detail in Chapter 3. Briefly stating, cycloheximide was added to a cell culture at a final concentration of 25 µg/ml and incubated for overnight. Figure 6-2 exhibits the images taken for the cell culture and clearly shows the morphology exhibited during apoptosis. The details in Table 6-1 under 'Morphological Features' can be used as a guideline for characterization.

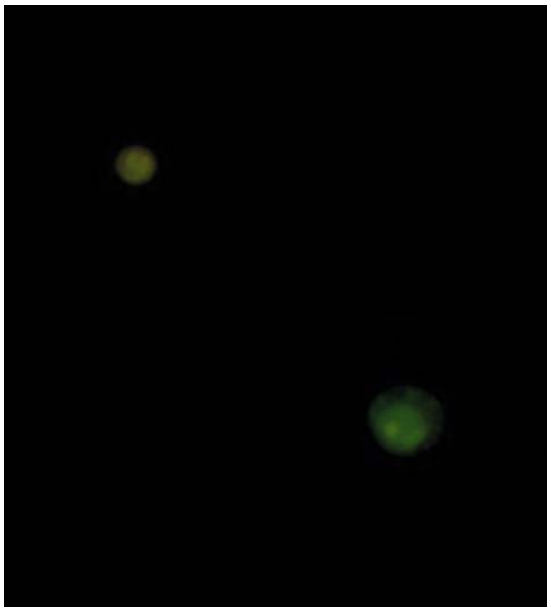

(a)

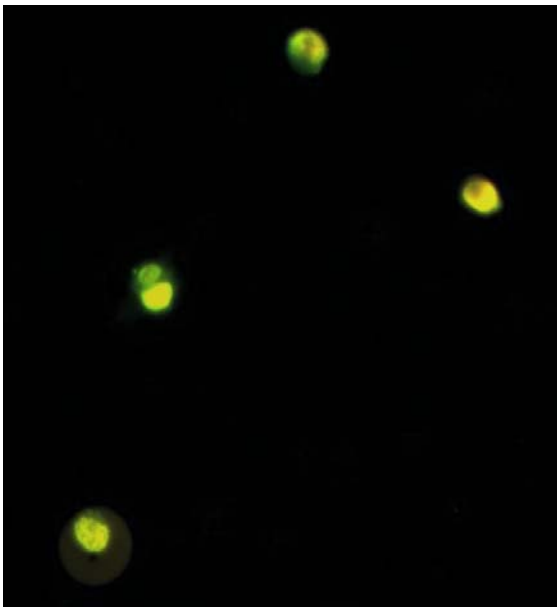

(b)

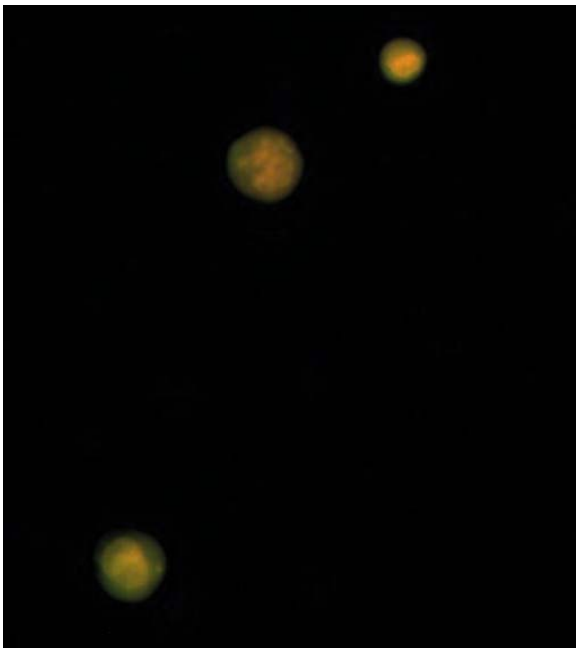

(c)

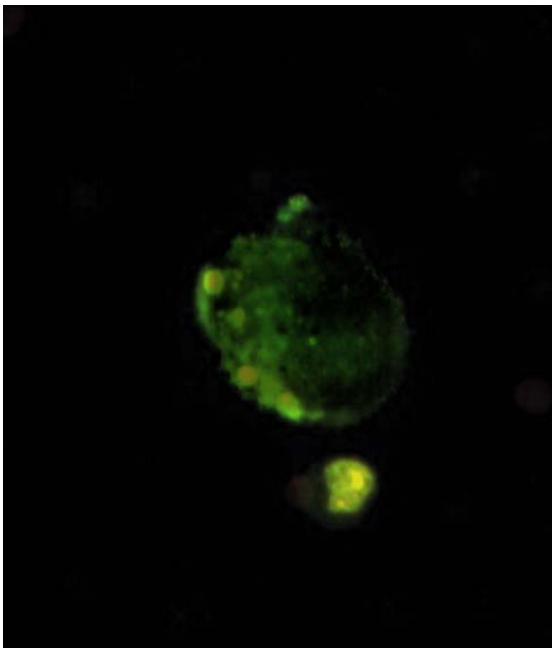

(d)

Continued on next page…

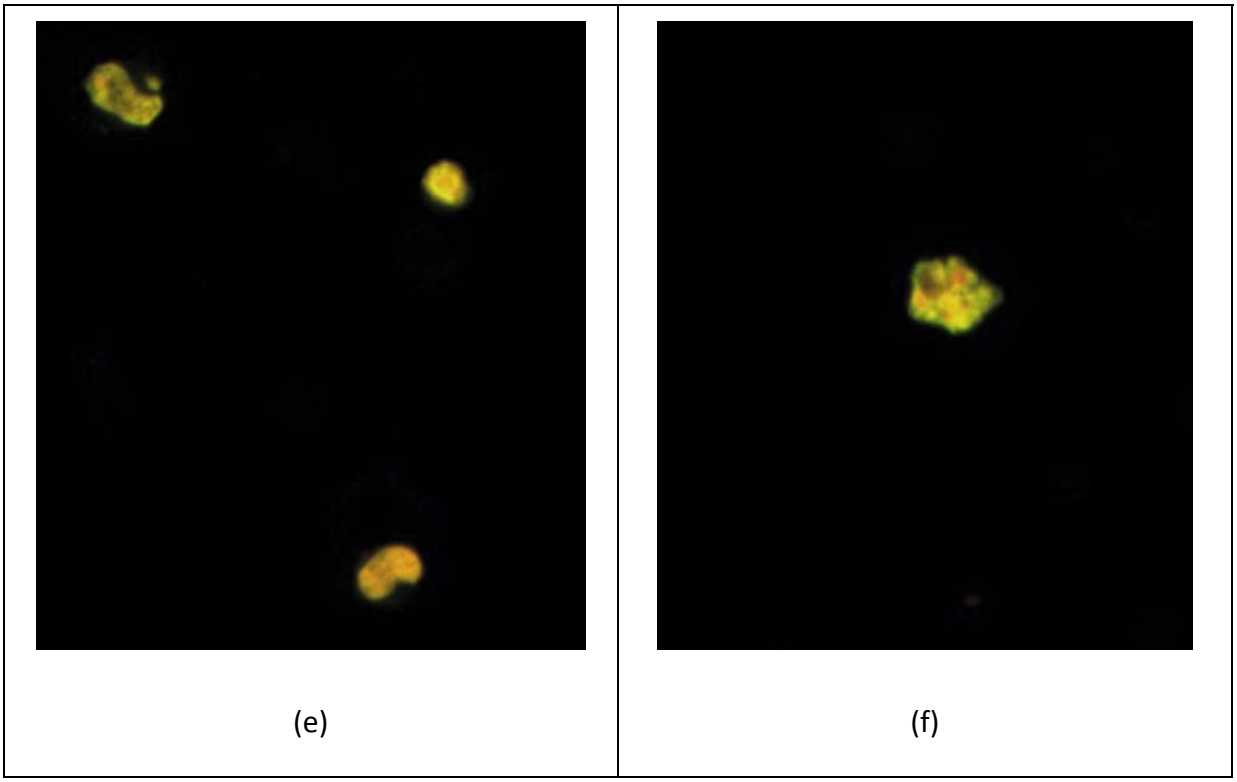

(e) (f)

Figure 6-2 Images of Apoptotic Cells Exhibiting Characteristic Associated Morphology

6.3.2.2 Induction of Necrosis

Method for induction of necrosis has been discussed in detail in Chapter 3. Briefly stating, HPLC grade ethanol was added to a cell culture at a final concentration of 25% v/v and incubated overnight. Figure 6-3 shows the images taken for the cell culture and clearly depicts the morphology exhibited during necrosis. The details in Table 6-1 under 'Morphological Features' can be used as a guideline for characterization.

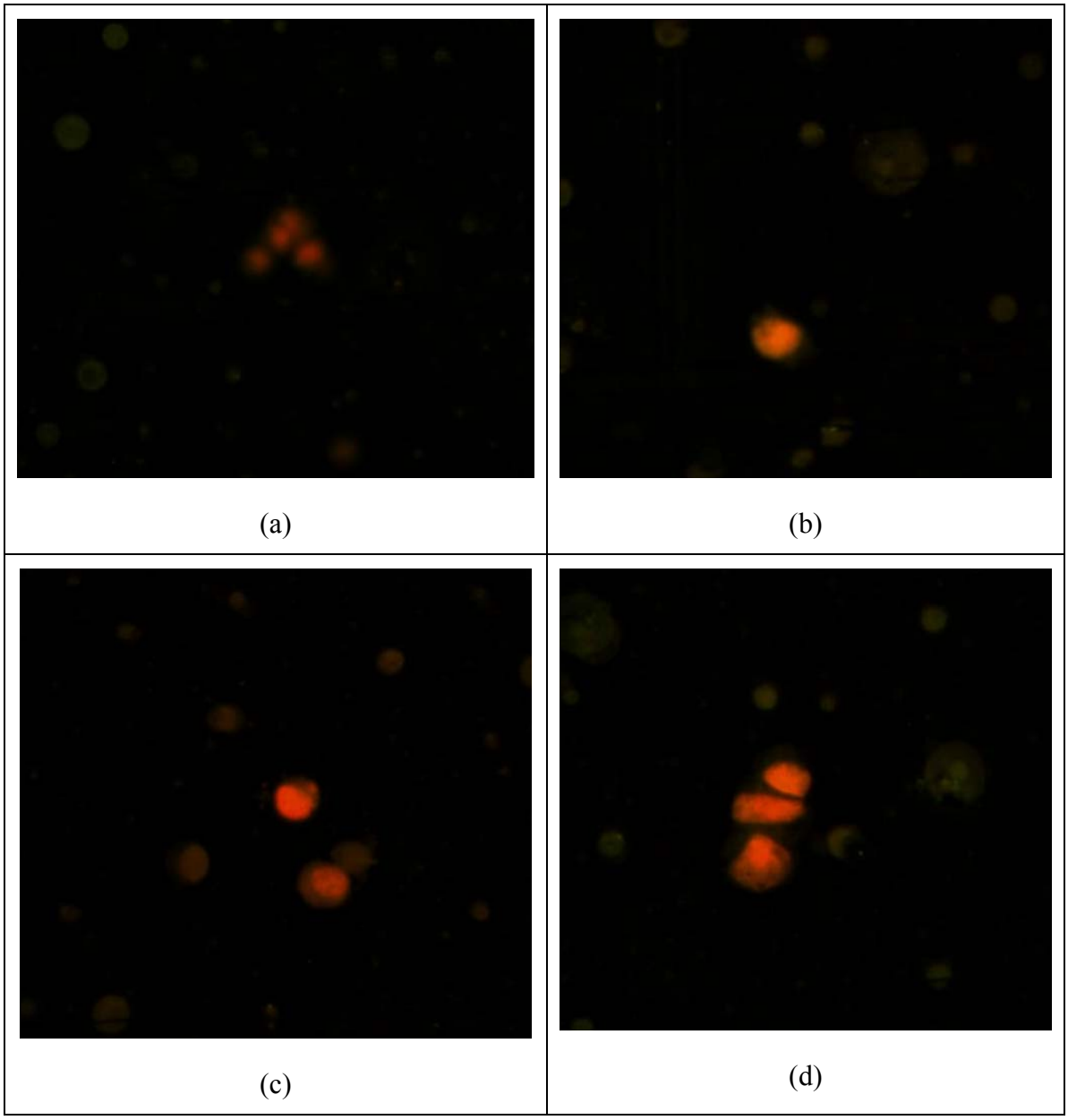

Figure 6-3 Images of Necrotic Cells Exhibiting Characteristic Associated Morphology

Based on the analysis of images for apoptotic and necrotic cell cultures, a general guideline for distinguishing the cell population was developed. Thus, the cells can be categorized as illustrated in Figure 6-4.

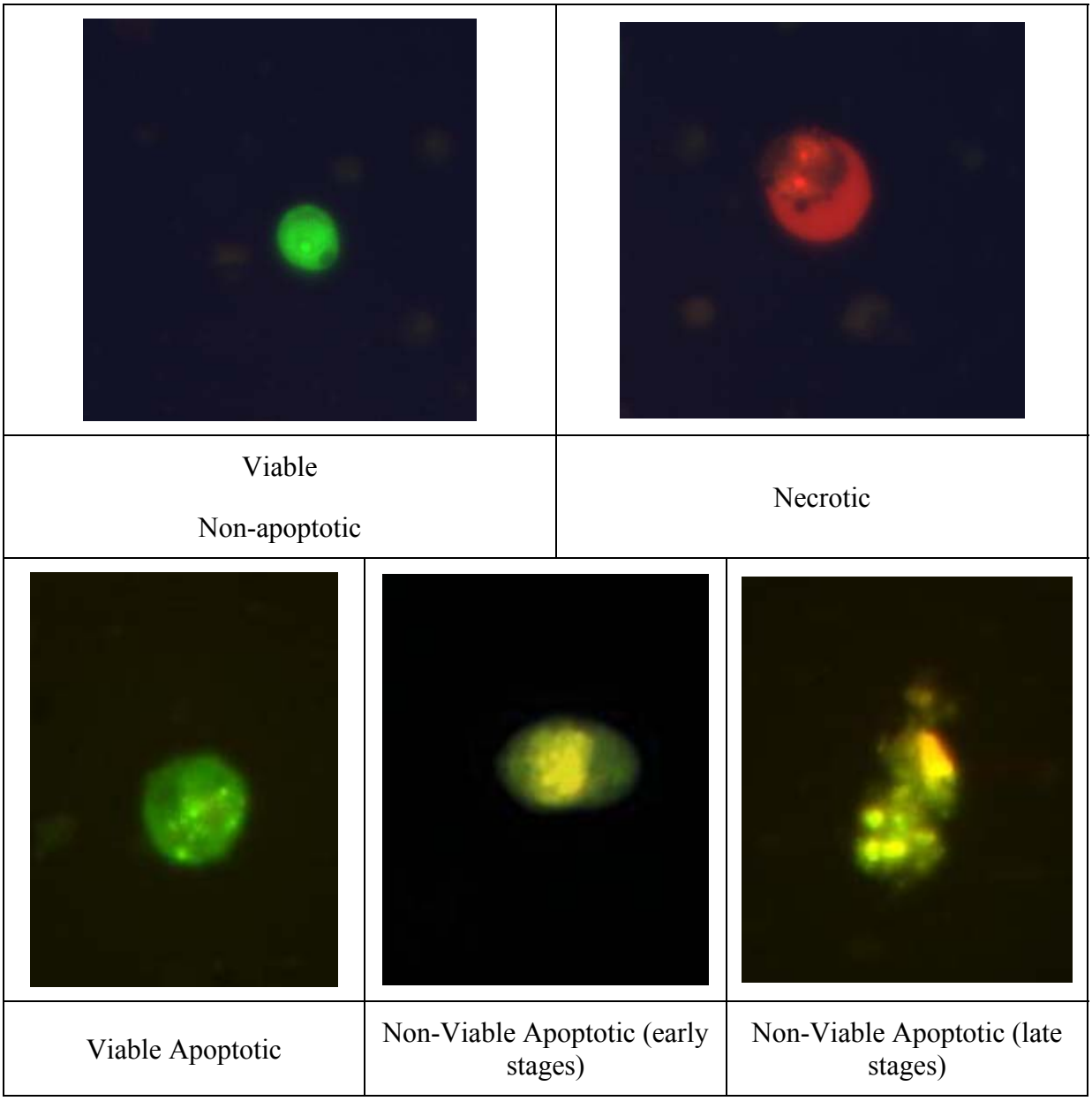

Figure 6-4 Images Exhibiting Characteristic Morphology for Cells in Different Stages of Growth/Death

6.4 Present Research Efforts

Efforts in the future focus on carrying out regular batch and fed-batch runs and characterization of the overall population into (i) Viable Non-apoptotic, (ii)Viable Apoptotic, (iii) Non-viable Apoptotic, (iv) Necrotic.

6.4.1 Preliminary Image Results for Batch Mode

Images shown in this section were obtained in experiments conducted with CHO IG1-9B8 for batch mode in spinners. Two frames for each day have been exhibited for a total duration of 12 days for which the experiment was run.

The culture was initiated on March 29 and incubated overnight. This period formed the lag period of the culture age. The images taken from the experiment have been illustrated in the figures that follow.

Figure 6-5 displays images taken after overnight incubation that revealed some chromatin condensation in the cell population indicating a slightly apoptotic cell population on day 1 of growth; the culture had not yet entered the exponential phase of growth. Images taken after another day of growth on day 2 illustrated an exponentially growing population with viable non-apoptotic cell population, i.e. green stained cells with a well-defined nucleus in their center.

March 30- Day 1	
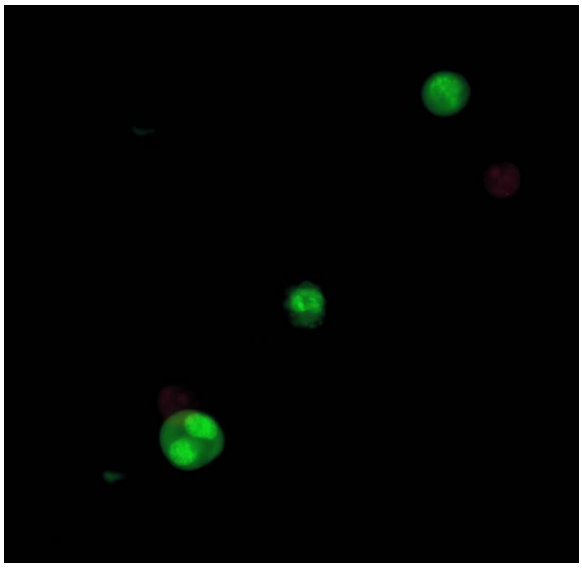	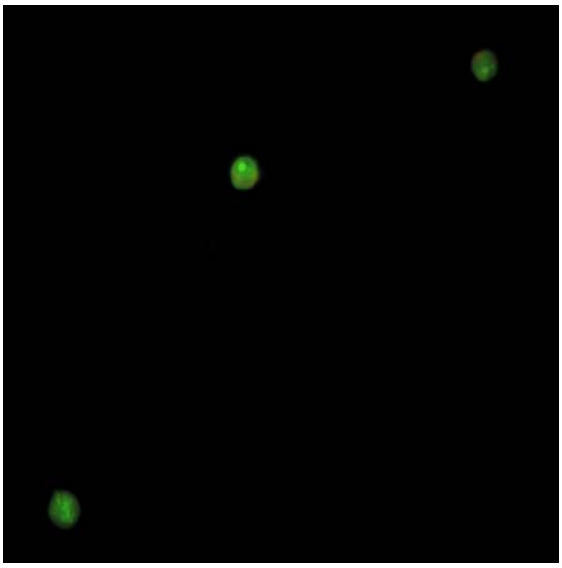
March 31-Day 2	
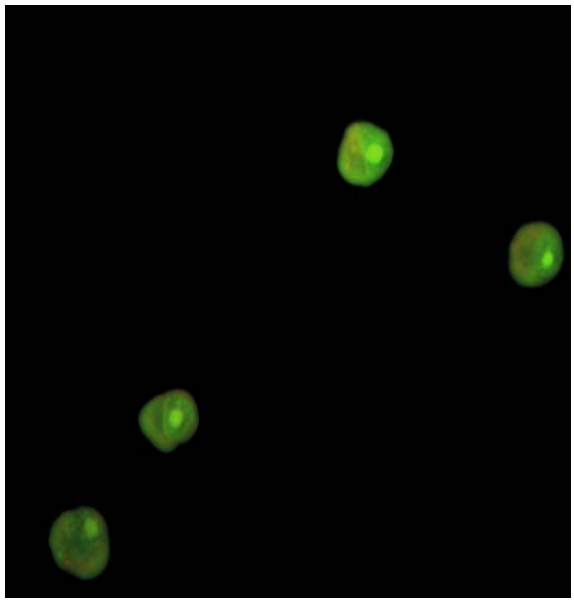	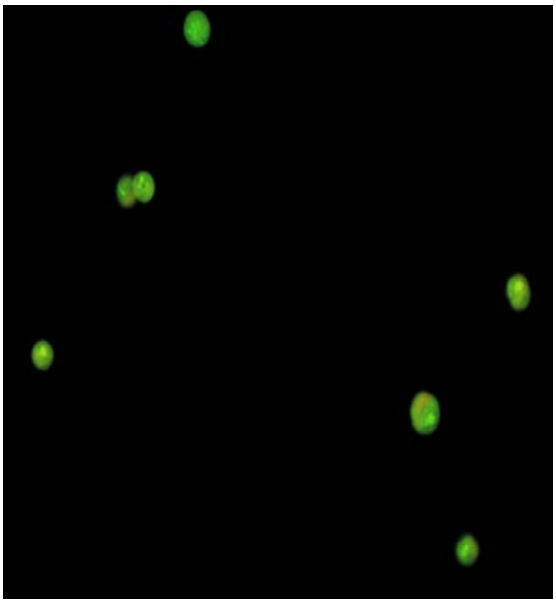

Figure 6-5 Day 1 and 2 of the Batch Culture Experiment

Figure 6-6 displays images taken on day 3 and 4 of culture. There was marked cell shrinkage and the appearance of “blebs” on the surface of the cells at the end of day 3 indicating the onset of apoptosis. On day 4, there was visible chromatin condensation in some of the cells with no loss of nuclear integrity further confirming apoptotic cell morphology.

April 1-Day 3	
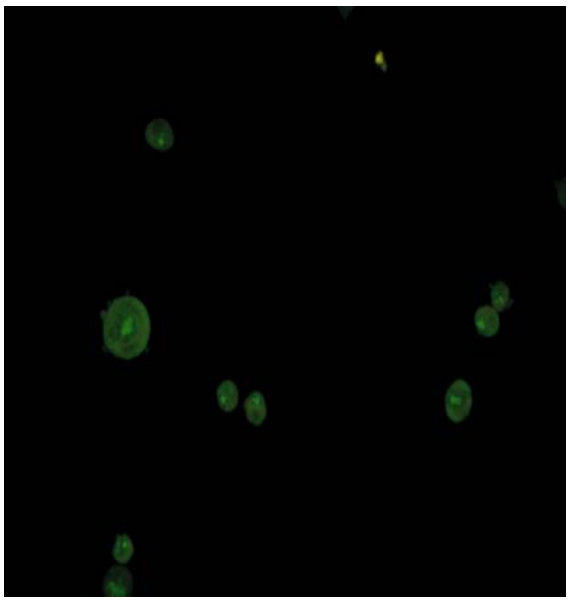	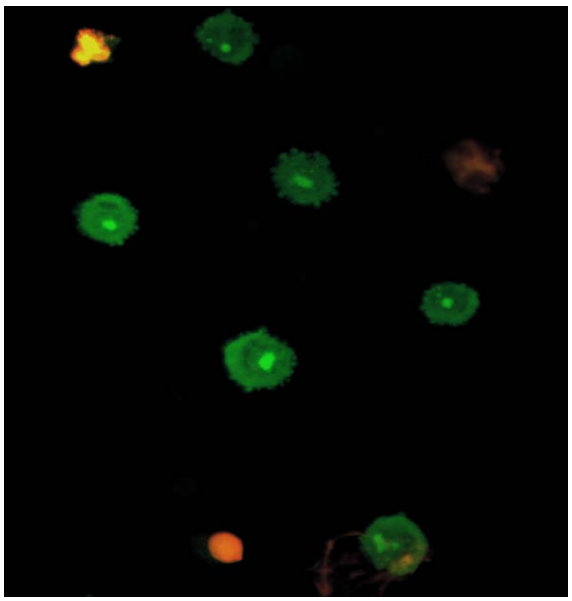
April 2-Day 4	
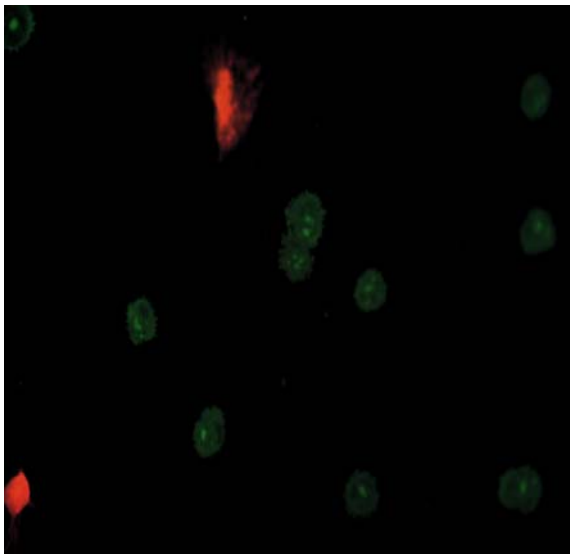	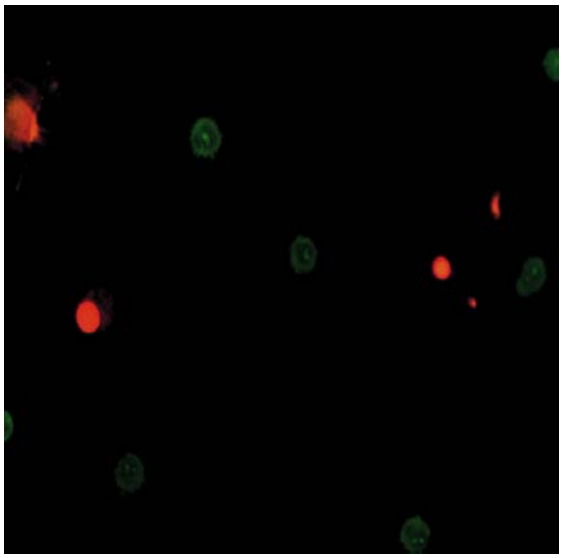

Figure 6-6 Day 3 and 4 of the Batch Culture Experiment

April 3-Day 5	
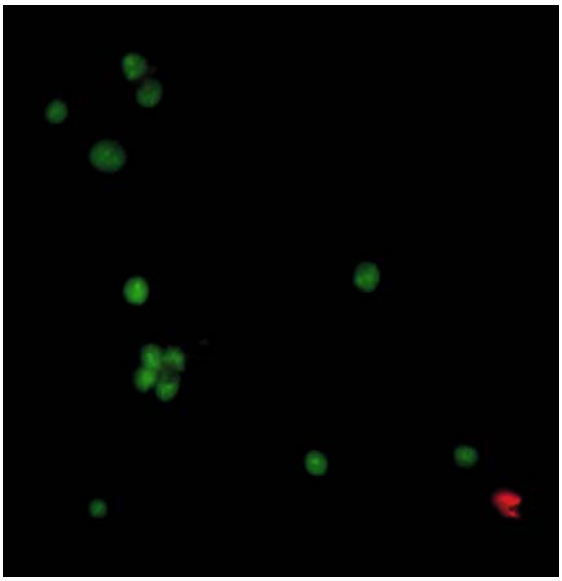	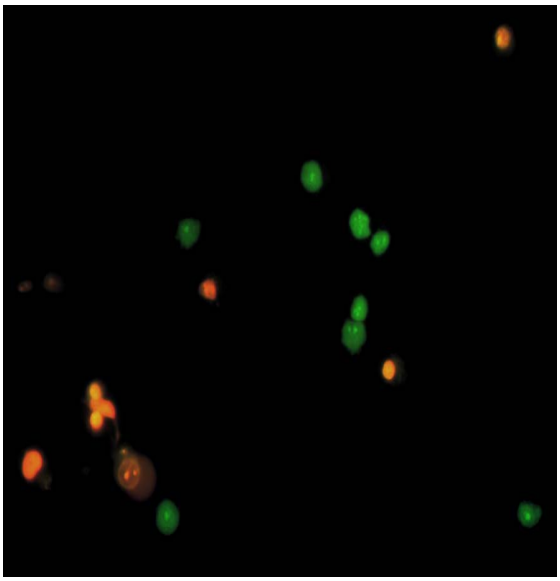
April 4-Day 6	
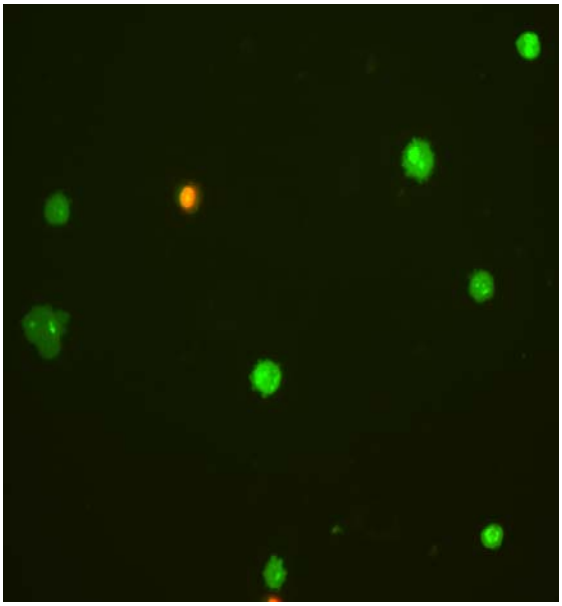	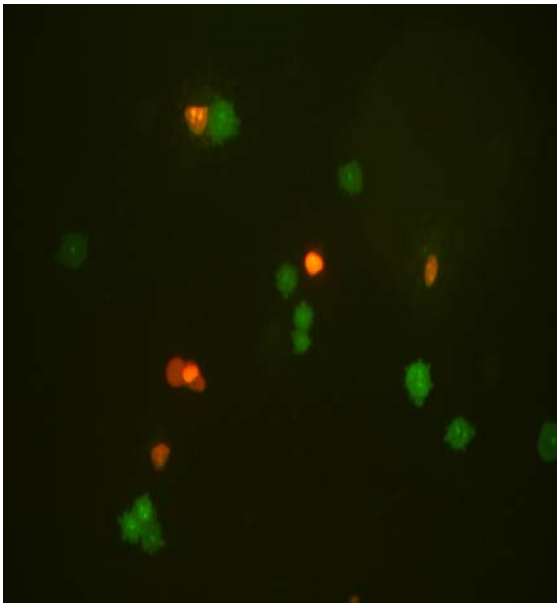

Continued on next page…

April 5-Day 7	
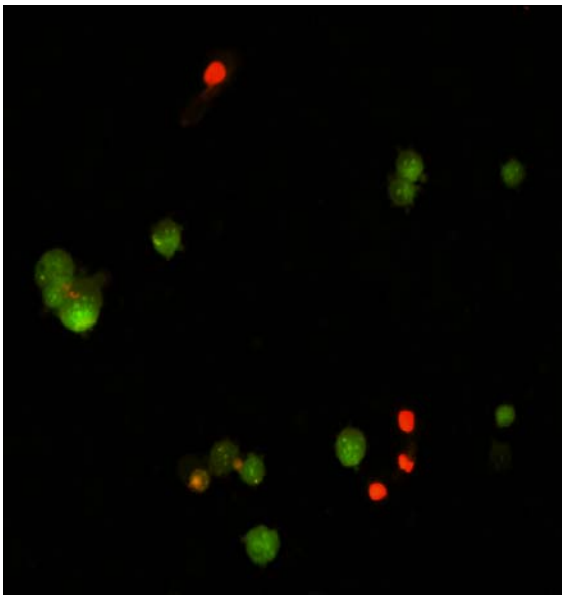	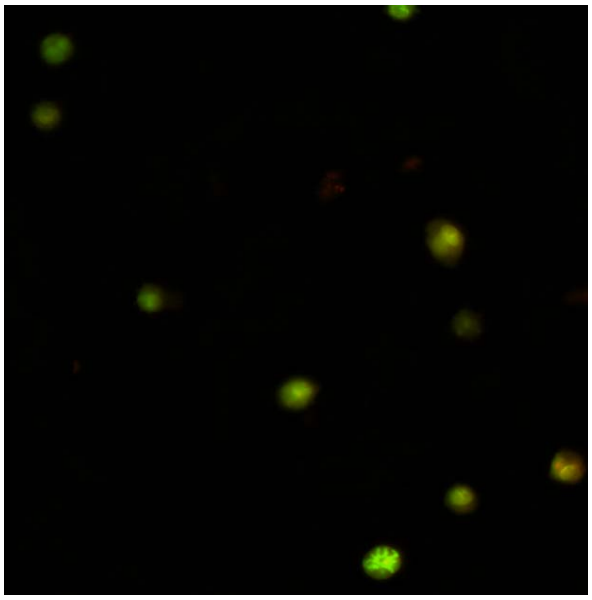

Figure 6-7 Day 5, 6 and 7 of the Batch Culture Experiment

As Figure 6-7 illustrates, on day 5 the chromatin condensation became more pronounced and widespread which is an indicator that the culture was largely apoptotic although apoptosis induction was still in its earlier stages. Over the progress of the day, some of the cells progressed to the late apoptotic stage where the cellular membrane exhibited permeability and stained orange. The trend continued on day 6 and 7 with some cells receding into the final stages of apoptotic death or secondary necrosis as indicated by the red stained cells. The cells stained green are also apoptotic since they show a large degree of chromatin condensation.

Figure 6-8 that follows on the next page confirms that the trend continued for the next two days with the progression of culture from early apoptosis to late apoptosis which is marked by a greater permeability of the cell membrane to Trypan Blue dye. This is confirmed by the results obtained from the Trypan Blue dye exclusion test in Figure 6-11 that displays a decline in cell viability.

April 6-Day 8	
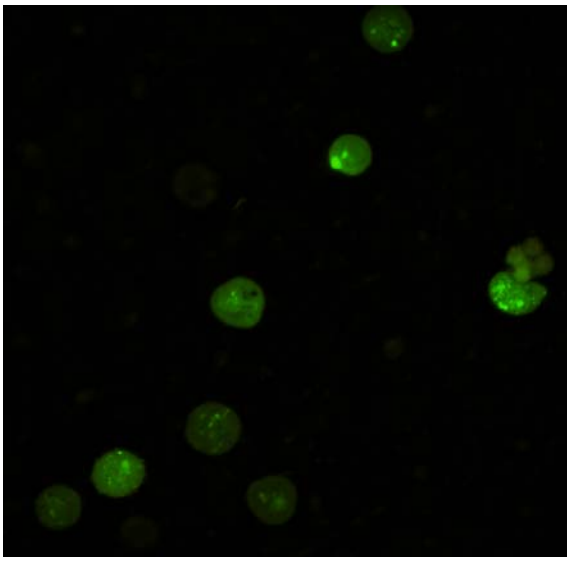	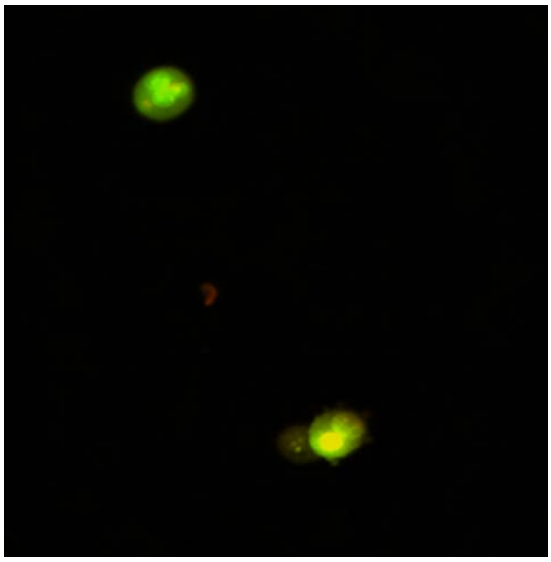
April 7-Day 9	
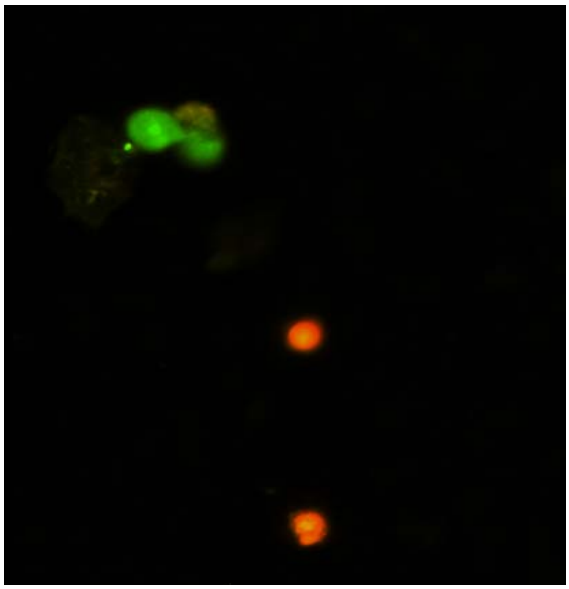	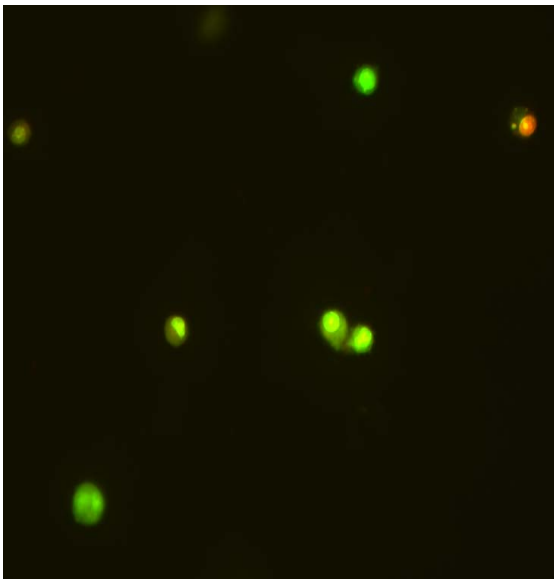

Figure 6-8 Day 8 and 9 of the Batch Culture Experiment

Figure 6-9 indicates that almost all cells in the culture had turned apoptotic by day 10 and this trend carried on to day 11 as evidenced by the formation of apoptotic bodies. By day 11, more than 50% of the cells had undergone death via apoptosis. There is sufficient reason to

believe that there was not sufficient primary necrosis as the cells did not show incidence of necrosis earlier in the run and the cells did not lose membrane integrity which is a salient characteristic of necrosis.

April 8-Day 10	
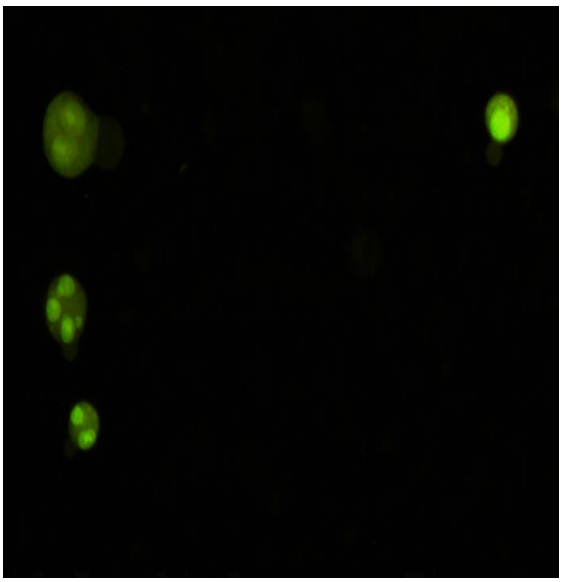	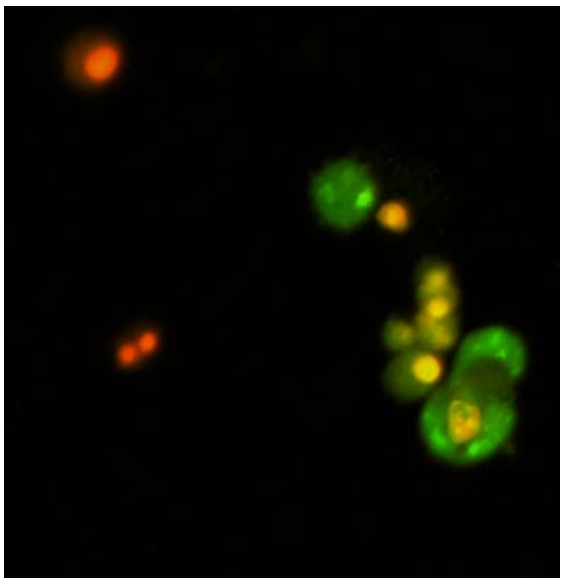
April 9-Day 11	
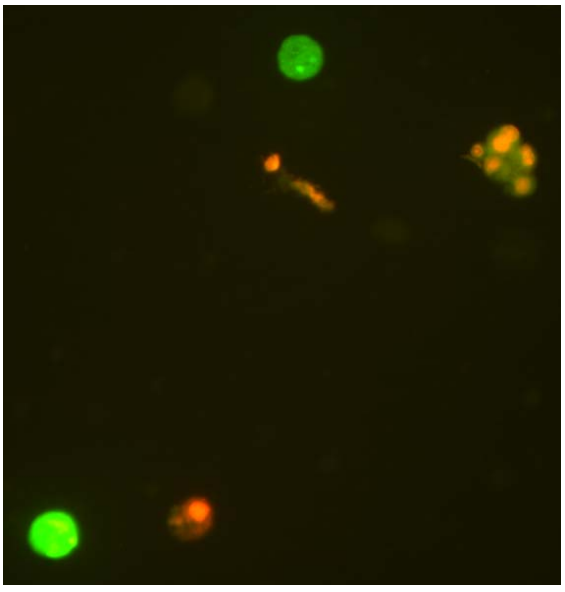	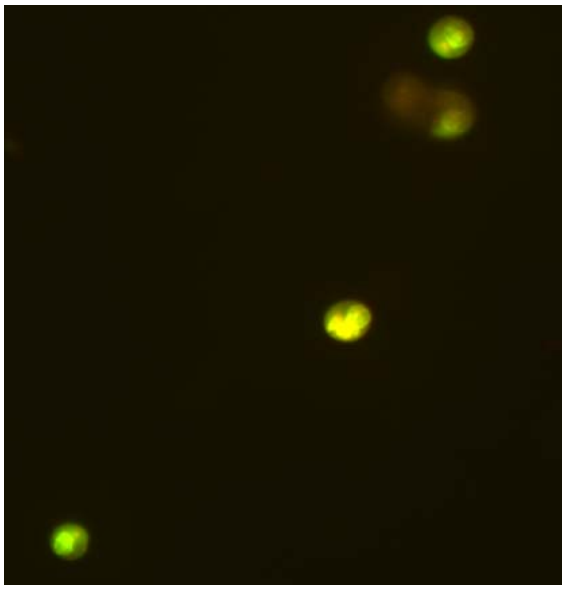

Figure 6-9 Day 10 and 11 of the Batch Culture Experiment

April 10- Day 12	
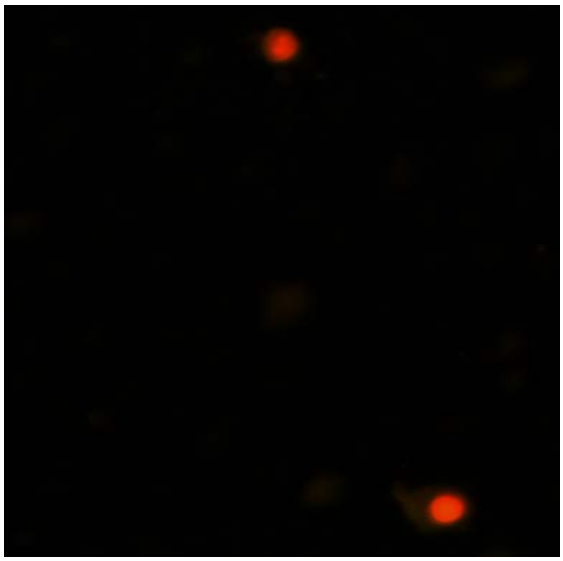	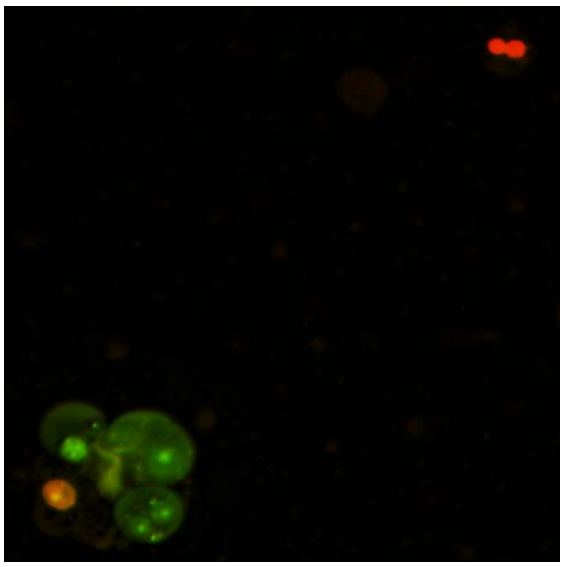
April 12-Day 14	
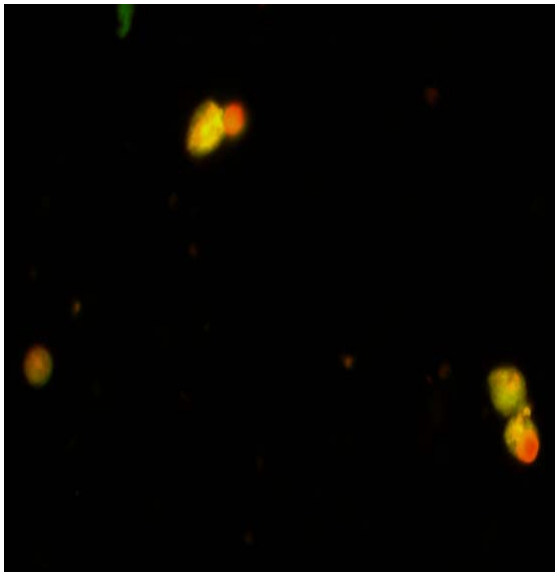	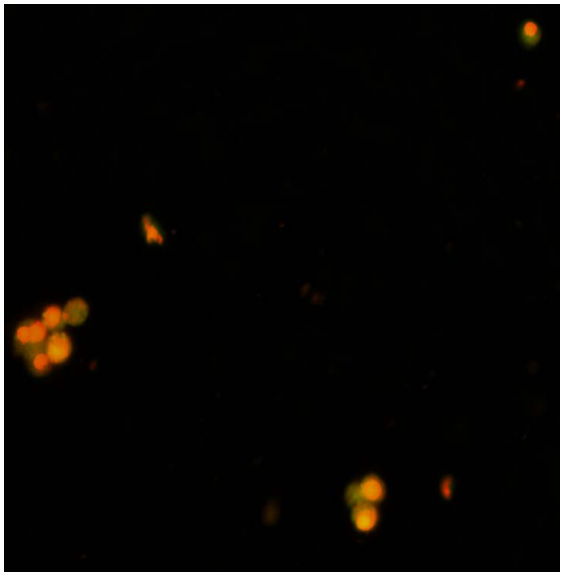

Figure 6-10 Day 12 and 14 of the Batch Culture Experiment

As is evident from Figure 6-10 and Figure 6-11, by the end of day 14, all cells were dead. This observation was supported by the results from the Trypan Blue dye exclusion test. The reader may see Appendix A for reference.

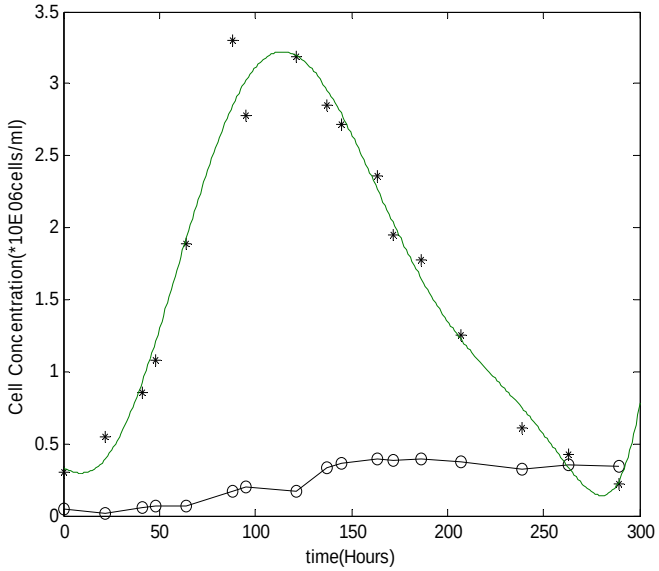

Figure 6-11 Viable(*) and Dead(o) Cell Concentration as per the Trypan Blue Exclusion Test

In addition, Mercille and Massie (1994) observed similar behavior in D5-hybridoma and attributed the induction of apoptosis in batch results to the exhaustion of glutamine. Further analysis of the culture supernatant sampled during the course of the experiment will yield valuable information about the possible factors leading to cell death by apoptosis and enable the analysis of MAb productivity.

Chapter 7
Conclusions and Recommendations

Dynamic models for batch and fed-batch operations were derived based on initial metabolic flux analysis. The simplified elementary fluxes and consequent model structure were similar for batch and fed-batch processes. However, differences in reaction rate constants were noted indicating a shift in energy metabolism during fed-batch operation. The results imply that the nutrients in fed-batch mode are essentially channeled towards cell-maintenance rather than growth.

It was observed from calculated flux values that while glutamine is not exhausted, the viable cell count was maintained at about 4.5×10^5 cells/ml and the dead cell count remained relatively low at 1×10^5 cells/ml until the very end of the experimental run. Also, during this period, the death rate k_d was significantly lower for fed-batch mode as compared to batch mode. Comparing the distribution of fluxes during batch and fed-batch operation, it is evident that the ratio of flux 8 (Pyr→Lac) to flux 2 (Pyr→TCA cycle) in batch culture is 2.41 while in fed-batch culture it equals 1.29, almost twice as high as in batch culture. Moreover, there is a slight increase in flux 1(Glc→Pyr) in fedbatch mode because there was no glucose limitation during fed-batch experiment. All these facts indicate that the energy-producing metabolism becomes more efficient in fed-batch as compared to batch. The reason could be a possible metabolic shift with higher emphasis on cellular maintenance rather than growth or metabolite accumulation. There is published evidence to support the above statement (Follstad, et al., 1999). Thus, although the set of significant fluxes remains the same in batch and fed-batch operations, the order of magnitude is different.

The model is an improvement over pre-existing models of similar nature as:

1. MFA has been applied to a fed batch situation in order to obtain a dynamic model for this mode of operation. The same structure of the dynamic model has been applied to both batch and fed-batch systems.
2. The viable and dead cell concentrations have been explicitly modeled. Correlation analysis has been used to investigate the dependencies of growth and death rates on nutrient and product concentrations.
3. The cell concentration model is coupled to the metabolite dynamic model that utilizes experimental starting values to generate an integrated model that predicts all significant system variables, including viable and dead cell concentrations, independent of subsequent experimental values.

However, there are some drawbacks in the model.

1. In the final predictions for the Integrated Model in fed-batch mode, there was a noticeable under-prediction of death and MAb concentration whose accurate prediction is the primary objective.
2. The proposed model does not account for viable apoptotic and non-apoptotic cells individually.

The difference between experimental data and corresponding predictions may be explained on the basis of the fact that viable cells can be further categorized as apoptotic and non-apoptotic. Available literature with regards to cell kinetics during fed-batch suggests that under nutrient limited conditions, the cells move from a viable, non-apoptotic state to a viable apoptotic state. This could lead to variation in antibody production rates and might explain inaccurate predictions for cell death and MAb in the current work. It is probable that these two different classes of viable cells have different rates of reaction or to be more specific, MAb production. Therefore, there is a possibility that the present model predicts an average rate of generation based on an averaging of apoptotic and non-apoptotic cells as

viable population. Thus, there is a clear motivation to monitor the evolution of apoptotic and non-apoptotic cells during operation.

Fluorescent images taken for batch experiments indicated that death of the CHO cells is primarily through apoptosis. This observation is similar to the work of Mercille and Massie (1994) who found that death of D5 hybridomas occurred primarily through apoptosis. They also found that such a trend coincided with the exhaustion of glutamine. Analysis of the culture supernatant is still pending and will yield valuable information in this regard. Such an analysis will yield useful information that can then be extended to fed-batch experiments and help in the modelling of individual cell populations present in culture more accurately and representing the trends of death and MAb production more accurately.

Additionally, it has been hypothesized in this work that under conditions of nutrient limitation there is a constant accumulation of apoptotic cells in the system. When the feeding is stopped, the apoptotic cells go into death mode almost instantaneously that would explain the sudden death scenario in fed-batch cultures. The current model only classifies the cell population as viable and dead. As a result, more detailed analysis of this switch from non-apoptotic to apoptotic state is required.

Based on the above, future work shall focus on the following points:

1. Use of fluorescence imaging as a tool to capture the changes in cell morphology along the course of experimental runs- batch and fed-batch and relate them to changes in concentrations of the various metabolites present in the system at any time.
2. Identification of an active death process such as apoptosis and the factors controlling it (as opposed to a passive one, i.e., necrosis) may lead to new strategies for the minimization of cell death during commercial operation of animal cell cultures. Specifically, this will aid in the design of an optimum fed-batch feeding regime with controlled nutrient supply that maximizes product formation with minimal toxin accumulation.

3. Modelling of the mechanisms leading to apoptosis at the intracellular level such as cell-cell signalling, activation of caspases and the correlation of this activation process to the extracellular metabolite levels.

Appendix A

Raw Experimental Data

SET-1

Batch Experiment-1

Time (hours)	Cell Hours	Viable Cell Concentration ($x10^6$ cells/mL)	% Viability	pH	IgG (mg/L)	GLC (g/L)	LAC (g/L)
1.00	0.0000	0.11	76.27	7.57			
25.10	4.8711	0.33	85.39	7.11			
49.50	20.8364	1.15	88.08	6.81			
73.50	47.1476	1.05	80.44	6.82			
76.00	0.0000	0.12	84.07	7.77			
98.50	2.3730	0.09	75.51	7.40			
123.50	8.0731	0.46	84.26	7.12			
143.00	23.1183	1.21	90.88	6.93			
145.00	0.0000	0.10	84.95	7.68	2.46	3.91	0.18
164.50	2.3505	0.15	85.29	0.00	2.92	3.62	0.44
192.00	12.4236	0.74	83.10	6.92	14.08	2.43	1.41
217.75	38.4855	1.34	94.19	6.90	26.54	1.70	1.68
239.00	61.4044	0.86	60.64	6.90	44.25	1.63	1.64
263.50	74.4412	0.30	18.62	7.16	33.08	1.63	1.63
287.00	77.9675	0.06	3.66	7.20	28.87	1.59	1.66
308.50	78.7504	0.02	1.32	7.15	35.93	1.67	1.77

Related Amino-acid Data

All the measurements for the amino-acid concentrations have been expressed in mmol/L.

Time (hours)	ASP	GLU	ASN	SER	GLN	HIS	GLY	THR	ALA	ARG
1.00	0.26	0.07	0.47	0.36	3.35	0.21	0.38	0.70	0.14	0.33
25.10	0.21	0.11	0.41	0.33	2.20	0.17	0.34	0.62	0.43	0.26
49.50	0.08	0.09	0.32	0.28	0.27	0.09	0.30	0.48	1.07	0.12
73.50	0.01	0.02	0.28	0.33	0.00	0.08	0.36	0.46	1.32	0.13
76.00	0.25	0.06	0.45	0.36	3.31	0.20	0.37	0.69	0.16	0.33
98.50	0.23	0.10	0.42	0.34	2.65	0.18	0.35	0.64	0.27	0.29
123.50	0.18	0.14	0.36	0.32	1.27	0.14	0.34	0.55	0.64	0.20
143.00	0.09	0.12	0.31	0.33	0.05	0.09	0.30	0.48	1.10	0.12
145.00	0.27	0.06	0.47	0.39	3.35	0.21	0.41	0.73	0.15	0.35
164.50	0.26	0.10	0.46	0.41	2.83	0.19	0.47	0.72	0.36	0.33
192.00	0.15	0.13	0.37	0.34	0.92	0.13	0.37	0.57	0.85	0.19
217.75	0.03	0.06	0.32	0.33	0.00	0.09	0.38	0.52	1.34	0.14
239.00	0.01	0.03	0.29	0.33	0.00	0.09	0.52	0.52	1.45	0.15
263.50	0.02	0.03	0.26	0.33	0.00	0.09	0.62	0.54	1.53	0.16
287.00	0.04	0.04	0.24	0.33	0.00	0.09	0.64	0.54	1.55	0.17
308.50	0.06	0.05	0.22	0.33	0.00	0.09	0.65	0.55	1.60	0.18

Time (hours)	TYR	VAL	MET	TRP	PHE	ILE	LEU	LYS	PRO
1.00	0.33	0.70	0.18	0.06	0.33	0.63	0.62	0.45	0.23
25.10	0.30	0.60	0.15	0.05	0.31	0.55	0.53	0.57	0.23
49.50	0.22	0.41	0.08	0.03	0.22	0.37	0.27	0.34	0.30

73.50	0.21	0.37	0.07	0.03	0.22	0.31	0.22	0.34	0.43
76.00	0.33	0.70	0.19	0.06	0.34	0.66	0.66	0.62	0.28
98.50	0.30	0.63	0.17	0.05	0.32	0.58	0.58	0.57	0.25
123.50	0.26	0.51	0.12	0.04	0.27	0.46	0.41	0.50	0.24
143.00	0.23	0.39	0.08	0.03	0.23	0.34	0.24	0.38	0.29
145.00	0.34	0.70	0.19	0.05	0.33	0.66	0.65	0.62	0.29
164.50	0.33	0.69	0.19	0.05	0.32	0.60	0.59	0.60	0.29
192.00	0.26	0.47	0.11	0.03	0.24	0.41	0.33	0.36	0.26
217.75	0.23	0.41	0.08	0.03	0.22	0.35	0.24	0.36	0.46
239.00	0.22	0.38	0.08	0.03	0.22	0.29	0.22	0.36	0.51
263.50	0.23	0.38	0.09	0.03	0.23	0.28	0.22	0.41	0.56
287.00	0.23	0.38	0.09	0.03	0.23	0.27	0.22	0.39	0.59
308.50	0.23	0.38	0.10	0.03	0.23	0.27	0.22	0.39	0.60

Batch Experiment-2

Time (hours)	**Viable Cell Concentration ($x10^5$ cells/mL)**	**%Viability**	**GLC (g/L)**	**LAC (g/L)**	**GLN (mmol/L)**	**GLT (mmol/L)**
0	1.00	86.52	4	0.003	4	0.106
1	1.31	71.43	2.99	0.135	3.92	0.307
19	1.04	70.76	2.48	0.191	3.66	0.585
23	1.58	77.78	3.64	0.688	2.21	0.18
27	1.53	79.22	3.52	0.745	2.21	0.206
43	3.88	84.24	2.81	1.38	1.62	0.213
47	4.15	90.71	2.68	1.49	1.3	0.238
51	5.43	88.93	2.58	1.59	1.08	0.24

52	5.80	88.93	2.45	1.5	1.04	0.233
55	6.55	93.24	2.4	1.66	0.824	0.242
56	6.81	93.24	2.37	1.71	0.767	0.223
67	8.05	90.06	2.14	1.84	0.125	0.207
68	8.16	90.06	2.12	1.87	0.103	0.221
71	8.90	89	2.1	1.84	0.043	0.221
72	9.14	89	2.09	1.86	0.029	0.212
75	10.00	80.65	2.08	1.85	0	0.229
76	10.30	80.65	2.09	1.86	0.003	0.194
80	9.60	85.33	2.03	1.84	0	0.21
81	9.41	85.33	1.99	1.83	0.004	0.194
96	6.95	63.47	1.89	1.8	0	0.212
97	6.81	63.47	1.86	1.82	0	0.225
100	7.75	59.16	1.85	1.83	0	0.218
101	8.08	59.16	1.83	1.81	0	0.223
104	6.85	56.61	1.88	1.87	0	0.237
105	6.47	56.61	1.83	1.84	0	0.22
116	5.00	50.25	1.84	1.84	0	0.24
120	5.50	52.88	1.9	1.84	0	0.247
124	4.20	39.81	1.9	1.81	0	0.242
140	4.15	33.6	1.79	1.73	0	0.28
144	2.60	22.61	1.86	1.79	0	0.289
148	3.15	26.25	1.87	1.87	0	0.293
164	1.60	11.99	1.86	1.83	0	0.289

168	1.85	15.88	1.82	1.75	0	0.323
172	0.46	13.96	1.84	1.75	0	0.315
189	0.80	5.67	1.85	1.84	0	0.329
194	0.65	5.94	1.84	1.77	0	0.333

Related Amino-Acid Data

All the concentration measurements for the amino-acids have been expressed in mmol/L.

Time (hours)	ASP	GLU	ASN	SER	GLN	HIS	GLY	THR	ALA	ARG
19	0.22	0.17	0.4	0.37	2.28	0.2	0.38	0.64	0.46	0.32
23	0.21	0.13	0.41	0.37	2.36	0.21	0.39	0.65	0.47	0.32
27	0.22	0.14	0.41	0.38	2.34	0.21	0.4	0.66	0.51	0.32
43	0.19	0.19	0.39	0.35	1.52	0.18	0.43	0.62	0.84	0.29
47	0.19	0.18	0.37	0.34	1.33	0.17	0.62	0.6	0.91	0.27
51	0.18	0.18	0.37	0.34	1.12	0.17	0.39	0.59	1.01	0.26
52	0.18	0.18	0.36	0.32	1.06	0.16	0.37	0.58	0.99	0.25
55	0.17	0.18	0.34	0.31	0.82	0.15	0.4	0.56	1.08	0.24
56	0.16	0.18	0.34	0.31	0.75	0.15	0.37	0.55	1.1	0.24
67	0.15	0.19	0.34	0.37	0.19	0.13	0.38	0.56	1.5	0.23
68	0.14	0.17	0.32	0.35	0.16	0.12	0.35	0.52	1.42	0.2
71	0.13	0.17	0.31	0.35	0.07	0.12	0.34	0.51	1.42	0.2
72	0.13	0.16	0.27	0.31	0.04	0.11	0.34	0.46	1.3	0.18
75	0.12	0.16	0.29	0.33	0.04	0.11	0.39	0.49	1.41	0.19
76	0.13	0.17	0.32	0.37	0.06	0.12	0.37	0.54	1.53	0.21
80	0.13	0.18	0.33	0.39	0.03	0.12	0.45	0.57	1.66	0.22
81	0.12	0.16	0.31	0.36	0.04	0.12	0.46	0.54	1.59	0.21
96	0.1	0.16	0.28	0.3	0.02	0.12	0.6	0.53	1.68	0.21

97	0.1	0.17	0.28	0.29	0.03	0.12	0.58	0.52	1.63	0.21
100	0.1	0.17	0.28	0.28	0.02	0.12	0.64	0.54	1.72	0.21
101	0.1	0.18	0.28	0.29	0.03	0.12	0.69	0.57	1.82	0.23
104	0.09	0.17	0.26	0.25	0.02	0.12	0.64	0.51	1.66	0.2
105	0.1	0.18	0.27	0.26	0.03	0.12	0.68	0.54	1.74	0.21
116	0.09	0.18	0.24	0.23	0.02	0.11	0.69	0.5	1.65	0.2
120	0.09	0.18	0.23	0.22	0.02	0.12	0.66	0.49	1.63	0.19
124	0.09	0.18	0.22	0.21	0.03	0.11	0.68	0.48	1.61	0.19
140	0.1	0.21	0.23	0.22	0.02	0.12	0.8	0.54	1.88	0.21
144	0.12	0.21	0.19	0.2	0.03	0.11	0.78	0.51	1.8	0.2
148	0.12	0.22	0.19	0.21	0.03	0.11	0.8	0.53	1.84	0.2
164	0.13	0.23	0.18	0.21	0.02	0.1	0.79	0.51	1.82	0.19
168	0.11	0.21	0.16	0.18	0.02	0.1	0.73	0.46	1.63	0.17
172	0.12	0.22	0.16	0.19	0.02	0.11	0.75	0.47	1.65	0.18
189	0.14	0.23	0.15	0.19	0.02	0.11	0.78	0.49	1.72	0.18
194	0.14	0.24	0.16	0.19	0.02	0.11	0.8	0.5	1.78	0.18

Time (hours)	**TYR**	**VAL**	**MET**	**TRP**	**PHE**	**ILE**	**LEU**	**LYS**	**PRO**
19	0.31	0.59	0.17	0.08	0.33	0.57	0.58	0.66	0.28
23	0.32	0.61	0.17	0.08	0.34	0.59	0.6	0.7	0.26
27	0.33	0.61	0.18	0.08	0.34	0.6	0.6	0.71	0.27
43	0.3	0.54	0.15	0.07	0.31	0.53	0.51	0.63	0.3
47	0.29	0.53	0.15	0.07	0.3	0.52	0.49	0.61	0.3
51	0.29	0.52	0.14	0.07	0.3	0.51	0.48	0.61	0.31
52	0.28	0.5	0.14	0.07	0.29	0.49	0.45	0.57	0.31
55	0.27	0.48	0.13	0.06	0.28	0.46	0.42	0.53	0.32
56	0.26	0.47	0.13	0.06	0.27	0.45	0.41	0.53	0.31

67	0.27	0.47	0.12	0.06	0.28	0.45	0.38	0.54	0.4
68	0.25	0.44	0.11	0.06	0.26	0.42	0.35	0.5	0.37
71	0.25	0.42	0.11	0.06	0.25	0.39	0.32	0.42	0.32
72	0.22	0.37	0.1	0.06	0.22	0.33	0.27	0.37	0.39
75	0.23	0.39	0.1	0.05	0.24	0.35	0.29	0.43	0.39
76	0.26	0.44	0.11	0.06	0.26	0.41	0.33	0.48	0.41
80	0.27	0.45	0.11	0.06	0.27	0.4	0.32	0.53	0.47
81	0.25	0.42	0.11	0.06	0.25	0.36	0.3	0.46	0.42
96	0.25	0.39	0.1	0.06	0.26	0.3	0.25	0.5	0.42
97	0.24	0.37	0.1	0.05	0.24	0.27	0.22	0.29	0.36
100	0.25	0.38	0.1	0.05	0.25	0.27	0.22	0.37	0.42
101	0.27	0.4	0.11	0.06	0.27	0.29	0.25	0.52	0.51
104	0.24	0.36	0.1	0.05	0.24	0.25	0.2	0.4	0.4
105	0.25	0.37	0.1	0.05	0.26	0.26	0.21	0.46	0.51
116	0.23	0.32	0.09	0.05	0.24	0.21	0.17	0.46	0.48
120	0.23	0.32	0.09	0.05	0.24	0.2	0.16	0.44	0.41
124	0.23	0.3	0.09	0.05	0.23	0.18	0.15	0.45	0.44
140	0.25	0.31	0.09	0.05	0.26	0.16	0.13	0.52	0.54
144	0.24	0.29	0.09	0.05	0.25	0.15	0.12	0.49	0.52
148	0.24	0.3	0.09	0.05	0.26	0.15	0.12	0.49	0.54
164	0.24	0.27	0.08	0.05	0.25	0.12	0.09	0.47	0.54
168	0.21	0.24	0.08	0.04	0.22	0.11	0.08	0.39	0.49
172	0.22	0.24	0.07	0.05	0.23	0.11	0.08	0.43	0.46
189	0.23	0.25	0.07	0.05	0.23	0.11	0.08	0.29	0.31
194	0.23	0.25	0.08	0.05	0.24	0.11	0.08	0.33	0.33

Fed-batch Experiment-1

Time (hours)	Viable Cell Concentration (x 10^5 cells/mL)	%Viability	GLC (g/L)	LAC (g/L)	GLN (mmol/L)	GLT (mmol/L)
0	1.00	86.52	4	0.003	4	0.106
1	0.78	76.54	3.01	0.13	3.89	0.303
19	0.88	84.85	2.54	0.171	3.63	0.576
23	1.18	82.46	3.68	0.668	2.29	0.187
27	1.61	76.79	3.57	0.721	2.4	0.2
43	2.15	86.87	2.98	1.26	1.88	0.23
47	3.35	87.01	2.8	1.36	1.54	0.254
51	3.53	87.58	2.75	1.52	1.38	0.263
52	3.46	87.58	2.79	1.55	1.47	0.266
55	4.08	90.06	2.57	1.52	1.27	0.243
56	3.24	90.06	2.45	1.19	1.85	0.214
67	5.50	90.16	2	1.49	1.1	0.233
68	4.97	90.16	2	1.33	1.4	0.215
71	5.05	88	1.91	1.39	0.832	0.252
72	4.70	88	1.85	1.29	1.37	0.216
75	4.10	93.71	1.84	1.45	1.17	0.227
76	3.58	93.71	1.7	1.26	1.34	0.202
80	4.80	91.43	1.62	1.49	1.15	0.224
81	3.97	91.43	1.69	1.11	1.62	0.202
96	5.60	92.56	0.99	1.66	1	0.221
97	5.32	92.56	1.06	1.63	1.1	0.213

100	5.05	83.47	0.951	1.67	0.944	0.213
101	4.59	83.47	1.05	1.69	1.04	0.216
104	5.50	87.4	0.989	1.69	0.938	0.204
105	4.69	87.4	1.24	1.27	1.5	0.197
116	4.65	84.55	0.962	1.6	1	0.211
120	5.80	87.88	0.893	1.6	0.799	0.222
124	4.65	85.32	0.802	1.61	0.645	0.223
125	4.29	85.32	0.826	1.7	0.681	0.201
140	6.70	79.76	0.598	1.7	0.277	0.235
144	5.30	70.2	0.507	1.79	0.137	0.235
148	3.95	62.7	0.485	1.92	0.084	0.235
164	4.00	55.17	0.342	1.96	0	0.24
168	3.55	51.08	0.327	1.84	0	0.227
172	0.60	38.4	0.336	1.88	0	0.243
189	1.65	20.5	0.333	1.98	0	0.267
194	1.05	13.82	0.322	1.88	0	0.265

Related Amino-acid Data

All the measurements for the amino acids have been expressed in mmol/L.

Time (hours)	MAb (mg/L)	ASP	GLU	ASN	SER	GLN	HIS	GLY	THR	ALA	ARG
19	5.33	0.22	0.12	0.44	0.39	2.76	0.2	0.4	0.71	0.43	0.34
23	6.90	0.21	0.11	0.41	0.38	2.66	0.19	0.36	0.7	0.45	0.32
27	5.97	0.23	0.14	0.43	0.4	2.73	0.2	0.39	0.75	0.52	0.34
43	8.46	0.2	0.17	0.4	0.36	1.97	0.18	0.37	0.69	0.82	0.31

47	9.31	0.2	0.19	0.41	0.37	1.84	0.18	0.39	0.71	0.97	0.31
51	10.30	0.19	0.18	0.37	0.33	1.47	0.17	0.35	0.64	0.99	0.27
52		0.19	0.18	0.37	0.33	1.54	0.16	0.35	0.66	0.98	0.27
55	10.87	0.17	0.17	0.36	0.32	1.3	0.15	0.35	0.63	1.06	0.26
56		0.2	0.15	0.39	0.35	2	0.17	0.36	0.69	0.83	0.29
67	13.23	0.18	0.18	0.38	0.34	1.29	0.15	0.4	0.67	1.25	0.28
68		0.19	0.15	0.37	0.33	1.55	0.17	0.36	0.65	1.02	0.28
71	14.99	0.18	0.15	0.36	0.33	1.37	0.15	0.37	0.65	1.13	0.27
72		0.19	0.16	0.4	0.35	1.49	0.16	0.4	0.69	1.21	0.3
75	17.96	0.19	0.16	0.38	0.34	1.56	0.16	0.85	0.69	1.14	0.29
76		0.2	0.16	0.4	0.35	1.64	0.19	0.39	0.7	1.12	0.29
80	13.69	0.17	0.15	0.36	0.3	1.28	0.15	0.37	0.63	1.16	0.27
81		0.18	0.12	0.36	0.31	1.76	0.15	0.39	0.64	0.86	0.28
96	16.74	0.18	0.17	0.39	0.37	1.17	0.15	0.37	0.68	1.4	0.29
97		0.18	0.17	0.38	0.37	1.32	0.15	0.37	0.69	1.32	0.29
100	21.22	0.16	0.16	0.37	0.38	1.03	0.14	0.36	0.65	1.39	0.28
101		0.17	0.16	0.37	0.37	1.09	0.15	0.39	0.65	1.36	0.28
104	15.24	0.16	0.15	0.35	0.34	0.98	0.14	0.35	0.62	1.32	0.26
105		0.17	0.12	0.36	0.34	1.5	0.15	0.36	0.64	1.03	0.28
116	20.82	0.17	0.15	0.38	0.34	1.12	0.15	0.42	0.67	1.38	0.29
120	21.12	0.17	0.16	0.38	0.34	0.97	0.18	0.41	0.66	1.45	0.28
124	23.23	0.15	0.15	0.35	0.34	0.74	0.13	0.37	0.61	1.44	0.26
125		0.16	0.15	0.34	0.34	0.76	0.13	0.37	0.61	1.43	0.26
140	31.63	0.16	0.17	0.36	0.35	0.32	0.12	0.47	0.66	1.85	0.28
144	32.17	0.15	0.17	0.32	0.32	0.16	0.11	0.53	0.64	1.92	0.27
148	38.65	0.16	0.18	0.34	0.32	0.1	0.12	0.59	0.67	2.06	0.28
164	44.55	0.13	0.16	0.26	0.21	0	0.09	0.62	0.57	1.87	0.23
168	44.45	0.13	0.17	0.26	0.2	0	0.09	0.66	0.58	1.91	0.23

172	50.46	0.14	0.18	0.28	0.2	0	0.1	0.7	0.6	1.99	0.24
189	53.27	0.15	0.2	0.28	0.19	0	0.1	0.8	0.64	2.14	0.26
194	68.94	0.14	0.2	0.26	0.17	0	0.1	0.83	0.6	2.02	0.24

Time (hours)	**TYR**	**VAL**	**MET**	**TRP**	**PHE**	**ILE**	**LEU**	**LYS**	**PRO**
19	0.33	0.67	0.17	0.1	0.35	0.63	0.64	0.71	0.31
23	0.31	0.66	0.16	0.05	0.33	0.62	0.62	0.69	0.28
27	0.34	0.69	0.17	0.05	0.35	0.64	0.63	0.55	0.23
43	0.32	0.63	0.15	0.05	0.34	0.62	0.61	0.79	0.31
47	0.33	0.65	0.15	0.05	0.34	0.62	0.6	0.76	0.31
51	0.29	0.57	0.13	0.04	0.29	0.52	0.49	0.34	0.18
52	0.29	0.58	0.13	0.03	0.29	0.51	0.47	0.29	0.24
55	0.29	0.56	0.13	0.04	0.3	0.54	0.51	0.65	0.29
56	0.31	0.64	0.15	0.04	0.33	0.62	0.6	0.71	0.3
67	0.3	0.59	0.13	0.04	0.31	0.56	0.52	0.61	0.36
68	0.3	0.59	0.13	0.04	0.3	0.56	0.53	0.45	0.22
71	0.29	0.59	0.13	0.04	0.31	0.57	0.53	0.65	0.32
72	0.31	0.62	0.14	0.04	0.32	0.59	0.55	0.64	0.35
75	0.31	0.62	0.14	0.04	0.32	0.59	0.55	0.62	0.35
76	0.31	0.63	0.14	0.04	0.33	0.61	0.57	0.49	0.23
80	0.28	0.57	0.13	0.04	0.3	0.54	0.5	0.59	0.33
81	0.28	0.58	0.14	0.04	0.29	0.55	0.52	0.53	0.3
96	0.31	0.61	0.14	0.05	0.32	0.6	0.55	0.69	0.35
97	0.31	0.62	0.14	0.04	0.32	0.59	0.54	0.61	0.37
100	0.29	0.58	0.13	0.04	0.3	0.55	0.5	0.55	0.38
101	0.29	0.58	0.13	0.04	0.29	0.54	0.49	0.29	0.28
104	0.28	0.55	0.12	0.04	0.28	0.52	0.47	0.28	0.26

105	0.28	0.59	0.14	0.04	0.3	0.56	0.54	0.58	0.33
116	0.3	0.61	0.14	0.04	0.31	0.59	0.54	0.64	0.39
120	0.3	0.6	0.13	0.04	0.31	0.58	0.53	0.61	0.39
124	0.27	0.55	0.12	0.04	0.28	0.52	0.47	0.51	0.36
125	0.27	0.55	0.12	0.03	0.28	0.52	0.47	0.52	0.36
140	0.29	0.58	0.13	0.04	0.3	0.56	0.49	0.54	0.51
144	0.28	0.56	0.12	0.03	0.29	0.53	0.47	0.54	0.5
148	0.3	0.59	0.13	0.04	0.31	0.57	0.5	0.64	0.55
164	0.25	0.47	0.1	0.03	0.25	0.42	0.35	0.43	0.49
168	0.25	0.48	0.1	0.02	0.25	0.41	0.35	0.44	0.52
172	0.26	0.49	0.1	0.03	0.27	0.42	0.36	0.46	0.51
189	0.28	0.51	0.11	0.03	0.28	0.42	0.36	0.51	0.61
194	0.26	0.48	0.1	0.03	0.27	0.4	0.35	0.52	0.54

Fed-batch Experiment-2

Time (hours)	**Viable Cell Concentration (x 10^5 cells/mL)**	**%Viability**	**GLC (g/L)**	**LAC (g/L)**	**GLN (mmol/L)**	**GLT (mmol/L)**
0	1.00	86.52	4	0.003	4	0.106
1	0.75	75.95	3.99	0.323	*3.95*	*0.309*
19	1.20	88.89	2.54	0.195	3.66	0.59
23	1.18	78.33	3.64	0.682	2.33	0.189
27	1.37	77.7	3.61	0.748	2.32	0.217
43	3.28	82.91	2.88	1.36	1.81	0.246
47	2.95	86.13	2.68	1.43	1.56	0.264
51	4.65	91.18	2.69	1.6	1.41	0.295
52	5.05	91.18	2.68	1.64	1.42	0.282

55	3.90	93.41	2.49	1.63	1.22	0.27
56	2.59	93.41	2.12	1.28	1.33	0.237
67	3.28	89.12	1.68	1.57	0.801	0.264
68	3.32	89.12	1.66	1.63	0.761	0.245
71	4.40	88	1.93	1.46	1.23	0.233
72	4.16	88	1.45	1.56	0.691	0.246
75	5.10	86.44	1.45	1.65	0.572	0.243
76	4.95	86.44	1.33	1.44	0.69	0.229
80	5.35	90.68	1.21	1.61	0.524	0.233
81	3.96	90.68	1.13	1.14	0.779	0.2
96	2.88	86.47	0.513	1.7	0.28	0.246
97	2.73	86.47	0.328	1.67	0.317	0.235
100	3.35	88.16	0.416	1.69	0.202	0.234
101	3.43	88.16	0.425	1.77	0.205	0.231
104	5.13	86.5	0.375	1.76	0.168	0.221
105	4.63	86.5	0.508	1.33	0.477	0.186
116	4.65	85.32	0.217	1.68	0.142	0.222
120	4.15	82.18	0.146	1.66	0.087	0.212
121	3.74	82.18	0.208	1.53	0.184	0.212
124	4.75	84.82	0.14	1.59	0.096	0.214
125	4.72	84.82	0.211	1.54	0.207	0.209
140	5.33	81.54	0.025	1.54	0	0.235
144	4.10	70.09	0.007	1.56	0	0.233
148	3.80	71.7	0.011	1.7	0	0.244
164	2.90	50	0	2.02	0	0.24

168	2.25	37.5	0	1.6	0	0.276
172	0.46	28.24	0.013	1.53	0	0.278
189	0.50	9.35	0.013	1.63	0	0.297
194	1.25	17.99	0.014	1.53	0	0.294

Related Amino-acid Data

All the measurements for the amino-acids have been expressed in mmol/L.

Time (hours)	MAb (mg/L)	ASP	GLU	ASN	SER	GLN	HIS	GLY	THR	ALA	ARG
0											
1											
19	5.89	0.22	0.15	0.4	0.38	2.49	0.2	0.38	0.66	0.42	0.31
23	7.78	0.2	0.13	0.39	0.36	2.53	0.18	0.48	0.67	0.45	0.32
27	7.35	0.2	0.14	0.38	0.36	2.45	0.17	0.41	0.66	0.48	0.31
43	9.95	0.18	0.19	0.37	0.34	1.82	0.16	0.41	0.64	0.81	0.29
47	11.73	0.18	0.2	0.37	0.34	1.65	0.15	0.43	0.64	0.92	0.28
51	13.88	0.18	0.21	0.37	0.33	1.48	0.15	0.41	0.64	1.01	0.28
52		0.18	0.21	0.37	0.33	1.48	0.15	0.41	0.64	0.98	0.28
55	14.07	0.18	0.21	0.36	0.32	1.28	0.15	0.41	0.63	1.06	0.28
56		0.18	0.17	0.36	0.33	1.36	0.15	0.39	0.64	0.79	0.28
67	17.38	0.18	0.2	0.37	0.31	0.88	0.14	0.44	0.64	1.12	0.29
68		0.18	0.2	0.36	0.31	0.86	0.14	0.43	0.64	1.13	0.28
71	15.57	0.2	0.22	0.41	0.35	0.81	0.16	0.49	0.72	1.35	0.31
72		0.2	0.21	0.41	0.35	0.73	0.15	0.49	0.71	1.3	0.31
75	16.34	0.21	0.21	0.43	0.37	0.85	0.16	0.5	0.75	1.23	0.33

76		0.2	0.21	0.41	0.36	0.85	0.15	0.49	0.72	1.23	0.31
80	17.04	0.19	0.21	0.4	0.33	0.64	0.15	0.5	0.7	1.24	0.31
81		0.24	0.19	0.44	0.38	1.04	0.18	0.52	0.79	0.97	0.35
96	20.39	0.22	0.23	0.43	0.37	0.39	0.15	0.54	0.77	1.33	0.33
97		0.22	0.24	0.45	0.39	0.44	0.16	0.57	0.81	1.36	0.35
100	22.37	0.21	0.22	0.42	0.37	0.25	0.14	0.55	0.76	1.39	0.33
101		0.18	0.2	0.38	0.34	0.24	0.13	0.5	0.69	1.23	0.3
104	23.11	0.19	0.2	0.37	0.32	0.19	0.13	0.51	0.69	1.23	0.29
105		0.2	0.16	0.38	0.32	0.5	0.15	0.47	0.68	0.94	0.3
116	23.23	0.18	0.18	0.41	0.27	0.22	0.12	0.64	0.67	1.11	0.29
120	24.88	0.19	0.2	0.38	0.29	0.1	0.13	0.54	0.7	1.2	0.3
121		0.2	0.2	0.4	0.31	0.22	0.14	0.59	0.73	1.16	0.31
124	26.97	0.19	0.2	0.38	0.3	0.12	0.13	0.54	0.7	1.17	0.3
125		0.2	0.18	0.37	0.29	0.25	0.14	0.5	0.68	1.01	0.29
140	32.95	0.18	0.18	0.33	0.23	0.01	0.12	0.55	0.64	1.09	0.26
144	36.48	0.18	0.19	0.33	0.22	ND	0.12	0.66	0.69	1.26	0.28
148	37.16	0.19	0.21	0.34	0.21	ND	0.12	0.73	0.72	1.34	0.3
164	45.27	0.2	0.24	0.33	0.15	ND	0.13	0.85	0.74	1.42	0.3
168	42.62	0.18	0.23	0.31	0.13	ND	0.11	0.79	0.69	1.33	0.28
172	44.52	0.19	0.23	0.3	0.12	ND	0.12	0.76	0.67	1.29	0.27
189	43.20	0.21	0.25	0.3	0.12	ND	0.15	0.78	0.72	1.33	0.29
194	56.9	0.19	0.25	0.29	0.11	ND	0.12	0.83	0.7	1.37	0.29

Time (hours)	TYR	VAL	MET	TRP	PHE	ILE	LEU	LYS	PRO
0									
1									
19	0.32	0.65	0.18	0.05	0.34	0.61	0.62	0.69	0.33
23	0.31	0.64	0.16	0.04	0.33	0.62	0.62	0.74	0.29
27	0.31	0.64	0.15	0.03	0.33	0.61	0.62	0.75	0.29
43	0.3	0.59	0.14	0.03	0.31	0.56	0.55	0.69	0.32
47	0.29	0.58	0.14	0.03	0.31	0.55	0.53	0.67	0.33
51	0.29	0.58	0.14	0.03	0.31	0.55	0.53	0.67	0.32
52	0.29	0.58	0.14	0.03	0.3	0.55	0.53	0.66	0.32
55	0.29	0.57	0.13	0.03	0.3	0.54	0.51	0.63	0.34
56	0.29	0.6	0.14	0.03	0.31	0.59	0.58	0.69	0.32
67	0.3	0.59	0.14	0.03	0.31	0.58	0.56	0.69	0.38
68	0.29	0.6	0.14	0.02	0.31	0.58	0.55	0.67	0.39
71	0.33	0.66	0.15	0.03	0.33	0.61	0.56	0.5	0.42
72	0.33	0.66	0.15	0.04	0.35	0.65	0.61	0.74	0.48
75	0.35	0.71	0.17	0.04	0.37	0.69	0.66	0.78	0.49
76	0.33	0.66	0.15	0.03	0.34	0.64	0.61	0.72	0.46
80	0.33	0.66	0.15	0.03	0.34	0.63	0.59	0.73	0.48
81	0.36	0.75	0.18	0.04	0.38	0.72	0.7	0.8	0.45
96	0.36	0.72	0.17	0.04	0.37	0.69	0.65	0.79	0.54
97	0.37	0.75	0.18	0.04	0.39	0.72	0.68	0.83	0.55
100	0.35	0.7	0.16	0.03	0.36	0.67	0.63	0.77	0.5
101	0.31	0.63	0.14	0.03	0.32	0.59	0.55	0.63	0.49

104	0.31	0.63	0.14	0.03	0.32	0.6	0.55	0.66	0.48
105	0.3	0.63	0.14	0.02	0.31	0.58	0.54	0.43	0.34
116	0.31	0.61	0.14	0.02	0.31	0.58	0.55	0.67	0.44
120	0.32	0.64	0.14	0.03	0.33	0.6	0.56	0.68	0.47
121	0.33	0.66	0.15	0.03	0.33	0.62	0.58	0.7	0.47
124	0.32	0.64	0.14	0.03	0.33	0.6	0.56	0.68	0.43
125	0.31	0.64	0.15	0.03	0.32	0.6	0.56	0.65	0.43
140	0.29	0.58	0.13	0.02	0.29	0.52	0.47	0.57	0.39
144	0.31	0.6	0.13	0.02	0.3	0.52	0.47	0.39	0.34
148	0.33	0.64	0.15	0.02	0.34	0.56	0.52	0.71	0.51
164	0.33	0.62	0.14	0.02	0.34	0.51	0.48	0.71	0.51
168	0.3	0.57	0.13	0.02	0.32	0.47	0.44	0.66	0.46
172	0.29	0.56	0.13	0.02	0.3	0.43	0.39	0.24	0.31
189	0.33	0.64	0.15	0.02	0.33	0.49	0.45	0.61	0.53
194	0.31	0.57	0.13	0.02	0.32	0.45	0.42	0.65	0.49

SET-2 (associated with imaging)

Batch Experiment-1

Time (hours)	**Viable Cell Concentration (x 10^6 cells/mL)**	**Dead Cell Concentration (x 10^6 cells/mL)**	**Total Cell Concentration (x 10^6 cells/mL)**	**%Viability**	**GLC (mM)**	**NH_3 (ppm)**	**NH_3 (mM)**
0	0.3	0.05	0.35	85.71429			
22	0.55	0.02	0.57	96.49123		0.72	1.122353
41.4	0.85	0.06	0.91	93.40659	16.2	1.14	1.777059
48.25	1.08	0.07	1.15	93.91304	13.1	1.46	2.275882

64	1.89	0.07	1.96	96.42857	10.4	1.88	2.930588
88	3.3	0.17	3.47	95.10086	8	2.41	3.756765
94.75	2.78	0.2	2.98	93.28859	6.3	2.5	3.897059
114	2.28	0.46	2.74	83.21168	4.3	2.65	4.130882
121.4	3.19	0.17	3.36	94.94048	3.7	2.7	4.208824
137	2.85	0.33	3.18	89.62264	2.2	2.76	4.302353
144.7	2.72	0.36	3.08	88.31169	1.3	2.67	4.162059
163.5	2.36	0.39	2.75	85.81818	0.9	2.8	4.364706
172	1.95	0.38	2.33	83.69099	1	3.08	4.801176
186.5	1.78	0.39	2.17	82.02765	LO	3.23	5.035
206.8	1.25	0.37	1.62	77.16049	LO	3.48	5.424706
238.75	0.61	0.32	0.93	65.5914	LO	3.71	5.783235
263.25	0.42	0.35	0.77	54.54545	LO	3.92	6.110588
289.1	0.22	0.34	0.56	39.28571	LO	4.27	6.656176
331.7	0	0.45	0.45	0	LO	4.25	6.625

Batch Experiment-2

Time (hours)	**Viable Cell Concentration (x 10^6 cells/mL)**	**Dead Cell Concentration (x 10^6 cells/mL)**	**Total Cell Concentration (x 10^6 cells/mL)**	**%Viability**	**GLC (mM)**	**NH_3 (ppm)**	**NH_3 (mM)**
0	0.3	0.05	0.35	85.71429			
22	0.43	0.08	0.51	84.31373		0.594	0.925941
41.4	0.92	0.05	0.97	94.84536	13.6	1.03	1.605588
48.25	1.37	0.09	1.46	93.83562	12.9	1.38	2.151176
64	2.47	0.17	2.64	93.56061	10.6	1.5	2.338235

88	2.84	0.13	2.97	95.6229	9.9	1.15	1.792647
94.75	2.09	0.23	2.32	90.08621	7.7	1.24	1.932941
114	2.14	0.25	2.39	89.53975	5.4	1.62	2.525294
121.4	3.38	0.14	3.52	96.02273	4.4	1.71	2.665588
137	2.4	0.4	2.8	85.71429	2.8	1.8	2.805882
144.7	2.36	0.61	2.97	79.46128	2.3	1.91	2.977353
163.5	2.17	0.62	2.79	77.77778	1.1	2.06	3.211176
172	1.95	0.57	2.52	77.38095	0.6	2.08	3.242353
186.5	1.76	0.41	2.17	81.10599	LO	2.16	3.367059
206.8	1.38	0.6	1.98	69.69697	LO	2.35	3.663235
238.75	1.07	0.57	1.64	65.2439	LO	2.64	4.115294
263.25	0.76	0.72	1.48	51.35135	LO	2.9	4.520588
289.1	0.85	0.77	1.62	52.46914	LO	3.13	4.879118
331.7	0.42	0.68	1.1	38.18182	LO	3.43	5.346765

Batch Experiment-3

Time (hours)	**Viable Cell Concentration (x 10^6 cells/mL)**	**Dead Cell Concentration (x 10^6 cells/mL)**	**Total Cell Concentration (x 10^6 cells/mL)**	**%Viability**	**GLC (mM)**	**NH_3 (ppm)**	**NH_3 (mM)**
0	0.3	0.05	0.35	85.71429			
22	0.5	0.03	0.53	94.33962		0.717	1.117676
41.4	0.81	0.05	0.86	94.18605	16.4	1.2	1.870588
48.25	1.15	0.16	1.31	87.78626	12.1	1.31	2.042059
64	1.51	0.11	1.62	93.20988	9.2	1.47	2.291471
88	1.56	0.05	1.61	96.89441	7.1	1.59	2.478529

94.75	1.76	0.19	1.95	90.25641	6.6	1.69	2.634412
114	1.44	0.33	1.77	81.35593	5.8	1.77	2.759118
121.4	1.21	0.33	1.54	78.57143	5.8	1.87	2.915
138.5	1.29	0.4	1.69	76.33136	5.5	1.93	3.008529
146.3	1.3	0.43	1.73	75.14451	5.6	2.1	3.273529
165.2	1.32	0.56	1.88	70.21277	5.1	2.3	3.585294
173	1.31	0.66	1.97	66.49746	4.5	2.35	3.663235
189.75	0.96	0.66	1.62	59.25926	4.2	2.42	3.772353
209	0.69	0.87	1.56	44.23077	4	2.51	3.912647
240.75	0.32	0.75	1.07	29.90654	3.1	2.62	4.084118
265.5	0.3	1.1	1.4	21.42857	2.3	2.7	4.208824
293.6	0.23	0.85	21	21.2963	2	2.81	4.380294
333	0.19	0.84	18.4	18.4466	1.6	2.84	4.427059

Batch Experiment-4

Time (hours)	**Viable Cell Concentration (x 10^6 cells/mL)**	**Dead Cell Concentration (x 10^6 cells/mL)**	**Total Cell Concentration (x 10^6 cells/mL)**	**%Viability**	**GLC (mM)**	**NH3 (ppm)**	**NH3 (mM)**
0	0.3	0.05	0.35	85.71429			
22	0.46	0.04	0.5	92		0.748	1.166
41.4	0.8	0.1	0.9	88.88889	14.2	1.29	2.010882
48.25	1.33	0.09	1.42	93.66197	13.1	1.61	2.509706
64	1.37	0.19	1.56	87.82051	9.1	1.69	2.634412
88	1.39	0.16	1.55	89.67742	7.7	1.82	2.837059

94.75	2.37	0.28	2.65	89.43396	6.2	1.9	2.961765
114	0.92	0.17	1.09	84.40367	6.2	2	3.117647
121.4	1.48	0.19	1.67	88.62275	6.1	2.24	3.491765
138.5	1.46	0.24	1.7	85.88235	5.2	2.3	3.585294
146.3	1.47	0.5	1.97	74.61929	5	2.34	3.647647
165.2	1.28	0.41	1.69	75.73964	4.2	2.46	3.834706
173	1.17	0.39	1.56	75	4	2.5	3.897059
189.75	1.2	0.42	1.62	74.07407	3.8	2.6	4.052941
209	1.06	0.43	1.49	71.14094	3.3	2.66	4.146471
240.75	0.78	0.53	1.31	59.54198	2.3	2.76	4.302353
265.5	0.75	0.62	1.37	54.74453	1.7	2.86	4.458235
293.6	0.75	0.56	57	57.25191	1.1	2.96	4.614118
333	0.65	0.62	51.1	51.1811	LO	3.11	4.847941

Appendix B

Calculated Results for Experiment Set-1

Calculated R-values for Batch Experiment-1 (*in mmol/10^9 cell hours*):

Metabolite	R_{exp}	R_{post}	R_{full}
Pyr	0	0	0
AcCoA	0	0	0
aKG	0	0	0
SuCCoA	0	0	0
FUM	0	0	0
OAA	0	0	0
Glc	-0.26731323	-0.00918419	-0.11199362
Lac	0.328126	0.00648532	0.12408664
Ala	0.02545904	0.00585721	0.0136512
Arg	-0.00459109	0.00084063	-0.00132343
Asp	-0.0060134	0.00043947	-0.00237187
Asn	-0.00348374	-0.00220295	-0.00252385
Cys	0	0	0
Gln	-0.06972616	0	-0.02718938
Glu	-0.00142231	-0.00040116	-0.00104844
Gly	-0.0019166	0.0067063	0.00311847
His	-0.00252123	0	-0.00100581
Ile	-0.00599654	-0.00193225	-0.00342958
Leu	-0.00844114	-0.00048008	-0.00352847
Lys	-0.00531528	0.00098747	-0.00135043
Met	-0.00266607	0.00039022	-0.00083956

Phe	-0.00236796	0.00028164	-0.00075062
Pro	0.00529764	0.00334811	0.00428066
Ser	-0.00184839	-7.3089E-19	-0.00067234
Thr	-0.00481256	0.00067186	-0.00151366
Tyr	-0.0024446	4.1605E-05	-0.00096518
Val	-0.00666095	-0.00072011	-0.00296679
BioMass	0.58469819	0.0843572	0.27580246
Mab	4.124E-09	6.5733E-10	2.4835E-09

Calculated R-values for a Batch Experiment-2 were unavailable.

Calculated R-values for a Fed-batch Experiment-1 (*in mmol/10^9 cell hours*):

Metabolite	R1	R2	R3	R4	R5	R6
Pyr	0	0	0	0	0	0
AcCoA	0	0	0	0	0	0
aKG	0	0	0	0	0	0
SuCCoA	0	0	0	0	0	0
FUM	0	0	0	0	0	0
OAA	0	0	0	0	0	0
Glc	-0.91769036	-1.08065625	-0.52007489	-0.332668	-0.26518165	-0.54181663
Lac	1.63726605	-0.29472443	0.69343319	0.44355733	1.52479448	0.85142614
Ala	0.09513467	0.07073386	0.08737258	0.07318696	0.02386635	0.07523511
Arg	-0.00823733	-0.00884173	-0.0020803	-0.00665336	-0.01193317	0.00139324
Asp	-0.00485846	-0.01768347	-0.0041606	-0.00665336	-0.01789976	8.5705E-18
Asn	-0.00648865	-0.00884173	-0.0020803	-0.00665336	-0.02386635	0.00417973
Cys	0	0	0	0	0	0

Gln	-0.16787599	-0.17683466	-0.15602247	-0.37791084	-0.11336516	-0.08638105
Glu	0.01153475	-0.00884173	0.0062409	7.014E-18	-0.00596659	0.00696621
Gly	-0.0016854	8.4354E-17	0.0083212	0.00665336	-0.01193317	-0.00278649
His	-0.00397651	-0.00884173	-0.0041606	-0.01330672	-0.02386635	4.2852E-18
Ile	-0.0130268	0.0265252	-0.0124818	0.00665336	-0.04176611	0.00696621
Leu	-0.01698807	0.03536693	-0.0166424	0	-0.04176611	0.00417973
Lys	-0.02052016	0.31830239	-0.020803	0.1330672	0.05966587	0.02229188
Met	-0.00510279	1.6871E-17	-0.0041606	8.4168E-18	-0.00596659	1.7141E-18
Phe	-0.0054271	0.00884173	-0.0041606	0.00665336	-0.01789976	0.00417973
Pro	-0.00432718	0.04420866	0.0124818	0.0665336	0.05966587	0.00696621
Ser	-0.0084569	-0.00884173	-0.0020803	0	-0.02983294	0.00835946
Thr	-0.0107647	-0.0265252	-0.0041606	-2.2445E-17	-0.04176611	0.00557297
Tyr	-0.00343409	4.4989E-17	-0.0020803	-0.00665336	-0.01789976	0.00417973
Val	-0.01406359	-0.01768347	-0.0104015	-3.9278E-17	-0.03579952	0.00417973
BioMass	0.75198001	0.94557514	0.96057049	0.27769063	1.57379337	0.43905398
Mab	4.3281E-09	2.5667E-09	3.0414E-09	5.7899E-09	-1.3819E-08	2.6698E-09

Continued…

Metabolites	**R7**	**R8**	**R9**	**R10**	**R11**	**R-average**
Pyr	0	0	0	0	0	0
AcCoA	0	0	0	0	0	0
aKG	0	0	0	0	0	0
SuCCoA	0	0	0	0	0	0
FUM	0	0	0	0	0	0
OAA	0	0	0	0	0	0
Glc	-0.38929962	-0.22391073	-0.26149181	-0.15367506	-0.09637471	-0.4686465

Lac	0.28572449	-6.7998E-16	0.4238765	-5.037E-16	0.11558634	0.55653537
Ala	0.04500161	-0.02642881	0.04711841	0.05095541	0.00807957	0.05421762
Arg	-0.0064288	-0.0132144	-0.00168588	0.00242645	-0.0027295	-0.00552553
Asp	-0.0128576	-0.0066072	-0.00162675	-3.4979E-18	-0.00132223	-0.00723472
Asn	-0.0064288	-0.0132144	-0.00017737	0.00242645	-0.00597122	-0.00611448
Cys	0	0	0	0	0	0
Gln	-0.1002893	-0.06739346	-0.09302404	-0.04901426	-0.01523901	-0.13881112
Glu	-0.0064288	-0.0066072	0.00377126	0.00242645	0.00135471	0.00030953
Gly	-0.0064288	-0.02642881	0.00234427	0.01213224	0.01957028	-0.00198116
His	-0.0064288	-0.0066072	-0.00049537	-0.00121322	-0.00155117	-0.00688965
Ile	-0.0257152	-0.0132144	-0.00267662	0.0048529	-0.01148075	-0.00638833
Leu	-0.0257152	-0.0132144	-0.00607076	0.00242645	-0.01073261	-0.00784238
Lys	-0.03857281	-0.0066072	-0.00491699	0.00242645	-0.00620734	0.04443336
Met	-0.0064288	-0.0066072	-0.00200388	0.00121322	-0.00195994	-0.00290566
Phe	-0.0128576	-0.0066072	-0.00130875	0.00242645	-0.00251277	-0.00261597
Pro	0.0064288	-0.0132144	0.00434815	0.01819836	0.00255338	0.02012899
Ser	0.0064288	-0.01982161	2.1352E-17	0.00121322	-0.01183493	-0.0053032
Thr	-0.0257152	-0.01982161	-0.00186325	0.00606612	-0.00407509	-0.01189776
Tyr	-0.0128576	-0.0066072	-0.00017737	0.00242645	-0.00210344	-0.00431035
Val	-0.0257152	-0.01982161	-0.00299462	0.00363967	-0.00706258	-0.01186601
BioMass	0.35874929	0.96782647	0.09698619	0.75481148	-0.17467905	0.71270371
Mab	1.4212E-08	-1.9978E-08	5.2112E-09	6.4446E-09	1.2136E-08	1.0467E-09

Calculated R-values for a Fed-batch Experiment-2 (*in mmol/10^9 cell hours*):

Metabolites	R1	R2	R3	R4	R5	R6
Pyr	0	0	0	0	0	0
AcCoA	0	0	0	0	0	0
aKG	0	0	0	0	0	0
SuCCoA	0	0	0	0	0	0
FUM	0	0	0	0	0	0
OAA	0	0	0	0	0	0
Glc	-0.78348215	-0.73388552	-1.10577638	-0.3236246	-0.6681828	0.08112545
Lac	1.45320187	1.05460311	1.05290927	0.91693635	1.21290882	0.41969614
Ala	0.07718603	0.09823633	-0.06218514	0.00485437	0.07017544	-0.05890319
Arg	-0.00528226	0.00124962	0.01184338	-9.1047E-18	-0.00389864	-0.02426654
Asp	-0.00300282	8.3442E-18	0.00592169	-0.00485437	-0.00389864	-0.01248045
Asn	-0.00230171	0.00124962	0.01184338	-0.00485437	-0.00194932	-0.0321678
Cys	0	0	0	0	0	0
Gln	-0.13191535	-0.16149418	-0.29397317	-0.08058252	-0.09727096	-0.05479145
Glu	0.01100109	0.00877817	-0.00414666	-4.5524E-18	0.00779727	-0.01580252
Gly	-0.00507293	0.01295385	0.00592169	0.00485437	0.00389864	-0.02472945
His	-0.00378085	-0.00292606	0.00177503	-9.1047E-18	-0.00584795	-0.01145478
Ile	-0.0097865	-0.00292606	0.04027341	-0.00485437	-0.00584795	-0.04843323
Leu	-0.01346818	-0.00752855	0.05034176	-0.00970874	-0.00974659	-0.05254951
Lys	-0.01182092	-0.00335287	0.12320664	0.00485437	-0.00194932	-0.0698406
Met	-0.00230171	2.7814E-18	0.01184338	-9.1047E-18	-0.00194932	-0.01580252
Phe	-0.00365727	1.1126E-17	0.0201367	0	-0.00194932	-0.02805152
Pro	0.0047688	0.01923278	0.03080166	0.00970874	0.01754386	-0.02623164

Ser	-0.00421741	-0.00585211	0.01184338	-0.01456311	-0.00194932	-0.02838281
Thr	-0.00380312	6.6754E-17	0.0195401	-0.00970874	-0.00389864	-0.04820177
Tyr	-0.00298056	0.00124962	0.01184338	-9.1047E-18	-3.6635E-18	-0.02449799
Val	-0.00898621	-0.00124962	0.02960846	-1.8209E-17	-0.00584795	-0.04820177
BioMass	0.92872045	0.50392085	1.07267435	0.15526114	-0.37273327	2.04348336
Mab	5.8912E-09	5.4185E-09	2.8252E-09	1.8211E-09	3.9913E-09	5.6419E-09

Continued…

Metabolites	R7	R8	R9	R10	R Average
Pyr	0	0	0	0	0
AcCoA	0	0	0	0	0
aKG	0	0	0	0	0
SuCCoA	0	0	0	0	0
FUM	0	0	0	0	0
OAA	0	0	0	0	0
Glc	-0.29830956	-0.29664529	-0.13709232	-0.00367211	-0.47398591
Lac	0.58515701	0.52349169	-1.8797E-16	0.040834	0.80210047
Ala	0.03685566	0.00785238	0.0106136	0.01502154	0.02052061
Arg	-0.00043848	-0.00785238	-0.0039801	0.00103861	-0.00362504
Asp	-0.00200779	-0.00785238	-0.0026534	0.00130199	-0.00342535
Asn	0.00131545	-0.01570475	-0.0053068	-0.00326323	-0.00531959
Cys	0	0	0	0	0
Gln	-0.05879136	-0.0691009	-0.02746269	0	-0.10837584
Glu	0.00540027	1.9041E-17	-9.7899E-19	0.00554199	0.00144751
Gly	0.01536999	-0.03926188	0.0066335	0.01847289	-0.00215914
His	-0.0035771	-0.00785238	-0.0026534	0.00074237	-0.00403528

Ile	0.00226165	-0.01570475	-0.0106136	-0.00684761	-0.00618127
Leu	0.00270013	-0.01570475	-0.0119403	-0.00542729	-0.00751164
Lys	0.03879422	-0.01570475	-0.0106136	0.00240902	0.00595257
Met	7.1749E-18	-0.00785238	-0.0026534	0.00015848	-0.00207955
Phe	0.00226165	-1.7921E-17	-0.0039801	0.00170518	-0.00169332
Pro	0.01908555	-0.0314095	-0.0053068	0.00644461	0.00424372
Ser	-0.00558489	-0.00785238	-0.0079602	-0.0107842	-0.00716876
Thr	0.00182317	-0.02355713	-0.0053068	0.0028836	-0.00812366
Tyr	0.00270013	-0.00785238	-0.0026534	0.00061375	-0.00246569
Val	0.00025386	-0.01570475	-0.0079602	-0.00102881	-0.00645424
BioMass	-0.05527199	1.5199253	0.23791102	-0.16405454	0.67043236
Mab	1.3585E-09	8.3533E-09	4.9765E-09	8.8458E-09	4.4753E-09

Calculated Average Flux Values for Batch Experiment 1and 2:

Flux Serial Number	Exponential	Post-exponential	Overall Average
j1	0.32051	2.35E-02	0.172007
j2	0.1606	0.049514	0.105057
j3	0.17153	0.053174	0.112352
j4	0.22796	0.06031	0.144135
j5	0.23433	0.062859	0.148595
j6	0.23536	0.062901	0.149131
j7	0.059652	0.0097467	0.034699
j8	0.50516	1.71E-04	0.252665
j9	0.000034119	3.97E-09	1.71E-05

j10	0.00047431	5.12E-12	0.000237
j11	7.1924E-08	3.61E-05	1.81E-05
j12	0.000092423	3.32E-07	4.64E-05
j13	0.00099849	1.91E-05	0.000509
j14	0.0021201	7.28E-04	0.001424
j15	0.001672	9.16E-08	0.000836
j16	0.0017275	0.0017975	0.001763
j17	0.00082258	1.94E-07	0.000411
j18	0.0015946	0.00058961	0.001092
j19	0.0012031	2.39E-05	0.000614
j20	0.00089793	1.95E-03	0.001424
j21	0.0013824	8.29E-11	0.000691
j22	0.009163	2.67E-03	0.005919
j23	0.060203	8.02E-03	0.034112
j24	0.056414	5.64E-03	0.031027
j25	0.0077077	1.20E-04	0.003914
j26	0.0097928	2.43E-10	0.004896
j27	0.040995	0.0071029	0.024049
j28	0.0042103	2.75E-08	0.002105
j29	0.000001654	1.68E-05	9.21E-06
j30	0.0060156	3.39E-11	0.003008
j31	0.54561	8.41E-02	0.314867
j32	3.7025E-08	8.97E-13	1.85E-08

Calculated Average Flux Values for Fed-batch Experiment 1and 2:

Flux Serial Number	Exponential	Post-exponential	Overall Average
j1	0.410662646	0.094383485	0.252523
j2	0.328097561	0.165048363	0.246573
j3	0.370968232	0.188169262	0.279569
j4	0.463434922	0.209142859	0.336289
j5	0.492940796	0.21703174	0.354986
j6	0.503836484	0.218014949	0.360926
j7	0.130015436	0.029872373	0.079944
j8	0.595659567	0.039084743	0.317372
j9	0.000118698	3.4262E-06	6.11E-05
j10	0.000347825	3.53203E-10	0.000174
j11	0.004400219	0.00576053	0.00508
j12	0.003965813	0.000496962	0.002231
j13	0.008532288	0.000951559	0.004742
j14	0.007477653	0.002089812	0.004784
j15	0.008935302	0.000467968	0.004702
j16	0.007083523	0.004711025	0.005897

j17	0.003640182	0.000584008	0.002112
j18	0.004154661	0.00424648	0.004201
j19	0.00310045	0.001875909	0.002488
j20	0.006086514	0.003664704	0.004876
j21	0.003742772	0.00062041	0.002182
j22	0.014824928	0.003763127	0.009294
j23	0.083039743	0.017780533	0.05041
j24	0.07743353	0.014471262	0.045952
j25	0.012304046	0.005342362	0.008823
j26	0.022636932	1.01842E-07	0.011319
j27	0.05566465	0.020315552	0.03799
j28	0.004822266	1.84138E-08	0.002411
j29	0.002193692	2.0545E-05	0.001107
j30	0.019378491	1.13792E-07	0.009689
j31	0.597395705	0.162979337	0.380188
j32	3.53801E-06	1.62832E-07	1.85E-06

Values of a-coefficients:

	Batch Exponential	Fed-Batch Exponential
a_1	0.159293	0.275055
a_2	0.01666	0.031789
a_3	0.002791	0.02178
a_4	0.010118	0.025652
a_5	0.038617	0.101629
a_6	0.035737	0.097108
a_7	0.587604	0.718849
a_8	0.004079	9.92E-04
a_9	4.15E-05	4.71E-04

	Batch Post-exponential	Fed-Batch Post-exponential
a_1	0.001277	0.062592
a_2	0.0023	0.002917
a_3	2.24E-15	4.01E-12
a_4	0.001655	3.58E-04
a_5	0.001914	0.018823
a_6	2.23E-15	0.016492
a_7	0.084084	3.46E-12
a_8	5.16-04	0.012079
a_9	2.22E-15	9.98E-04

Appendix C

MATLAB Codes

Predictions for Dynamic Model- Batch and Fed-batch Mode- Main File:

```
clear all
%run data file for DYNAMIC MODEL of METABOLITES for EXPS.
%xdata1 = Experiment 250-3
%xdata2 = Experiment 1000-2
%xdata3 = Experiment 7(3)
%xdata4 = Experiment 7(4)
%xdata5 = Experiment 7(1)
global X
global xp
global swittch
global a
load a8%a8 for batch and a12 for fedbatch
    a= aExA

load xxxdata
xdatae = xdata5;
XvData = xdatae(:,33);
DataTime = xdatae(:,1);
start = min(DataTime);
fin = max(DataTime);
ttt = (min(DataTime):0.5: max(DataTime));
XX = interp1 (DataTime, XvData, ttt);

batch=0;%0 for Batch , 3 for Exp(3), 4 for Exp7(4)
x10f(:,1) =xdatae(:,9);          %GLC
x10f(:,2) =xdatae(:,17);         %GLN
x10f(:,3) =xdatae(:,10);         %LAC
x10f(:,4) =xdatae(:,11);         %AMM.
x10f(:,5) =xdatae(:,18)*10;      %GLU
x10f(:,6) =xdatae(:,15);         %ASN
x10f(:,7) =xdatae(:,14);         %ASP
x10f(:,8) =xdatae(:,12);         %ALA
x10f(:,9) =xdatae(:,26);         %PRO
x10f(:,10)=xdatae(:,31);         %BIOMASS
x10f(:,11)=xdatae(:,32)*1E6;     %MAb

%load initial values
x10(1) =xdatae(1,9);
x10(2) =xdatae(1,17);
x10(3) =xdatae(1,10);
x10(4) =xdatae(1,11);
x10(5) =xdatae(1,18)*10;
x10(6) =xdatae(1,15);
x10(7) =xdatae(1,14);
x10(8) =xdatae(1,12);
x10(9) =xdatae(1,26);
```

```
x10(10)=xdatae(1,31);
x10(11)=xdatae(1,32)*1E6;
Y(1,:)=x10; % x10 is the initial value vector

%number of iterations
mn = (fin-start)*2
for i=1:mn
    i;
 time = start + (i-1)/2;

%switch to post-exponential phase
if time>=76 %for both 7(3) and 7(4)=140, 250-3:72, 1000-2:75, 7(1):76
   a = aPos;
end

 ooo(i)=i;
 X = XX(i);
 [t,x01]=ode23('Testing_a_b_function',[i i+1],x10);

 A1=[t,x01];
 [a1,b1]=size(A1);

if batch==3 %Exp7(3), Dilutions are initiated in total 0.5 hrs before
diluted point
   batch
     if time==51
       for u = 1:11
           node=2;
           dist=DataTime(node+1)-DataTime(node); %node=Number of Data Node
before Dilutio
           v=i+1-2*dist;
           x10(u)=Y(v,u)+(x10f(node+1,u)-x10f(node,u));

       end
   elseif time==55
       for u = 1:11
           node=4;
           dist=DataTime(node+1)-DataTime(node); %node=Number of Data Node
before Dilution
           v=i+1-2*dist;
           x10(u)=Y(v,u)+(x10f(node+1,u)-x10f(node,u));
       end
   elseif time==56
       for u = 1:11
           node=5; dist=DataTime(node+1)-DataTime(node); %node=Number of
Data Node before Dilution
           v=i+1-2*dist;
           x10(u)=Y(v,u)+(x10f(node+1,u)-x10f(node,u));
       end
   elseif time==71
       for u = 1:11
           node=8; dist=DataTime(node+1)-DataTime(node); %node=Number of
Data Node before Dilution
```

```
            v=i+1-2*dist;
            x10(u)=Y(v,u)+(x10f(node+1,u)-x10f(node,u));
        end
    elseif time==75
        for u = 1:11
            node=10; dist=DataTime(node+1)-DataTime(node); %node=Number of
Data Node before Dilution
            v=i+1-2*dist;
            x10(u)=Y(v,u)+(x10f(node+1,u)-x10f(node,u));
        end
    elseif time==80
        for u = 1:11
            node=11; dist=DataTime(node+1)-DataTime(node); %node=Number of
Data Node before Dilution;
            v=i+1-2*dist;
            x10(u)=Y(v,u)+(x10f(node+1,u)-x10f(node,u));
        end
    elseif time==96
        for u = 1:11
            node=13; dist=DataTime(node+1)-DataTime(node) ;%node=Number of
Data Node before Dilution
            v=i+1-2*dist;
            x10(u)=Y(v,u)+(x10f(node+1,u)-x10f(node,u));
        end
    elseif time==100
        for u = 1:11
            node=16; dist=DataTime(node+1)-DataTime(node) %node=Number of
Data Node before Dilution
            v=i+1-2*dist
            x10(u)=Y(v,u)+(x10f(node+1,u)-x10f(node,u))
        end
    elseif time==104
        for u = 1:11
            node=17; dist=DataTime(node+1)-DataTime(node); %node=Number of
Data Node before Dilution
            v=i+1-2*dist;
            x10(u)=Y(v,u)+(x10f(node+1,u)-x10f(node,u));
        end
    elseif time==120
        for u = 1:11
            node=20; dist=DataTime(node+1)-DataTime(node); %node=Number of
Data Node before Dilution
            v=i+1-2*dist;
            x10(u)=Y(v,u)+(x10f(node+1,u)-x10f(node,u));
        end
    else
        x10=x01(a1,:);
    end

elseif batch==4 %Exp7(4), Dilutions  are initiated in total 0.5 hrs before
diluted point
     if time==43
         for u = 1:11
```

```
            node=2;
            dist=DataTime(node+1)-DataTime(node);%node=Number of Data Node
before Dilution
            v=i+1-2*dist;
            x10(u)=Y(v,u)+(x10f(node+1,u)-x10f(node,u));
        end
    elseif time==54
         for u = 1:11
            node=5;
            dist=DataTime(node+1)-DataTime(node); %node=Number of Data Node
before Dilution
            v=i+1-2*dist;
            x10(u)=Y(v,u)+(x10f(node+1,u)-x10f(node,u));
        end
   elseif time==71
         for u = 1:11
            node=8;
            dist=DataTime(node+1)-DataTime(node) ;%node=Number of Data Node
before Dilution
            v=i+1-2*dist;
            x10(u)=Y(v,u)+(x10f(node+1,u)-x10f(node,u));
        end
   elseif time==75
         for u = 1:11
            node=12;
            dist=DataTime(node+1)-DataTime(node); %node=Number of Data Node
before Dilution
            v=i+1-2*dist;
            x10(u)=Y(v,u)+(x10f(node+1,u)-x10f(node,u));
        end
   elseif time==80
         for u = 1:11
            node=14;
            dist=DataTime(node+1)-DataTime(node); %node=Number of Data Node
before Dilution
            v=i+1-2*dist;
            x10(u)=Y(v,u)+(x10f(node+1,u)-x10f(node,u));
         end
   elseif time==96
         for u = 1:11
            node=16;
            dist=DataTime(node+1)-DataTime(node); %node=Number of Data Node
before Dilution
            v=i+1-2*dist;
            x10(u)=Y(v,u)+(x10f(node+1,u)-x10f(node,u));
        end
   elseif time==104
         for u = 1:11
            node=20;
            dist=DataTime(node+1)-DataTime(node); %node=Number of Data Node
before Dilution
            v=i+1-2*dist;
            x10(u)=Y(v,u)+(x10f(node+1,u)-x10f(node,u));
```

```
        end
    elseif time==120
         for u = 1:11
            node=23;
            dist=DataTime(node+1)-DataTime(node); %node=Number of Data Node
before Dilution
            v=i+1-2*dist;
            x10(u)=Y(v,u)+(x10f(node+1,u)-x10f(node,u));
         end
     elseif time==124
         for u = 1:11
            node=25;
            dist=DataTime(node+1)-DataTime(node); %node=Number of Data Node
before Dilution
            v=i+1-2*dist;
            x10(u)=Y(v,u)+(x10f(node+1,u)-x10f(node,u));
        end

   else
        x10=x01(a1,:);
        t10=A1(a1,1);
    end
 else % for Batch Experiments without Dilution
 x10=x01(a1,:);
 end

   %*********************all outputs are positive***************
   for j=1:11
        if x10(j)<0
            x10(j)=0;
        end
   end


   Y(i+1,:)=x10;
   Ydif(i+1,:)=xp;


end

save Y1308F Y Ydif

%Plot of the model prediction and the measured data

length=fin;

%ttt=tttt

figure(1)
subplot(2,3,1)
scatter (DataTime,XvData,6,'ko','filled')
hold on
```

```
xlabel('time(hour)');
ylabel('Xv(xE06/mL)');
axis([start length min(XX) max(XX)])

subplot(2,3,2)
F = Y(:,1);
E = xdatae(:,9);
plot(ttt,F,'-k')
hold on
scatter(DataTime,E,6,'ko','filled')
xlabel('time(hour)');
ylabel('GLC(mM)')
axis([start length min(min(F),min(E)) max(max(F),max(E))])

subplot(2,3,3)
F = Y(:,2);
E = xdatae(:,17);
plot(ttt,F,'-k')
hold on
scatter(DataTime,E,6,'ko','filled')
xlabel('time(hour)');
ylabel('GLN(mM)')
axis([start length min(min(F),min(E)) max(max(F),max(E))])

subplot(2,3,4)
F = Y(:,3);
E = xdatae(:,10);
plot(ttt,F,'-k')
hold on
scatter(DataTime,E,6,'ko','filled')
xlabel('time(hour)');
ylabel('LAC(mM)')
axis([start length min(min(F),min(E)) max(max(F),max(E))])

subplot(2,3,5)
F = Y(:,10);
E = xdatae(:,31);
plot(ttt,F,'-k')
hold on
scatter(DataTime,E,6,'ko','filled')
xlabel('time(hour)');
ylabel('Biomass(mM)')
axis([start length min(min(F),min(E)) max(max(F),max(E))])

subplot(2,3,6)
F = Y(:,11)*1E-6; %Mab goes in with 1E6 the value, to get a reasonable a-
coefficient during the QP
E = xdatae(:,32);
plot(ttt,F,'-k')
hold on
%scatter(DataTime,E,6,'go','filled')
xlabel('time(hour)');
ylabel('MAb(mM)')
```

```
axis([start length min(min(F),min(E)) max(max(F),max(E))])

figure(2)
subplot(2,3,1)
F = Y(:,8);
E = xdatae(:,12);
plot(ttt,F,'-k')
hold on
scatter(DataTime,E,6,'ko','filled')
xlabel('time(hour)');
ylabel('ALA(mM)')
axis([start length min(min(F),min(E)) max(max(F),max(E))])

subplot(2,3,2)
F = Y(:,9);
E = xdatae(:,26);
plot(ttt,F,'-k')
hold on
scatter(DataTime,E,6,'ko','filled')
xlabel('time(hour)');
ylabel('PRO(mM)')
axis([start length min(min(F),min(E)) max(max(F),max(E))])

subplot(2,3,3)
F = Y(:,7);
E = xdatae(:,14);
plot(ttt,F,'-k')
hold on
scatter(DataTime,E,6,'ko','filled')
xlabel('time(hour)');
ylabel('ASP(mM)')
axis([start length min(min(F),min(E)) max(max(F),max(E))])

subplot(2,3,4)
F = Y(:,6);
E = xdatae(:,15);
plot(ttt,F,'-k')
hold on
scatter(DataTime,E,6,'ko','filled')
xlabel('time(hour)');
ylabel('ASN(mM)')
axis([start length min(min(F),min(E)) max(max(F),max(E))])

subplot(2,3,5)
F = Y(:,5)*0.1;
E = xdatae(:,18);
plot(ttt,F,'-k')
hold on
scatter(DataTime,E,6,'ko','filled')
xlabel('time(hour)');
ylabel('GLU(mM)')
axis([start length min(min(F),min(E)) max(max(F),max(E))])
```

```
subplot(2,3,6)
F = Y(:,4);
plot(ttt,F,'-k')
hold on
xlabel('time(hour)');
ylabel('NH3(mM)')
axis([start length min(F) max(F)])
```

Sub-routine for the Dynamic Model:

```
function xp=DynamicModel(t,x)
%a-coefficients are calculated from averages of Exp7(3) and Exp 250-3

global X
global xp
global switch
global a


if batch==0
      kG=4;kQ=0.03;
      kU=0.01;kS=0.02;kF=0.05;
end
if batch>0
      kG=0.5;kQ=0.5;
      kU=0.01;kS=0.12;kF=0.05;
end

G=x(1);Q=x(2);L=x(3);N=x(4);U=x(5);S=x(6);F=x(7);B=x(8);P=x(9);M=x(10);A=x
(11);
%G-Glucose; Q-GLutamine; L-Lactate; N-Ammonia; U-GlutamicAcid;
%S-Asparagine; F-Aspartic Acid; B-Alanine; P-Proline; M-Biomass; A-MAb
%**********************
load KK

%reaction rates
r(1)=a(1)*G*X/(kG+G);
r(2)=a(2)*G*U*X/((kG+G)*(kU+U));
r(3)=a(3)*G*U*X/((kG+G)*(kU+U));
r(4)=a(4)*U*X/(kU+U);
r(5)=a(5)*S*X/(kS+S);
r(6)=a(6)*Q*F*X/((kQ+Q)*(kF+F));
r(7)=a(7)*X*Q/(kQ+Q);
r(8)=a(8)*X*Q/(kQ+Q);
r(9)=a(9)*Q*X/(kQ+Q);

r=r';
jay = size(r);
K1;
xp=K1*r;
xp=xp;
```

Prediction for Integrated Model- Batch and Fedbatch Mode:

```
clear all
%run data file for INTEGRATED MODEL of METABOLITES for BATCH & FED-BATCH
EXPS.
%xdata1 = Experiment 250-3
%xdata2 = Experiment 1000-2
%xdata33 = Experiment 7(3)
%xdata4 = Experiment 7(4)
%xdata5 = Experiment 7(1)
global xp
global X
global batch
global a
load a8 %for batch and early fed-batch before feeding
    a= aExA;

% load experimental data
load xxxdata

%fix xdata and batch no. manually
xdata = xdata5;
batch=0;%0 for Batch , 3 for Exp(3), 4 for Exp7(4)

DataTime = xdata(:,1);
ttt=DataTime';
start = min(DataTime);
fin = max(DataTime);

x10f(:,2) =xdata(:,9);                              %Glucose
x10f(:,3) =xdata(:,17);                             %Glutamine
x10f(:,4) =xdata(:,10);                             %Lactate
x10f(:,5) =xdata(:,11);                             %Ammonia
x10f(:,6) =xdata(:,18)*10;                          %Glutamic Acid
x10f(:,7) =xdata(:,15);                             %ASN
x10f(:,8) =xdata(:,14);                             %ASP
x10f(:,9) =xdata(:,12);                             %Alanine
x10f(:,10) =xdata(:,26);                            %Prolin
x10f(:,11)=xdata(:,31);                             %Biomass
x10f(:,12)=xdata(:,32)*1E6;                         %MAb
x10f(:,1)=xdata(:,33);                              %Xv
x10f(:,13)=xdata(:,34);                             %Xd
jack=size(x10f);

%load initial values

x10(2) =xdata(1,9);                             %Glc
x10(3) =xdata(1,17);                            %Gln
x10(4) =xdata(1,10);                            %Lac
x10(5) =xdata(1,11);                            %Amm
x10(6) =xdata(1,18)*10;                         %Glu
x10(7) =xdata(1,15);                            %ASN
```

```
x10(8) =xdata(1,14);                          %ASP
x10(9) =xdata(1,12);                          %Ala
x10(10) =xdata(1,26);                         %Pro
x10(11)=xdata(1,31);                          %Biomass
x10(12)=xdata(1,32)*1E6;                      %MAb
x10(1)=xdata(1,33) ;                          %Xv
x10(13)=xdata(1,34);                          %Xd
Y1(1,:)=x10; % x10 is the initial value vector
Y(1,:)=x10;
eli=size(Y1)

%switch to post-exponential phase
if batch==0 %for batch experiments
   mn = (fin-start);
   ttt = (min(DataTime):1: max(DataTime));
 for i=1:mn
    i;
 time = start + (i-1)/2;
 if time>=76 %fix switch for 250-3=80, 7(1)=76
   a = aPos;
end

 [t,x01]=ode23('Testing_a_function',[i i+1],x10);
 A1=[t,x01];
 [a1,b1]=size(A1);
 x10=x01(a1,:);
 t10=A1(a1,1);
   for j=1:12
       if x10(j)<0
           x10(j)=0;
       end
   end

   Y(i+1,:)=x10;
   T(i+1,:)=t10;
end
end

if batch>0
 %number of iterations
 mn = (fin-start)*2;
 ttt = (min(DataTime):0.5: max(DataTime));
 for i=1:mn
    i;
 time = start + (i-1)/2;

%switch to fed-batch a-values
 if time>47 %51 for 7(3) and 47 for 7(4)
    load a12
    a= aExA;
 end

%switch to post-exponential phase
```

```
 if time>=140 %switch for 7(3)=140, for 7(4)=140
    load a12
    a = aPos;
 end
 [t,x01]=ode23('Testing_a_function',[i i+1],x10);
 A1=[t,x01];
 [a1,b1]=size(A1);

 if batch==3 %Exp7(3), Dilutions are initiated in total 0.5 hrs before
diluted point
   if time==51
       for u = 1:12
           node=2;
           dist=DataTime(node+1)-DataTime(node); %node=Number of Data Node
before Dilution
           v=i+1-2*dist;
           x10(u)=Y(v,u)+(x10f(node+1,u)-x10f(node,u));
        end
   elseif time==55
       for u = 1:12
           node=4;
           dist=DataTime(node+1)-DataTime(node); %node=Number of Data Node
before Dilution
           v=i+1-2*dist;
           x10(u)=Y(v,u)+(x10f(node+1,u)-x10f(node,u));
       end
   elseif time==56
       for u = 1:12
           node=5; dist=DataTime(node+1)-DataTime(node); %node=Number of
Data Node before Dilution
           v=i+1-2*dist;
           x10(u)=Y(v,u)+(x10f(node+1,u)-x10f(node,u));
       end
   elseif time==71
       for u = 1:12
           node=8; dist=DataTime(node+1)-DataTime(node); %node=Number of
Data Node before Dilution
           v=i+1-2*dist;
           x10(u)=Y(v,u)+(x10f(node+1,u)-x10f(node,u));
       end
   elseif time==72
       for u = 1:12
           node=9; dist=DataTime(node+1)-DataTime(node); %node=Number of
Data Node before Dilution
           v=i+1-2*dist;
           x10(u)=Y(v,u)+(x10f(node+1,u)-x10f(node,u));
       end
       elseif time==75
       for u = 1:12
           node=10; dist=DataTime(node+1)-DataTime(node); %node=Number of
Data Node before Dilution
           v=i+1-2*dist;
           x10(u)=Y(v,u)+(x10f(node+1,u)-x10f(node,u));
```

```
        end
    elseif time==80
        for u = 1:12
            node=11; dist=DataTime(node+1)-DataTime(node); %node=Number of
Data Node before Dilution
            v=i+1-2*dist;
            x10(u)=Y(v,u)+(x10f(node+1,u)-x10f(node,u));
        end
    elseif time==96
        for u = 1:12
            node=13; dist=DataTime(node+1)-DataTime(node); %node=Number of
Data Node before Dilution
            v=i+1-2*dist;
            x10(u)=Y(v,u)+(x10f(node+1,u)-x10f(node,u));
        end
    elseif time==100
        for u = 1:12
            node=16; dist=DataTime(node+1)-DataTime(node); %node=Number of
Data Node before Dilution
            v=i+1-2*dist;
            x10(u)=Y(v,u);+(x10f(node+1,u)-x10f(node,u));
        end
    elseif time==104
        for u = 1:12
            node=17; dist=DataTime(node+1)-DataTime(node); %node=Number of
Data Node before Dilution
            v=i+1-2*dist;
            x10(u)=Y(v,u)+(x10f(node+1,u)-x10f(node,u));
        end
    elseif time==120
        for u = 1:12
            node=20; dist=DataTime(node+1)-DataTime(node); %node=Number of
Data Node before Dilution
            v=i+1-2*dist;
            x10(u)=Y(v,u)+(x10f(node+1,u)-x10f(node,u));
        end
    else
        x10=x01(a1,:);
        t10=A1(a1,1);
    end

elseif batch==4 %Exp7(4), Dilutions  are initiated in total 0.5 hrs before
diluted point
         if time==43
         for u = 1:12
            node=2;
            dist=DataTime(node+1)-DataTime(node);%node=Number of Data Node
before Dilution
            v=i+1-2*dist;
            x10(u)=Y(v,u)+(x10f(node+1,u)-x10f(node,u));
        end
     elseif time==54
         for u = 1:11
```

```
            node=5;
            dist=DataTime(node+1)-DataTime(node); %node=Number of Data Node
before Dilution
            v=i+1-2*dist;
            x10(u)=Y(v,u)+(x10f(node+1,u)-x10f(node,u));
        end
    elseif time==71
         for u = 1:11
            node=8;
            dist=DataTime(node+1)-DataTime(node) ;%node=Number of Data Node
before Dilution
            v=i+1-2*dist;
            x10(u)=Y(v,u)+(x10f(node+1,u)-x10f(node,u));
        end
    elseif time==75
         for u = 1:11
            node=12;
            dist=DataTime(node+1)-DataTime(node); %node=Number of Data Node
before Dilution
            v=i+1-2*dist;
            x10(u)=Y(v,u)+(x10f(node+1,u)-x10f(node,u));
        end
    elseif time==80
         for u = 1:11
            node=14;
            dist=DataTime(node+1)-DataTime(node); %node=Number of Data Node
before Dilution
            v=i+1-2*dist;
            x10(u)=Y(v,u)+(x10f(node+1,u)-x10f(node,u));
         end
    elseif time==96
         for u = 1:11
            node=16;
            dist=DataTime(node+1)-DataTime(node); %node=Number of Data Node
before Dilution
            v=i+1-2*dist;
            x10(u)=Y(v,u)+(x10f(node+1,u)-x10f(node,u));
        end
    elseif time==104
         for u = 1:11
            node=20;
            dist=DataTime(node+1)-DataTime(node); %node=Number of Data Node
before Dilution
            v=i+1-2*dist;
            x10(u)=Y(v,u)+(x10f(node+1,u)-x10f(node,u));
        end
    elseif time==120
         for u = 1:11
            node=23;
            dist=DataTime(node+1)-DataTime(node); %node=Number of Data Node
before Dilution
            v=i+1-2*dist;
            x10(u)=Y(v,u)+(x10f(node+1,u)-x10f(node,u));
```

```
        end
    else
        x10=x01(a1,:);
        t10=A1(a1,1);
    end
 else % for Batch Experiments without Dilution
 x10=x01(a1,:);
 end
  %*******************all outputs are positive**************

    for j=1:12
        if x10(j)<0
            x10(j)=0;
        end
    end

    Y(i+1,:)=x10;
    T(i+1,:)=t10;
end
end
save Y1308F Y
jane=size(Y);
jane=Y(1,:);

%Plot of the model prediction and the measured data

length=fin;

figure(1)
subplot(2,3,1)
F = Y(:,1);
E = x10f(:,1);
plot(ttt,F,'k-')
hold on
plot(DataTime,E,'k.')
xlabel('time(hour)');
ylabel('Xv(xE06/mL)');
axis([start length min(min(F),min(E)) max(max(F),max(E))])

subplot(2,3,2)
F = Y(:,2);
E = xdata(:,9);
plot(ttt,F,'k-')
hold on
plot(DataTime,E,'k.')
xlabel('time(hour)');
ylabel('GLC(mM)')
axis([start length min(min(F),min(E)) max(max(F),max(E))])

subplot(2,3,3)
F = Y(:,3);
E = xdata(:,17);
plot(ttt,F,'k-')
```

```
hold on
plot(DataTime,E,'k.')
xlabel('time(hour)');
ylabel('GLN(mM)')
axis([start length min(min(F),min(E)) max(max(F),max(E))])

subplot(2,3,4)
F = Y(:,4);
E = xdata(:,10);
plot(ttt,F,'k-')
hold on
plot(DataTime,E,'k.')
xlabel('time(hour)');
ylabel('LAC(mM)')
axis([start length min(min(F),min(E)) max(max(F),max(E))])

subplot(2,3,5)
F = Y(:,13);
E = x10f(:,13);
plot(ttt,F,'k-')
hold on
plot(DataTime,E,'k.')
xlabel('time(hour)');
ylabel('Xd(xE06/mL)');
axis([start length min(min(F),min(E)) max(max(F),max(E))])

subplot(2,3,6)
F = Y(:,12)*1E-6; %Mab goes in with 1E6 the value, to get a reasonable a-
coeffcient during the QP
E = xdata(:,32);
plot(ttt,F,'k-')
hold on
plot(DataTime,E,'k.')
xlabel('time(hour)');
ylabel('MAb(mM)')
axis([start length min(min(F),min(E)) max(max(F),max(E))])


figure (2)

subplot(2,3,1)
F = Y(:,11);
E = xdata(:,31);
plot(ttt,F,'k-')
hold on
plot(DataTime,E,'k.')
xlabel('time(hour)');
ylabel('Biomass(mM)')
axis([start length min(min(F),min(E)) max(max(F),max(E))])

subplot(2,3,2)
F = Y(:,9);
E = xdata(:,12);
```

```
plot(ttt,F,'k-')
hold on
plot(DataTime,E,'k.')
xlabel('time(hour)');
ylabel('ALA(mM)')
axis([start length min(min(F),min(E)) max(max(F),max(E))])

subplot(2,3,3)
F = Y(:,10);
E = xdata(:,26);
plot(ttt,F,'k-')
hold on
plot(DataTime,E,'k.')
xlabel('time(hour)');
ylabel('PRO(mM)')
axis([start length min(min(F),min(E)) max(max(F),max(E))])

subplot(2,3,4)
F = Y(:,7);
E = xdata(:,15);
plot(ttt,F,'k-')
hold on
plot(DataTime,E,'k.')
xlabel('time(hour)');
ylabel('ASN(mM)')
axis([start length min(min(F),min(E)) max(max(F),max(E))])

subplot(2,3,5)
F = Y(:,8);
E = xdata(:,14);
plot(ttt,F,'k-')
hold on
plot(DataTime,E,'k.')
xlabel('time(hour)');
ylabel('ASP(mM)')
axis([start length min(min(F),min(E)) max(max(F),max(E))])

subplot(2,3,6)
F = Y(:,6)*0.1;
E = xdata(:,18);
plot(ttt,F,'k-')
hold on
plot(DataTime,E,'k.')
xlabel('time(hour)');
ylabel('GLU(mM)')
axis([start length min(min(F),min(E)) max(max(F),max(E))])

figure(3)
F = Y(:,5);
plot(ttt,F,'k-')
hold on
xlabel('time(hour)');
ylabel('NH3(mM)')
```

```
axis([start length min(min(F),min(E)) max(max(F),max(E))])
```

Sub-routine for the Integrated Model:

```
function xp=Testing_a_function(t,x)
%a-coefficients are calculated from averages of Exp7(3) and Exp 250-3

global batch
global xp
global a
t=t;
a(1);

if batch==0
   kg=0.04;%0.05; 0.04 for fb; 0.04 for batch
   kd=0.001;
   kG=4;kQ=0.03;
   kU=0.01;kS=0.02;kF=0.05;
end

if batch>0
    kG=4;kQ=0.05;
    kU=0.01;kS=0.12;kF=0.05;
    if t<=47
    kg=0.04;
    kd=0.001;
    else
    kg=0.04;
    kd=0.0001;
    end
end

kgQ=0.05;
kdQ=0.43;

X=x(1);G=x(2);Q=x(3);L=x(4);N=x(5);U=x(6);S=x(7);F=x(8);B=x(9);P=x(10);M=x
(11);A=x(12);
%G-Glucose; Q-GLutamine; L-Lactate; N-Ammonia; U-GlutamicAcid;
%S-Asparagine; F-Aspartic Acid; B-Alanine; P-Proline; M-Biomass; A-MAb;
%X=Viable cells; **********************
load KK

%reaction rates
r(1)=a(1)*G*X/(kG+G);
r(2)=a(2)*G*U*X/((kG+G)*(kU+U));
r(3)=a(3)*G*U*X/((kG+G)*(kU+U));
r(4)=a(4)*U*X/(kU+U);
r(5)=a(5)*S*X/(kS+S);
r(6)=a(6)*Q*F*X/((kQ+Q)*(kF+F));
r(7)=a(7)*X*Q/(kQ+Q);
r(8)=a(8)*X*Q/(kQ+Q);
r(9)=a(9)*Q*X/(kQ+Q);
```

```
r=r';
size(r);
xp(2:12,:)=K1*r;

Xv=(kg*X*Q/(Q+0.05))-(kd*X*L/(Q+0.43)); %rate equation for viable cells
Xd=(kd*X*L/(Q+0.43)); %rate equation for dead cells

xp(1)=Xv;
xp(13)=Xd;
size(K1);%size of K1 is 11X9
size(xp);% size of xp excl Xd is 12X1
xp=xp;
size(xp);
```

Optimization for Biomass Model

Main File for Optimizing k_g and k_d in Biomass Model :

```
% MAIN PROGRAM FOR FED-BATCH EXPERIMENT: 2EQN
clear all;
lb = [0.0001;0.001];
ub =[0.05;0.3];
[paramt]=fmincon(@(k)...fedb_whole7_2(k),[0.001;;0.2],[],[],[],[],lb,ub,[]
,...optimset('TolFun',1e-01,'Display','iter'))
```

Sub-routine for Optimizing k_g and k_d- Fedbatch Mode:

```
% clear all;
%Experiment 7(2) 2EQN 2TERM
function ss = fedb_deathonly(k)
global tspan
% k
k = [0.0004;0.4303];
kd = k(1);
a4 = k(2);
ZZ0 = 0.237;
tspan = [27; 43];
[t1,X1] = ode23s(@ode_fedb_deathonly,tspan,ZZ0,[],kd,a4);
YY1 = X1(max(size(X1)));
ZZ1 = 0.812*X1(max(size(X1)),:);%after 43

tspan = [43; 47; 51];
[t2,X2] = ode23s(@ode_fedb_deathonly,tspan,ZZ1,[],kd,a4);
b2 = max(size(X2));
YY2 = X2(2:max(size(X2)));
ZZ2 = (0.865)*X2(max(size(X2)),:);%after 51

tspan = [51; 52; 55];
[t3,X3] = ode23s(@ode_fedb_deathonly,tspan,ZZ2,[],kd,a4);
```

```
b3 = max(size(X3));
YY3 = X3(2:max(size(X2)));
ZZ3 = X3(b3);%after 55

tspan = [55; 56; 67];
[t4,X4] = ode23s(@ode_fedb_deathonly,tspan,ZZ3,[],kd,a4);
b4 = max(size(X4));
YY4 = X4(2:b4);
ZZ4 = 0.88*X4(b4);%after 67

tspan = [67; 68; 71];
[t5,X5] = ode23s(@ode_fedb_deathonly,tspan,ZZ4,[],kd,a4);
b5 = max(size(X5));
YY5 = X5(2:b5);
ZZ5 = 0.874*X5(b5);%after 71

tspan = [71; 72; 75];
[t6,X6] = ode23s(@ode_fedb_deathonly,tspan,ZZ5,[],kd,a4);
b6 = max(size(X6));
YY6 = X6(2:b6);
ZZ6 = 0.774*X6(b6);%after 75

tspan = [75; 76; 80];
[t7,X7] = ode23s(@ode_fedb_deathonly,tspan,ZZ6,[],kd,a4);
b7 = max(size(X7));
YY7 = X7(2:b7);
ZZ7 = 0.794*X7(b7);%after 80

tspan = [80; 81; 96];
[t8,X8] = ode23s(@ode_fedb_deathonly,tspan,ZZ7,[],kd,a4);
b8 = max(size(X8));
YY8 = X8(2:b8);
ZZ8 = 0.884*X8(b8);

tspan = [96; 97; 100];
[t9,X9] = ode23s(@ode_fedb_deathonly,tspan,ZZ8,[],kd,a4);
b9 = max(size(X9));
YY9 = X9(2:b9);
ZZ9 = 0.88*X9(b9);%after 100

tspan = [100; 101];
[t10,X10] = ode23s(@ode_fedb_deathonly,tspan,ZZ9,[],kd,a4);
b10 = max(size(X10));
YY10 = X10(b10);
ZZ10 = 0.87*X10(b10);%after 101

tspan = [101; 104];
[t11,X11] = ode23s(@ode_fedb_deathonly,tspan,ZZ10,[],kd,a4);
b11 = max(size(X11));
YY11 = X11(b11);
ZZ11 = 0.78*X11(b11);%after 104
```

```
tspan = [104; 105; 116];
[t12,X12] = ode23s(@ode_fedb_deathonly,tspan,ZZ11,[],kd,a4);
b12 = max(size(X12));
YY12 = X12(2:b12);
ZZ12 = 0.925*X12(b12);

tspan = [116; 120; 124];
[t13,X13] = ode23s(@ode_fedb_deathonly,tspan,ZZ12,[],kd,a4);
b13 = max(size(X13));
YY13 = X13(2:b13);
ZZ13 = 0.87*X13(b13);%after 124

tspan = [124; 140; 144];
[t14,X14] = ode23s(@ode_fedb_deathonly,tspan,ZZ13,[],kd,a4);
b14 = max(size(X14));
YY14 = X13(2:b14);
ZZ14 = X14(b14); %after 144

tspan = [144; 148; 164];
[t15,X15] = ode23s(@ode_fedb_deathonly,tspan,ZZ14,[],kd,a4);
b15 = max(size(X15));
YY15 = X15(2:b15);
ZZ15 = X15(b15); %after 164

tspan = [164; 168; 172; 189; 194];
[t16,X16] = ode23s(@ode_fedb_deathonly,tspan,ZZ15,[],kd,a4);
b16 = max(size(X16));
YY16 = X16(2:b16);
ZZ16 = X16(b16);

%tspan=[tspan1;tspan2(2:b2);tspan3(2:b3);tspan4(2:b4);tspan5(2:b5);tspan6(
2:b6);tspan7(2:b7);tspan8(2:b8);tspan9(2:b9);tspan10(2);tspan11(2);tspan12
(2:b12);tspan13(2:b13);tspan14(2:b14);tspan15(2:b15);tspan16(2:b16)];
X=ZZ0;YY1;YY2;YY3;YY4;YY5;YY6;YY7;YY8;YY9;YY10;YY11;YY12;YY13;YY14;YY15;YY
16];
t = [ 27; 43; 47; 51; 52; 55; 56; 67; 68; 71; 72; 75;76; 80; 81; 96; 97;
100; 101; 104; 105; 116; 120; 124; 140; 144; 148; 164; 168; 172; 189; 194
];%time
% Xv = [1.41, 2.8, 4.75, 4, 3.7, 4, 6.23 4, 3.65, 7.20, 6.44, 5.05, 4.10,
5, 3.97, 6.55, 5.96, 5.70, 5.12, 5.1, 4.06, 4.9, 6.45, 6.05, 6.15, 7.10,
6.25, 4.05, 2.65, 0.85, 1.50, 1.05]';%viable cell concentration
Xd = [0.237, 0.5238, 0.5248, 0.5998, 0.548, 0.4999, 0.7787, 0.85, 0.7758,
0.4997, 0.4470, 0.5, 0.406, 0.35 0.2778, 0.7497, 0.6821, 0.8002, 0.7188,
0.6002, 0.4778, 0.6, 1.05, 0.9996, 2.05, 2.4997, 1.95, 5.5, 5, 1.1748,
5.9, 8.3 ]';%dead cell concentration
size(Xd);
ss = sum((X-Xd).^2)
```

Sub-routine called to the MAT file above- Fed-batch Mode:

```
%... for experiment 7(2): 2 EQN 2 TERM after correlation
```

```
function dX = ode_fedb_deathonly(t,X,kd,a4)
global tspan
a5 = 1;

%time = 27 to 43 hrs
if tspan(1) == 27
Glnp = -0.03375*t+3.21125;
Lacp = (1000/90)*(0.038125*t-0.29);
te = [27;43];
Xv = [1.41;2.8];
Xe = interp1(te,Xv,t);
dX = Xe*kd*(Lacp)*a5/(Glnp+a4);
dX;
t;
Xe;
end
%time = 43 to 51 hrs
if tspan(1) == 43
Glnp = -0.065*t+4.555;
Lacp = (1000/90)*(0.025*t+0.275);
te = [43;51];
Xv = [2.8;4];
Xe = interp1(te,Xv,t);
dX = Xe*kd*(Lacp)*a5/(Glnp+a4);
end
%time = 51 to 55
if tspan(1) == 51
Glnp = -0.065*t+4.555+0.11;
Lacp = (1000/90)*(0.025*t+0.275-0.05);
te = [52; 55];
Xv = [3.7;4];
Xe = interp1(te,Xv,t,'linear','extrap');
dX = Xe*kd*(Lacp)*a5/(Glnp+a4);
end
%time = 55 to 67 hrs
if tspan(1) == 55
Glnp = -0.065*t+4.555+0.7;
Lacp = (1000/90)*(0.025*t+0.275-0.4);
te = [55;75];
Xv = [4;5.05];
Xe = interp1(te,Xv,t);
dX = Xe*kd*(Lacp)*a5/(Glnp+a4);
t;
end
%time = 67 to 71
if tspan(1) == 67
Glnp = -0.065*t+4.555+0.8;
Lacp = (1000/90)*(0.025*t+0.275-0.5);
te = [67;71];
Xv = [4;7.2];
Xe = interp1(te,Xv,t);
dX = Xe*kd*(Lacp)*a5/(Glnp+a4);
end
```

```
%time = 71 to 75
if tspan(1) == 71
Glnp = -0.065*t+4.555+1.2;
Lacp = (1000/90)*(0.025*t+0.275-0.7);
te = [55;75];
Xv = [4;5.05];
Xe = interp1(te,Xv,t);
dX = Xe*kd*(Lacp)*a5/(Glnp+a4);
end
%time = 75 to 80
if tspan(1) == 75
Glnp = -0.065*t+4.555+1.6;
Lacp = (1000/90)*(0.025*t+0.275-0.9);
te = [76; 80];
Xv = [4.1;5];
Xe = interp1(te,Xv,t,'linear','extrap');
dX = Xe*kd*(Lacp)*a5/(Glnp+a4);
end
%time = 80 to 96
if tspan(1) == 80
Glnp = -0.065*t+4.555+2.2;
Lacp = (1000/90)*(0.03933*t-2.086);
te = [81; 96];
Xv = [3.97;6.55];
Xe = interp1(te,Xv,t,'linear','extrap');
dX = Xe*kd*(Lacp)*a5/(Glnp+a4);
end
%time = 96 to 100
if tspan(1) == 96
Glnp = -0.065*t+4.555+2.8;
Lacp = (1000/90)*(0.03933*t-2.086-0.2);
te = [96; 97; 100];
Xv = [6.55;5.96;5.70];
Xe = interp1(te,Xv,t);
dX = Xe*kd*(Lacp)*a5/(Glnp+a4);
end
%time = 100 to 101
if tspan(1) == 100
Glnp = -0.065*t+4.555+3;
Lacp = (1000/90)*(0.03933*t-2.086-0.4);
te = [100; 101];
Xv = [5.70;5.12];
Xe = interp1(te,Xv,t);
dX = Xe*kd*(Lacp)*a5/(Glnp+a4);
end
%time = 101 to 104
if tspan(1) == 101
Glnp = -0.065*t+4.555+3;
Lacp = (1000/90)*(0.03933*t-2.086-0.4);
te = [101; 104];
Xv = [5.12;5.10];
Xe = interp1(te,Xv,t);
dX = Xe*kd*(Lacp)*a5/(Glnp+a4);
```

```
end
%time = 104 to 116
if tspan(1) == 104
Glnp = -0.05*t+4.555+2.1;
Lacp = (1000/90)*(0.03933*t-2.086-0.85);
te = [104; 105; 116];
Xv = [5.10;4.06;4.90];
Xe = interp1(te,Xv,t);
dX = Xe*kd*(Lacp)*a5/(Glnp+a4);
end
%time = 116 to 124
if tspan(1) == 116
Glnp = -0.05*t+4.555+2.1;
Lacp = (1000/90)*(0.01875*t-0.625);
te = [116;124];
Xv = [4.90;6.05];
Xe = interp1(te,Xv,t);
dX = Xe*kd*(Lacp)*a5/(Glnp+a4);
end
%time = 124 to 144
if tspan(1) == 124
Glnp = (-0.023*t+3.3658);
Lacp = (1000/90)*(0.00625*t+0.895);
te = [124;144];
Xv = [6.05;7.10];
Xe = interp1(te,Xv,t);
dX = Xe*kd*(Lacp)*a5/(Glnp+a4);
end
%time = 144 to 164
if tspan(1) == 144
Glnp = (-0.003*t+0.5);
Lacp = (1000/90)*(0.00625*t+0.895);
te = [144; 148; 164];
Xv = [7.1;6.25;4.05];
Xe = interp1(te,Xv,t);
dX = Xe*kd*(Lacp)*a5/(Glnp+a4);
dX;
end
%time = 164 to 194
if tspan(1) == 164
Glnp = 0;
Lacp = (1000/90)*(0.00625*t+0.895);
te = [164;189; 194];
Xv = [4.05;1.5;1.05];
Xe = interp1(te,Xv,t);
dX = Xe*kd*(Lacp)*a5/(Glnp+a4);
dX;
end
```

Sub-routine for Optimizing k_e and k_d- Batch Mode :

```
% clear all;
%Experiment 250(3) 2EQN 2TERM
```

```
function ss = b250_3_lin(k)
global tspan
k=[0.0004;0.43];
% k = [0.05;0.05];
kg = 0.05;
a1 = 0.05;
ZZ0 = [1.5,0.258];
tspan = [22;49;75;96;121;144;166];
[t1,X] = ode23s(@odeb250_3_lin,tspan,ZZ0,[],kg,a1,k);

size(t1)
size(X)

t=[22,49,75,96,121,144,166]';
Xv = [1.6,7.8,10.5,8.8,6.1,2.3,1.6]';
Xd = [0.258,1.504,0.826,5.582,13.111,15.793,14.951]';
size(t)
size(Xv)
size(Xd)
ss = sum((X(:,2)-Xd).^2);
% ss = sum((X(:,1)-Xv).^2) + sum((X(:,2)-Xd).^2);
xlabel('Time(in hrs)')
hold on
ylabel('Cell conc. (in 10^5cells/mL)')
plot(t,Xv,'-r*')
plot(t,Xd,'-r*')
plot(t,X(:,1),'g.-')
plot(t,X(:,2),'g.-')
hold off
```

Sub-routine called to the MAT file above- Batch Mode:

```
%... for experiment 250(3): 2 EQN 2 TERM after correlation
function dX = odeb250_3_lin(t,X,kg,a1,k)
global tspan
kd = k(1);
a2 = k(2);
dX = zeros(2,1);
t;   %i= i+1;
te = [22,49,75,96,121,144,166];
Ge = [2.83,0.92,0,0,0,0,0];
Le = (1000/90)*[0.44,1.41,1.68,1.64,1.63,1.66,1.77];
Glnp = interp1(te,Ge,t);
Lacp = interp1(te,Le,t);
dX(1) = kg*X(1)*(Glnp/(Glnp+a1)) -  kd*X(1)*Lacp/(Glnp+a2);
dX(2) =  kd*X(1)*Lacp/(Glnp+a2);
```

.

Bibliography

Abraham, K.A., Eikom, T.S., Dowben, R.S., Dowben R. M. and Garatun-Tjeldsto, O. *Cell-free translation of messenger RNA for myeloma light chain prepared from synchronized plasmacytoma cells*. Eur. J. Biochem., Volume 65, pp. 79-86 (1976).

Agrawal, P., Koshy, G. and Ramseier, M. *An algorithm for Operating a Fed-Batch Fermentor at Optimum Specific Growth Rate*. Biotechnology and Bioengineering, Volume 33, pp.115 -125 (1989).

Al-Rubeai, M., Emery, A.N., Chalder, S. and Jan, D.C. *Specific monoclonal antibody productivity and the cell cycle comparisons of batch, continuous and perfusion cultures*. Cytotechnology, Volume 9, pp. 85-97 (1992).

Andrews, G.F. *The yield equations in the Modelling and control of bioprocesses*. Biotechnol Bioeng., Volume 42, pp. 549-556 (1993).

Bailey, J.E. and Ollis, D.F. *Biochemical Engineering Fundamentals*. Mc Graw Hill, New York, 2nd Edition (1986).

Banerjee, U.C., *Evaluation of Different Bio-Kinetic parameters of Curvularia Lunata at Different Environmental Conditions*. Biotechnology Techniques, Volume 7, No. 9, pp. 635-638 (1993).

Barford, J.P., Phillips, P. J. and Harbour, C. *Simulation of animal cell metabolism*. Cytotechnology, Volume 10, pp. 63-74 (1992).

Bidlingmeyer, B.A. *Rapid Analysis of Amino Acids Using Pre-Column Derivatization*. Journal of Chromatography, Elsevier, Amsterdam, 336, 93-104 (1984).

Bonarius, H.P.J., Hatzimanikatis, V., Meesters K.P.H., Gooijer, C.D., Schmid, G., Tramper, J. *Metabolic Flux Analysis of Hybridoma Cells in Different Culture Media Using Mass Balances*. Biotechnology and Bioengineering, Volume 50, pages 299-318 (1996).

Cazzador, L. and Mariani, L. *Growth and production modelling in hybridoma continuous cultures*. Biotechnology Bioengineering, Volume 42, pp. 1322-1330 (1993).

Chisti, Y., Animal cell culture in stirred bioreactors: *Observations on scale-up*. Bioprocess and Biosystems Engineering, Volume 9, No. 5, pp. 1616-1705 (1993).

Coligan, J.E. *Current Protocols in Immunology*. John Wiley and Sons, Inc., New York, Section IV (1994).

Cruz, H.J., Moreira, J.L. and Carrondo, M.J.T. *Metabolic shifts by nutrient manipulation in continuous cultures of BHK cells*. Biotechnol Bioeng., Volume 66, pp.104–112 (1999).

Darynkiewicz, Z., Juan. G., Li, X., Gorczyca, W., Murakami, T. and Traganos, F. *Cytometry in cell necrobiology: analysis of apoptosis and accidental cell death (necrosis)*. Cytometry, Volume 57, 1835-40 (1997).

De Alwis Seneviratne, D. M., *Hybridoma Cell Culture: Medium Optimization & Application to Fed-batch*. Thesis (MASc). University of Waterloo (2004).

Dutton, R.L., Scharer J.M. and Moo-Young, M. *Descriptive parameter evaluation in mammalian cell culture*. Cytotechnology, Volume 26, pp. 139-152 (1998).

Eakman, J. M., Fredrickson, A. G. and Tsuchiya, H. M. *Statistics and Dynamics of Microbial Cell Populations*. Chem. Eng. Prog. Syrup. Series No. 69, 62, pp. 37-49 (1966).

Europa, A.F., Gambhir, A., Fu, P.C. and Hu, W.S. *Multiple steady states with distinct cellular metabolism in continuous culture of mammalian cells*. Biotechnol Bioeng., Volume 67, pp. 25–34 (2000).

Frame, S. and Balmain, A. *Integration of positive and negative growth signals during ras pathway activation in vivo*. Curr. Opin. Genet. Dev. Volume 10, pp. 106-113 (2000).

Franek, F. and Dolnikova, J. *Hybridoma growth and monoclonal antibody production in iron-rich protein-free medium: Effect of nutrient concentration*. Cytotechnology, Volume 7, pp. 33-38 (1991a).

Follstad, B. D., Balcarcel, R. R., Stephanopolous G. and Wang D.I.C. *Metabolic Flux Analysis of Hybridoma Continuous Steady State Multiplicity*. John Wiley and Sons, Inc. (1999).

Fredrickson, A.G. *Formulation of structured growth models*. Biotechnology Bioengineering, Volume 18, pp. 1481-1486 (1976).

Gambhir, A., Korke, R., Lee, J., Fu, P., Europa, A., Hu, W. *Analysis of Cellular Metabolism of Hybridoma Cells at Distinct Physiological States*. Journal of Bioscience and Bioengineering, Volume 95, No. 4, pp. 317-327 (2003).

Gao, J., Gorenflo, V., Scharer, J.M. and Budman, H.M. *Dynamic metabolic Modelling for the optimization and control of bioprocesses*. To be published (2006).

Garatun-Tjeldstr, O., Pryme, I.F., Weltman, J.K. and Dowben, R.M. *Synthesis and secretion of light-chain immunoglobulin in two successive cycles of synchronized plasmacytoma cells*. J. Cell Biol., Volume 68, pp. 232-239 (1976).

Glacken, M.W., Adema, E. and Sinskey A.J. *Mathematical Descriptions of Hybridoma culture kinetics: I. Initial Metabolic Rates.* Biotechnology ad Bioengineering, Volume 32, pp. 491-506 (1988).

Glacken, M.W., Haung, C. and Sinskey, A.J. *Mathematical descriptions of hybridoma culture kinetics. III. Simulation of fed-batch bioreactors*. Journal of Biotechnology, Volume 10, pp. 39-66 (1989b).

Glacken, M.W., Fleischaker, R.J. and Sinskey, A.J. *Mammalian cell culture: engineering principles and scale-up*. Trends in Biotechnology, Volume 1, pp.102–108 (1983).

Gombert A.K. and Nielson, J. *Mathematical Modelling of metabolism*. Current Opinion in Biotechnology, Volume 11, pp. 180-186 (2000).

Griffiths, J.B. *Overview of cell culture systems and their scale up*. Animal cell biotechnology, Chapter 7, Vol. 3, Spier RE and Griffiths JB (Eds) Academic Press, London, pp. 179–220 (1988).

Hanko, V.P., Heckenberg, A. and Jeffrey, S.R. *Determination of Amino Acids in Cell Culture and Fermentation Broth Media Using Anion-Exchange Chromatography with Integrated Pulsed Amperometric Detection*. Journal of Biomolecular Techniques, Volume 15, pp.317-324 (2004).

Hatzis, C., Srienc, F., and Fredrickson, A. G. *Multistaged corpuscular models of microbial growth: Monte Carlo simulations*. Biosystems Volume 36, pp. 19-35 (1995).

Henderson, M.H., Ting-Beall, H.P. and Tran-Son-Tay R. *Shear sensitivity of mitotic doublets in GAP A3 hybridoma cells*. ASME Bioprocess Engineering Symposium BED-Volume 23, 7 (1992).

Henson, M.A. *Review*. Current Opinion in Biotechnology, Volume 14, pp. 460–467 (2003).

Hu, W.S. and Himes, V.B. *Stoichiometric considerations of mammalian cell metabolism in bioreactors*. In: Fiechter A, Okada H & Tanner RD (eds.) Bioproducts and Bioprocesses, Second conference to promote Japan/US joint projects and cooperation in biotechnology, Lake Biwa, Japan, Sept. 27-30, 1986, Springer-Verlag, Berlin, pp. 33-46 (1989).

Kerr, J.F.R., Wyllie, A.H. and Currie, A.R. *Apoptosis: a basic biological phenomenon with wide ranging implications in tissue kinetics*. Br J Cancer, Volume 26, pp. 239-57 (1972).

Liberti, P. and Baglioni, C. *Synthesis of immunoglobulin and nuclear protein in synchronized mouse myeloma cells.* J. Cell, Physiol., Volume 82, pp.113-120 (1973).

Linardos, T.I., Kalogerakis, N. and Behie, L.A. *Cell cycle model for growth rate and death rate in continuous suspension hybridoma cultures*. Biotechnol. Bioeng., Volume 40, pp. 359-368 (1992).

Linz, M., Zeng, A.P., Wagner, R. and Deckwer, W.D. *Stoichiometry, kinetics, and regulation of glucose and amino acid metabolism of a recombinant BHK cell line in batch and continuous cultures*. Biotech. Progr., Volume 13, pp. 453–463 (1997).

Liou, J.J., Srienc, F. and Fredrickson, A.G. *Solutions of population balance models based on a successive generations approach*. Chemical Eng. Sci., Volume 52, pp. 1529–1540 (1997).

Ljunggren, J. and Haggstrom, L. *Catabolic Control of Hybridoma Cells by Glucose and Glutamine Limited Fed Batch Cultures*. Biotechnology and Bioengineering, Volume 44, pp. 808-818 (1994).

Longobardi, G. P. *Fed-Batch versus Batch Fermentation*. Bioprocess Engineering, Volume 10, pp. 185-194 (1994).

Mantzaris, N., Liou, J., Daoutidis, P. and Srienc, F. *Numerical solution of a mass structured cell population balance model in an environment of changing substrate concentration*. J. Biotechnol., Volume 71, pp. 157-174 (1999).

Mantzaris, N.V., Daoutidis, P. and Srienc, F. *Numerical solution of multi-variable cell population balance models: I. Finite difference methods*. Computers and Chemical Engineering, 25, 1411-1440 (2001a).

McNeil, B. and Harvey, L. M. *Fermentation, a Practical Approach*. IRL Press, Tokyo (1990).

Mercille, S. and Massie, B. *Induction of Apoptosis in Nutrient-Derived Cultures of Hybridoma and Myeloma Cells*. Biotechnology and Bioengineering, Volume 44, pp. 1140-1154 (1994).

Mitchison, J.M. *The Biology of the Cell Cycle*. Cambridge University Press, Cambridge (1971).

Moore, S., Spackman, D.H. and Stein, W.H. *Analytical Chemistry*, Volume 30, pp. 1185 (1958).

Mousavi, S.A.A. and Geoffrey D.R. *Entry into the stationary phase is associated with a rapid loss of viability and an apoptotic-like phenotype in the opportunistic pathogen Aspergillus fumigates*. Fungal Genetics and Biology, Volume 39, pp. 221–229 (2003).

Needham, D., Ting-Beall, H.P., and Tran-Son-Tay, R. *Morphology and mechanical properties of GAP A3 hybridoma cells as related to cell cycle*. ASME Bioprocess Engineering Symposium BED-Volume 16, pp. 5-10 (1990).

Newland, M., Greenfield, P.F. and Reid, S. *Hybridoma growth limitations: The roles of energy metabolism and ammonia production.* Cytotechnology, Volume 3, pp. 215-229 (1990).

Noe, D.A. and Delenick, J.C. *Quantitative analysis of membrane and secretory protein processing and intracellular transport*. J. Cell Sci, Volume 92, pp. 449-459 (1989).

Papoutsakis, E.T. and Lee, S.Y. *Metabolic Engineering*. Marcel Dekker Inc., New York (1999).

Paredes, C., Prats, E., Cairo, J.J., Azorin, F., Cornudella, L. and Godia, F. *Modification of glucose and glutamine metabolism in hybridoma cells through metabolic engineering*. Cytotechnology, Volume 30, pp. 85–93 (1999).

Portner, R. and Schafer, T. *Modelling hybridoma cell growth and metabolism- a comparison of selected models and data*. Journal of Biotechnology, Volume 49, pp. 119-135 (1996).

Provost, A. and Bastin, G. *Dynamic metabolic modelling under the balanced growth condition*. Journal of Process Control, Volume 14, pp. 717-728 (2004).

Ramirez, O.T. and Mutharasan, R. *Cell cycle- and growth phase dependent variations in size distribution, antibody productivity, and oxygen demand in hybridoma cultures*. Biotechnol. Bioeng., Volume 36, pp. 839-848 (1990).

Renvoize, C., Biola, A., Pallardy, M. and Breard, J. *Apoptosis: Identification of dying cells*. Cell Biology and Cell Toxicology, Volume 14, pp.111-120 (1997).

Riccardi C. and Nicoletti. I. *Analysis of apoptosis by propidium iodide staining and flow cytometry*. Nature Protocols 1, pp.1458 – 1461 (2006)

Sambanis, A., Lodish, H.F. and Stephanopoulos, Gr. *A model of secretory protein trafficking in recombinant ART-20 cells*. Biotechnol. Bioeng., Volume 38, pp.280-295 (1991).

Sanderson, C.S. *The Development and Application of a Structured Model for Animal Cell Metabolism*. Ph.D. Thesis, University of Sydney, Sydney, Australia (1997).

Seamans, T.C. and Hu, W.S. *Kinetics of growth and antibody production by a hybridoma cell line in a perfusion culture*. J. Ferment. Bioeng., Volume 70(4), pp.241-245 (1990).

Sears, R.C. and Nevins, J.R. *Signaling networks that link cell proliferation and cell fate*. J. Biol. Chem., 277, 11617-11620 (2002).

Shapiro, P. *Ras-MAP kinase signaling pathways and control of cell proliferation: relevance to cancer therapy*. Crit. Rev. Clin. Lab. Sci., 39, 285-330 (2001).

Shuler, M.L. *Single-cell models: promise and limitations*. Journal of Biotechnology, Volume 71, pp. 225–228 (1999).

Shuler, M.L., and Kargi, F. *Bioprocess Engineering- Basic Concepts*. Prentice Hall, New Jersey.

Sidoli, F.R., Mantlaris, A. and Asprey S.P. *Modelling of mammalian cells and cell culture processes*. Cytotechnology, Volume 44, pp. 27-46 (2004).

Sidoli, F.R., Asprey S.P. and Mantlaris, A. *A Coupled Single Cell-Population-Balance Model for Mammalian Cell Cultures*. Ind. Eng. Chem. Res., 45, 5801-58811 (2006).

Simpson, N.H., Milner A. E. and Al-Rubeai, M. *Prevention of Hybridoma Cell Death by bcl-2 During Suboptimal Culture Conditions*. John Wiley & Sons, Inc. Biotechnology Bioengineering, Volume 54, pp. 1-16(1997).

Singh, R.P., Al-Rubeai, Gregory, C.D. and Emery, A.N. *Cell Death in bioreactors: A role for apoptosis*. Biotechnology Bioengineering, Volume 44, pp. 720-726 (1994).

Suzuki, E. and Ollis, D.F. *Cell cycle model for antibody production kinetics*. Biotechnol. Bioeng., Volume 35, pp.1398-1402 (1989).

Suzuki, E. and Ollis, D.F. *Enhanced antibody production at slowed rates: Experimental demonstration and a simple structured model*. Biotechnol. Prog., Volume 6, pp. 231-236 (1990).

Tziampazis, E. and Sambanis, A. *Modelling of cell culture processes*. Cytotechnology, Volume 14, pp. 191-204 (1994).

Upton, J, Mulliken JB, Murray JE. *Major intravenous extravasation injuries*. Am J Surgery, 137,497-506 (1979).

Villadsen, J. Short Communication. *On the use of population balances*. J. Biotech., Volume 71, pp.251-253 (1999).

Wyllie, A. H. *Apoptosis, Cell Death and Cell Proliferation*. Roche Applied Science, 3rd Edition, pp. 1-4 (2004).

Wyllie, A.H., Morris, R.G., Smith, A.L. and Dunlop, D. *Chromatin Cleavage in Apoptosis: Association with Condensed Chromatin Morphology and Dependence on Macromolecular Synthesis*. Journal of Pathology, Volume 142, pp. 67-77 (1984).

Xiang, X., Gerard, L. V., Huang, C. B., Anderson, D. C., Payan, D.G. and Luo, Y. *Detection of programmed cell death using fluorescence energy transfer*. Nucleic Acids Research, Oxford University Press, Vol. 26, No. 8, pp. 2034–2035 (1998).

Ziegler, U. and Groscurth, P. *Morphological Features of Cell Death*. News Physiol Sci, Volume 19, pp. 124-128 (2004).

Zhou, F., Bi, J., Zeng, A. and Yuan, J. *Alteration of mammalian cell metabolism by dynamic nutrient feeding*. Cytotechnology,Volume 24, pp. 99–108 (1997).

Invitrogen website "http://www.invitrogen.com", copyright © 2007, Invitrogen Corporation, accessed July, 2007.

"http://www.cellsalive.com", copyright © 2006, Quill, accessed July, 2007.

"http://www.wikipedia.org" Wikipedia- registered trademark of the Wikimedia Foundation Inc., accessed July, 2007.

"http://www.extravasation.org.uk", copyright © 2000-2007, The National Extravasation Information Service, accessed July, 2007.

"http://fachschaft.bci.unidortmund.de/Skripte/Zellbiologische%20Systeme/Zellbiologische%20Systeme%201_Stunde6.pdf", accessed July, 2007.

Ngee Ann website. "http://www.np.edu.sg/home/sitemap.html", copyright ©, Ngee Ann Polytechnic, accessed July, 2007.

"http://www.raifoundation.org", copyright © 2007, Rai Foundation Colleges, accessed July, 2007.

"http://rsb.info.nih.gov/ij/features.html", public domain, accessed July, 2007.

"http://users.rcn.com/jkimball.ma.ultranet/BiologyPages/A/Apoptosis.html", accessed July, 2007.

"http://users.rcn.com/jkimball.ma.ultranet/BiologyPages/C/CellCycle.html", accessed July, 2007.